„Significance of Neuroplastin and its Paralog Basigin for Plasma Membrane-associated Ca^{2+} ATPases in the Central and Peripheral Nervous System“

Thesis

For the degree of

doctor rerum naturalium (Dr. rer. nat.)

approved by the Faculty of Natural Sciences of Otto von Guericke University Magdeburg

by **M.Sc. Xiao Lin**

born on October 02. 1990 in Shaanxi (China)

Examiner: Prof. Dr. Eckart D. Gundelfinger

Prof. Dr. Stefan Kindle

Submitted on: March 26. 2021

Defended on: October 15. 2021

Abbreviations

AD	Alzheimer's Disease
AP5	2-Amino-5-Phosphonovaleric Acid
AZs	Active Zones
BSA	Bovine Serum Albumin
CAM	Cell Adhesion Molecule
cDNA	Complementary Deoxyribonucleic Acid
CSD	Current Source Density
CE	Carboxyeosin
CNQX	6-Cyano-7-Nitroquinoxaline-2,3-Dione
DIV	Day In Vitro
DTT	Dithiothreitol
DMEM	Dulbecco's Modified Eagle's Medium
ENU	N-ethyl-N-nitrosaurea
E.coli	Escherichia Coli
EDTA	Ethylenediaminetetraacetic acid
EF	Endotoxin Free
ELISA	Enzyme-linked Immunosorbent Assay
ER	Endoplasmic Reticulum
FGFR	Fibroblast Growth Factor Receptor
$GABA_AR$	A-type of Gamma-amino Butyric Acid Receptor
GFP	Green Fluorescent Protein
GRB2	Growth Factor receptor-bound protein 2
HBSS	Hank's Balanced Salt Solution
HEK	Human Embryonic Kidney Cell
IHC	Immunohistochemistry
IHCs	Inner Hair Cells
Ig	Immunoglobulin
KO	Knockout mice
LTD	Long Term Depression
LTP	Long Term Potentiation
NCX	Na^+/Ca^{2+} - exchangers
Nptn	Neuroplastin
MCT2	Monocarboxylate Transporter 2
MET	Mechanotranduction
MMP	Matrix Metalloproteinase
OHCs	Outer Hair Cells
PMCAs	Plasma membrane-associated Ca^{2+} ATPases
PSD95	Postsynaptic Densities
RFPT	Red Fluorescent Protein
SERCA	Sarco-endoplasmic reticulum Calcium ATPase
SGN	Spiral Ganglion Neuron

SNPs	Single Nucleotide Polymorphisms
SJ	Synaptic Junction
TMD	Transmembrane Domain
TRAF	Tumor necrosis factor Receptor Associated Factor
TTX	Tetrodotoxin
VDCCs	Voltage Dependent Calcium Channels
VEGF	Vascular Endothelial Growth Factor
WT	Wild-Type

Summary

Neuroplastin (Nptn), a transmembrane protein of the immunoglobulin superfamily categorized as a cell adhesion molecule (CAM), has been implicated in long term synaptic plasticity and synapse formation/stabilization. Moreover, studies on Nptn-mutant mice uncovered a crucial role in learning and memory. Recently, plasma membrane calcium ATPases (PMCAs) emerged as first order binding partners of Nptn. This suggested a role for Nptn in Ca^{2+} homeostasis, which was supported by studies on various cell types. The actual impact of Nptn loss on the various PMCA isoforms in the brain remained largely unaddressed. Moreover, the mode of interaction between Nptn and PMCAs was not explored in detail, before this work was initiated. Here, I present a detailed analysis of the effects of constitutive and conditional loss of Nptn on PMCAs in various central brain areas and in the cochlea. While principally leading to reduced PMCA levels, the different isoforms were affected to surprisingly various extent and in a brain-region specific manner. Knockdown of Nptn was accompanied by strikingly increased levels of Basigin, a close paralog of Nptn. Cell culture assays confirmed the hypothesis that Basigin can partially compensate for loss of Nptn. The well-conserved transmembrane domain in Nptn and Basigin was identified as the crucial determinant for stabilizing PMCAs. Further analyses point to an interdependent relation between PMCAs and Nptn or Basigin. In a second major part of this thesis, I analyzed the role of Nptn in the auditory system, demonstrating that deafening in Nptn mutants is a rapidly progressing process mainly due to loss of Nptn in hair cells of the cochlea, which is accompanied by profound reduction of PMCAs and subsequent cell death. In summary, these data corroborate and specify the crucial role of Nptn for stabilizing PMCAs. They also add another level of complexity by uncovering redundancy with Basigin. While leading to surprisingly differential profiles of PMCA reduction in the central nervous system, loss of Nptn in the inner ear causes altered Ca^{2+} homeostasis and as a consequence hearing deficits due to hair cell degeneration.

Zusammenfassung

Neuroplastin (Nptn), ein Zelladhäsionsmolekül der Immunoglobulin-Superfamilie, ist funktionell eng mit synaptischer Langzeitplastizität und der Bildung und Stabilisierung von Synapsen assoziiert. Untersuchungen an Nptn-mutanten Mäusen offenbarten zudem eine wichtige Rolle für Lernen und Gedächtnis. Kürzlich wurden Plasmamembran-assoziierte Calcium ATPasen (PMCAs) als enge Interaktionspartner von Nptn identifiziert. Dies legt eine Rolle für Nptn bei der Ca^{2+} Homöostase nahe, was anhand verschiedener Zelltypen bestätigt wurde. Weitgehend unbeantwortet waren bei Beginn der Arbeit Fragen nach dem Einfluß von Nptn auf die verschiedenen PMCA Isoformen sowie nach dem Interaktionsmodus. In dieser Arbeit präsentiere ich eine detaillierte Analyse der Effekte des konstitutiven oder konditionalen Ausfalls von Nptn auf PMCAs in verschiedenen Hirnarealen und in der Cochlea. Abgesehen von einer prinzipiellen Reduktion der PMCA-Levels, zeigte sich, dass die verschiedenen Isoformen in überraschend unterschiedlichem Maße und in regionsspezifischer Weise vermindert waren. Der Knockdown von Nptn war zudem stets mit einer auffallenden Zunahme von Basigin, einem eng verwandten Paralogon von Nptn, verbunden. Zellkulturversuche bestätigten die Hypothese, dass Nptn zumindest teilweise durch Basigin ersetzt werden kann. Die gut konservierte Transmembrandomäne von Nptn und Basigin wurde als entscheidende Determinante für die PMCA-Stabilisierung identifiziert. Weitere Analysen deuten auf wechselseitige Abhängigkeiten zwischen PMCAs und Nptn bzw. Basigin. Der zweite Hauptteil meiner Arbeit befasst sich mit der Rolle von Nptn im auditorischen System. Dort wird gezeigt, dass der Hörverlust in Nptn-Mutanten ein rasch voranschreitender Prozess ist, der vornehmich auf dem Verlust von Nptn in Haarzellen der Cochlea basiert und mit einer drastischen PMCA-Reduzierung und anschließendem Absterben der Zellen einhergeht. Zusammengefasst belegen die Befunde die Bedeutung von Nptn für die Stabilisierung von PMCAs, illustrieren aber auch eine erhöhte Komplexität durch die partielle Redundanz mit Basigin. Während Nptn-Defizienz im Zentralnervensystem unterschieliche Auswirkungen auf die PMCA-Expression hat, führt der Verlust in der Cochlea zu gravierender Degeneration der Haarzellen und verursacht so Taubheit.

Contents

1 Introduction

1.1 Calcium function in the nervous system

Ionic calcium, Ca^{2+}, serves as a universal second messenger in all cell types. Indeed, it has been implicated in a variety of cellular processes and pathways including gene expression, regulation of enzymatic activities, cell motility, neurite elongation, neuronal growth and neurotransmission (Berridge *et al.,* 2000, Carafoli *et al.,* 2001, Clapham 2007, Lisek *et al.,* 2018). Given such versatility, proper control of intracellular Ca^{2+} concentration is as important as demanding and involves several proteins that control Ca^{2+} flux across various cellular compartment boundaries (Fig.1). At resting state, the concentration of free Ca^{2+} ($[Ca^{2+}]_i$) in the cytosol is typically in the range of only 50 to 100 nM, i.e. about 10.000 times less than in the extracellular space (~1 to 2 mM) and still some 10 to 1000 times less than in mitochondria and the endoplasmic reticulum (ER), respectively (Fig.1). The influx of Ca^{2+} through ion channels from outside the cell or from intracellular compartments into the cytosol is thus strongly promoted by a steep gradient, whereas the clearance of Ca^{2+} from the cytoplasm requires the energy-consuming activity of membrane-resident transporters (Brini *et al.,* 2013, Lisek *et al.,* 2018). To allow for various cellular Ca^{2+} responses, the regulation of Ca^{2+} levels needs to be spatially and temporally precise and adjustable over a wide dynamic range (Augustine *et al.,* 2003). For example, Ca^{2+} entering through voltage-dependent calcium channels (VDCCs) at presynaptic active zones (AZs) triggers the release of synaptic vesicles within microseconds and remains restricted to a domain of a few hundred nanometers (Gundelfinger and Fejtova 2012, Neher and Sakaba 2008, Nishimune *et al.,* 2012). On the other hand, some Ca^{2+}-dependent cellular functions such as discrete transcriptional activities are operated based on Ca^{2+} oscillations that may last for minutes and may be propagated within a cell (Sneyd *et al.,* 2017). In neurons, Ca^{2+} plays a pivotal role in signal transduction associated with synaptic plasticity, including both long term plasticity for both potentiation (LTP) and depression (LTD), which in turn are crucial for learning and memory (Evans and

Blackwell 2015). Furthermore, disturbances of Ca^{2+} homeostasis have been correlated with amyotrophic lateral sclerosis ALS (von Lewinski and Keller 2005), Huntington's disease (Zuccato *et al.,* 2010), Alzheimer's disease (Dreses-Werringloer *et al.,* 2008, Stutzmann *et al.,* 2006), Parkinson's disease (Gandhi *et al.,* 2009, Surmeier and Schumacker 2013) and also with Ataxias (Airaksinen *et al.,* 1997, Liu *et al.,* 2009).

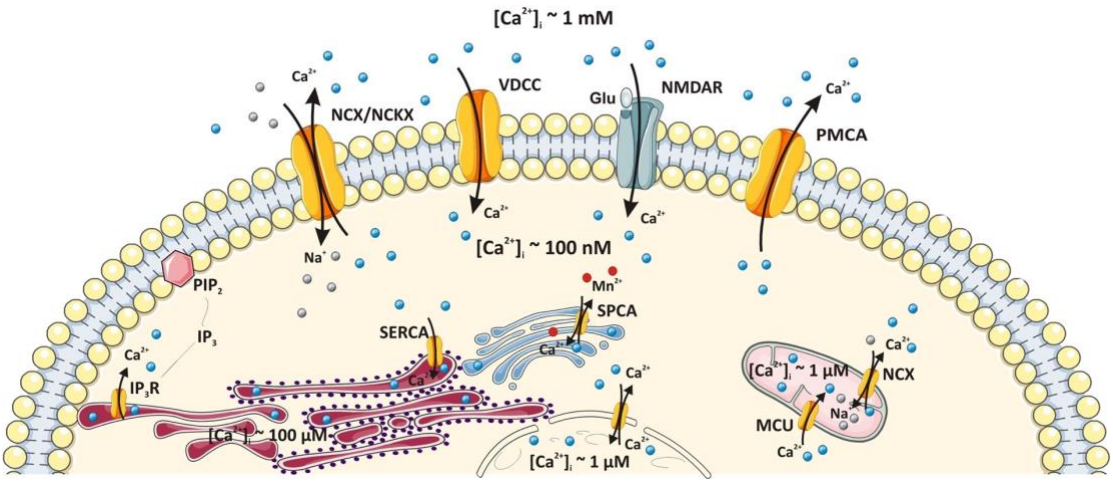

Fig.1. The schematic representation of Ca^{2+} homeostasis in neurons.

Ca^{2+} regulation involves Ca^{2+} influx through voltage-dependent and ionotropic channels (VDCCs, NMDARs) and extrusion across the plasma membrane by pumps (PMCA) or exchangers (NCX/NCKX). Intracellular compartments contribute by sequestration and release of Ca^{2+}.

Abbreviations: IP_3R, inositol 1,4,5-trisphosphate receptor; SERCA, sarco/endoplasmic reticulum Ca^{2+} ATPase; PIP_2, phosphatidylinositoln4,5-bisphosphate; NCX/NCKX, sodium calcium (Na^+/Ca^{2+}) exchanger/sodium calcium potassium exchanger (Na^+/Ca^{2+}-K^+); VDCC, voltage dependent Ca^{2+} channel; SPCA, secretory pathway Ca^{2+} ATPase; NMDAR, N-methyl-D-aspartate receptor; Glu, glutamate; PMCA, plasma membrane Ca^{2+} ATPase; MCU, mitochondrial Ca^{2+} uniporter. Image was taken from Lisek M, et al. (2018)

The principal molecular players and mechanisms of Ca^{2+} homeostasis are known for long time and have been investigated in both normal and neuropathogical brains (Brini *et al.,* 2014, DeCoster 1995), Next to soluble Ca^{2+} buffers, two families of transport proteins in the plasma membrane have emerged as particularly relevant for Ca^{2+} homeostasis in neurons. Na^+/Ca^{2+} - exchangers (NCX, NCKX) exploit the Na^+ gradient to extrude Ca^{2+}, whereas plasma membrane ATPases (PMCAs) use ATP hydrolysis

to pump Ca^{2+} out of cells. NCX have lower affinity for Ca^{2+} but higher transport capacitiy than PMCAs (Regehr, 1997). The relative contribution of NCX/NCKX and PMCAs to the extrusion of Ca^{2+} varies between cell types and even between different types of neurons (Blaustein *et al.,* 2002, Brini and Carafoli 2011, DiPolo and Beauge 1983)

1.2 Plasma membrane Ca^{2+} ATPase and Ca^{2+} homeostasis

PMCA was first identified in erythrocytes (Schatzmann 1966) and classified as a member of P-type pump family which extrudes Ca^{2+} out of the cell against a steep gradient at a 1:1 Ca^{2+} /ATP ratio (Niggli *et al.,* 1981). PMCA contains 10 transmembrane domains (TMDs), and both the N- and C-terminus face the cytoplasm (Fig. 2). Two larger cytosolic loops are formed between TMDs 2 and 3 and between TMDs 4 and 5, respectively. The former contains a site that is important for pump activation by acidic phospholipids. The second loop harbors the catalytic center including an ATP binding site and a crucial aspartate residue that is phosphorylated to yield an intermediate state in the catalytic cycle of the enzyme. Sequences in both loops have been implicated in the autoinhibition through an intramolecular interaction with a Ca^{2+}/calmodulin binding region in the C-terminal tail (Lopreiato *et al.,* 2014). The pump will be released from autoinhibition once Ca^{2+}/calmodulin binds to the calmodulin binding site. As deduced from studies on other P-type ATPases (mostly Sarco-endoplasmic calcium ATPase, SERCA), pump activity involves stepwise conformational changes. In brief, following displacement of the autoinhibitory segment from the core enzyme, cytosolic Ca^{2+} binds with high affinity to an intramembraneous pocket of the enzyme (E1-ATP state) and following intermediate states it will be replaced by $H^{+,}$ when the pump opens towards the extracellular space (E2P-open state) (Brini *et al.,* 2017, Bublitz *et al.,* 2011) (Fig.2). In addition to the generic regulation by Ca^{2+}/CaM and the aforementioned activation through phospholipids, various other modes of regulation have been found to affect the activity of PMCAs, but often in an isoform- or even splice variant-specific manner. The effect of phosphorylation by PKC,

for instance, was shown to affect the different family members in different ways, depending on their cytoplasmic tail sequences (Brini *et al.,* 2017).

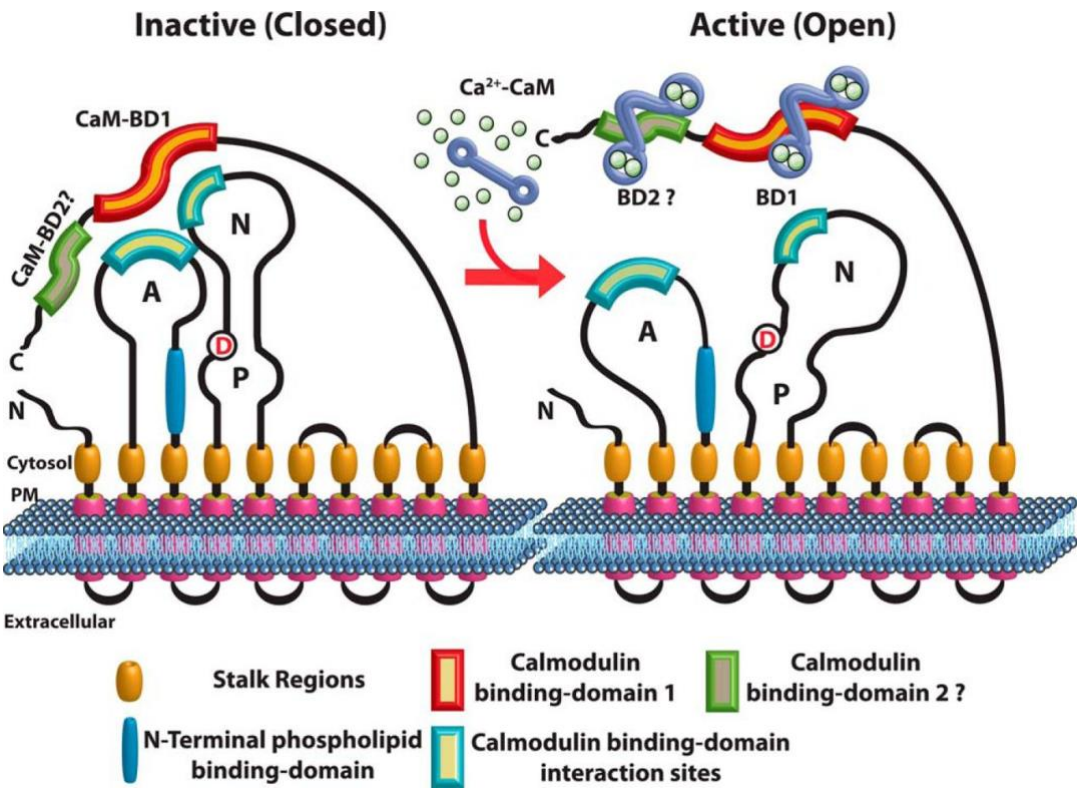

Fig.2. Topology of inactive and active PMCA.

The pump has 10 transmembrane domains depicted as red boxes (domain 1 to 10 is from left to right side). The cytosolic part contains two large loops with actuator (A), phosphorylation (P) and nucleotide-binding (N) domains. ATP-dependent phosphorylation of a catalytic aspartate residue (D) in P, which is blocked by binding of the cytoplasmic tail to A and N (left), occurs when binding of Ca^{2+}/CaM-triggered to the cytoplasmic tail releases this autoinhibition (right). Studies on the PMCA in *Arabidopsis thaliana* (Tidow *et al.,* 2012) suggest the existence of two binding sites with different affinities for Ca^{2+}/CaM (CaM-BD1, -BD2). Image was taken from Lopreiato R, et al. (2014).

In vertebrates, four PMCA isoforms (PMCA1-4), each encoded by a different gene, were identified. The various PMCA isoforms display remarkable differences with respect to their kinetics. PMCA2 and 3 emerged as relatively fast acting pumps whereas PMCA1 and PMCA4 displayed lower Ca^{2+} extrusion rates (Caride *et al.,* 2001). In addition, alternative splicing gives rise to several variants of each of the isoforms, affecting the first cytoplasmic loop and the C-terminal tail. The latter results

in two principal variants, "a" and "b". Only the b-variants harbor a C-terminal motif, which can mediate binding to PDZ domains in scaffold proteins such as PSD-95 and its paralogs (DeMarco and Strehler 2001, Kim *et al.,* 1998) or NHERF (Padanyi *et al.,* 2010), a two PDZ domain protein. This type of interaction may link PMCAs indirectly to other PDZ binding proteins. The a-variants show reduced affinity for Ca^{2+}/CaM, but for PMCA2 it has been demonstrated that the a-variant displays higher Ca^{2+} extrusion rates than the respective b-variant (Caride *et al.,* 2001, Jensen *et al.,* 2007). The impact of splice variation in the first intracellular loop is less well studied, but it has been suggested that it may affect the targeting of PMCAs to subregions of the plasma membrane, their activation by phospholipids or the autoinhibition (Chicka and Strehler 2003). The variability of physiological properties of the PMCAs and their splice variants is paralleled by distinct patterns of expression: PMCA1 and PMCA4 are expressed in virtually all tissues, whereas PMCA2 and PMCA3 are predominantly expressed in the nervous system and in some non-neuronal but excitable cells. (Burette *et al.,* 2003, Strehler *et al.,* 2007a, Strehler *et al.,* 2007b). In line with their differential expression, the various PMCA isoforms also display remarkable differences with respect to their kinetics. PMCA2 and 3 emerged as relatively fast acting pumps whereas PMCA4 is the slowest isoform (Caride *et al.,* 2001).

1.3 PMCA in neuronal plasticity

Given the principal role of PMCA isoforms in Ca^{2+} homeostasis one may expect that these enzymes are involved in the regulation of synaptic function and neuronal excitability. There are, however, relatively few studies implicating PMCAs in specific forms of neuronal plasticity. Studies on PMCA2-knockout mice revealed enhanced paired-pulse facilitation, i.e. altered presynaptic short- term plasticity at cerebellar synapses (Jensen *et al.,* 2007). Increased PMCA activity, in turn, has also been linked to altered plasticity. Pharmacological inhibition of PMCAs allowed to induce LTP in otherwise reluctant CA2 hippocampal neurons (Simons *et al.,* 2009) and induction of presynaptic homeostatic plasticity was found to be accompanied by reduction of the

highly active PMCA variant 2a in CA3 hippocampal neurons (Jensen *et al.,* 2009). Likewise, PMCA inactivation has been shown to contribute to spike-timing dependent plasticity (Scheuss *et al.,* 2006). On axons, downregulation of PMCA may be involved in reducing the excitability of sensory neurons (Gomez-Varela *et al.,* 2012). The redundancy among PMCA isoforms, the wide-spread expression of PMCAs across cell types but also along various subcompartments of neuronal plasma membranes as well as limited efficiency of pharmacological drugs makes it difficult to approach specific PMCA functions.

1.4 Neuroplastin as a prominent interaction partner of PMCAs

Only few proteins have been identified that can bind to all PMCA paralogs, including PSD-95-like scaffold molecules and Ca^{2+}/calmodulin (Caride *et al.,* 2007, DeMarco and Strehler 2001, Kim *et al.,* 1998). Several other binding partners, such as the signaling molecule 14-3-3e (Rimessi *et al.,* 2005), the scaffold molecule Homer 2 (Yang *et al.,* 2014) or the PDZ domain proteins NHERF2 (Padanyi *et al.,* 2010), CLP36 (Bozulic *et al.,* 2007) or CASK (Schuh *et al.,* 2003) have been assorted to individual isoforms and/or discrete, non-neuronal tissues only. They all bind to the cytoplasmic part of PMCAs and have been proposed to contribute to the membrane targeting and/or Ca^{2+} extrusion function of the pumps (Di Leva *et al.,* 2008, Kruger *et al.,* 2010). A proteomic analysis conducted by Dr. Karl-Heinz Smalla, Dr. Patricia Klemmer (LIN, Magdeburg) and Dr. Thilo Kähne (Institute of Experimental Internal Medicine, OvGU) aimed at identifying synaptic partners of Neuroplastin (Nptn), a putative cell adhesion molecule (CAM), disclosed all PMCA paralogs as tight interaction partners (Fig.3). In fact, the PMCAs emerged as the only high-score interaction partners when digitonin (rather than other detergents such as Triton or NP40) was used as a detergent to dissolve synaptic membrane fractions prior to immunoprecipitation with an antibody against Neuroplastin (Fig.3) (Leistner, 2016). This finding suggested a very close, if not direct interaction between PMCAs and Nptn. This hypothesis was further corroborated in the course of this work but also in parallel studies performed in central

neurons and immune cells (Gong *et al.,* 2018, Herrera-Molina *et al.,* 2017, Korthals *et al.,* 2017, Schmidt *et al.,* 2017). Moreover, Basigin, a paralog of Nptn, was found in association with PMCA4 in T cells (Supper *et al.,* 2016).

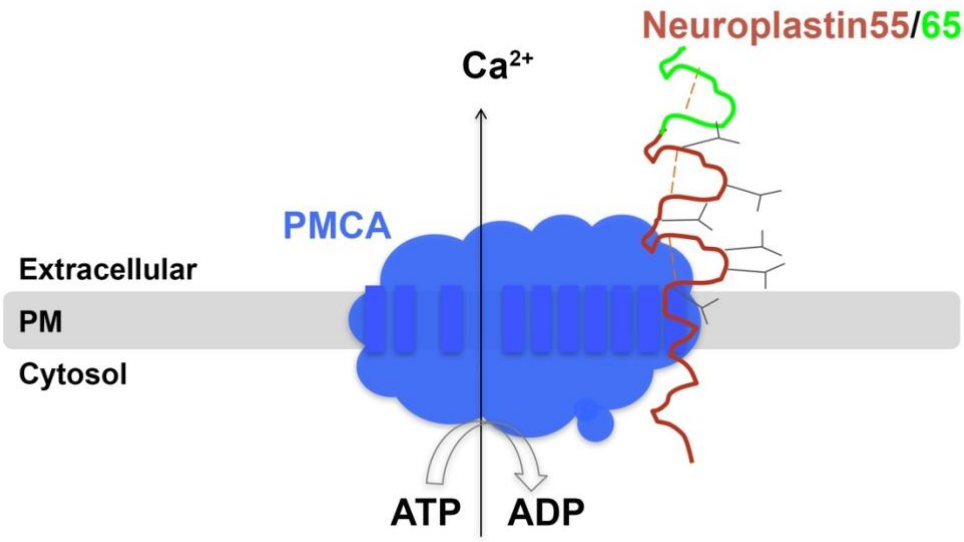

Fig.3. Interaction between Neuroplastin and PMCA.

The PMCA is depicted in blue. The single-pass membrane protein Nptn has two Ig domains in its short variant (Np55) and an additional Ig domain (green) in its long form Np65. The Ig domains 2 and 3 carry six N-glycosylation sites. Recent data from Gong et al. (2018) show that TMDs 9 and 10 and the TMD of Nptn are closely involved in the interaction.

1.5 Structure, expression and subcellular localization of Nptn

Neuroplastin (Nptn) was first identified as a pair of glycoproteins from rat brain synaptic membrane fractions (Hill *et al.,* 1988, Willmott *et al.,* 1992) with apparent molecular weights of 65 and 55 kDa (referred to as Np65 and Np55, respectively). Both forms are encoded by one single gene. After alternative splicing, the single transmembrane-spanning proteins with three (Np65) or two (Np55) immunoglobulin–like (Ig) domains (Figs. 3 and 4). In fact, Np65 and Np55 are identical except for the first, i.e. outer Ig-domain (Ig1) of Np65. Importantly, in contrast to the Ig domains common to both variants (Ig2 and 3), the Np65-specific Ig1 domain was found to mediate homophilic adhesion (Owczarek *et al.,* 2011, Smalla *et al.,* 2000). Alternative splicing may also

affect the short cytoplasmic tail in both Np55 and Np65, leading to variants that either come with a 4 aa acidic Asp-Asp-Glu-Pro (DDEP) insert or without it (Np55/65 versus Np55/65$^{\Delta DDEP}$) (Kreutz *et al.,* 2001, Langnaese *et al.,* 1997). N-glycosylation sites are located on the Ig2 and Ig 3 domains (Figs. 3 and 4) and *in vitro* deglycosylation shifted the apparent molecular weights down to 40 and 28 kDa for Np65 and Np55, respectively.

Different glycoforms of Np55 were identified in many tissues (Langnaese *et al.,* 1997, Langnaese *et al.,* 1998). Np65, in contrast, is mainly expressed in the brain. Np55 and Np65 also display differential expression within the brain. Np65 is highly expressed in the cortex, hippocampus and striatum as part of the forebrain. It is expressed at lower level in the midbrain, e.g. in the thalamus and hypothalamus, and is hardly detectable in the brainstem as well as in peripheral nerves (Hill *et al.,* 1988, Marzban *et al.,* 2003, Smalla *et al.,* 2000). Np55 is detectable in nearly all brain areas and it is the major isoform in mouse cerebellum where it is also found at the synapses of Purkinje cells (Marzban *et al.,* 2003). Both variants are predominantly localized to the plasma membrane of neurons and are found in both synaptic and extrasynaptic membrane areas. Moreover, both Np55 and Np65 can be found at excitatory and inhibitory synapses (Herrera-Molina *et al.,* 2014). Of note, neither Np55 nor Np65 has been reported to be expressed in glia. Nptn shows striking similarity to Basigin (also known as CD147 or EMMPRIN), and, to a lesser extent, to Embigin (also known as gp70). While the three proteins form a subfamily of Ig domain proteins they share highest homology in their transmembrane domains (Fig.4) (Beesley *et al.,* 2014). Basigin has not been found to be a synaptic component in the central mammalian brain and very little is known about putative roles in neurons.

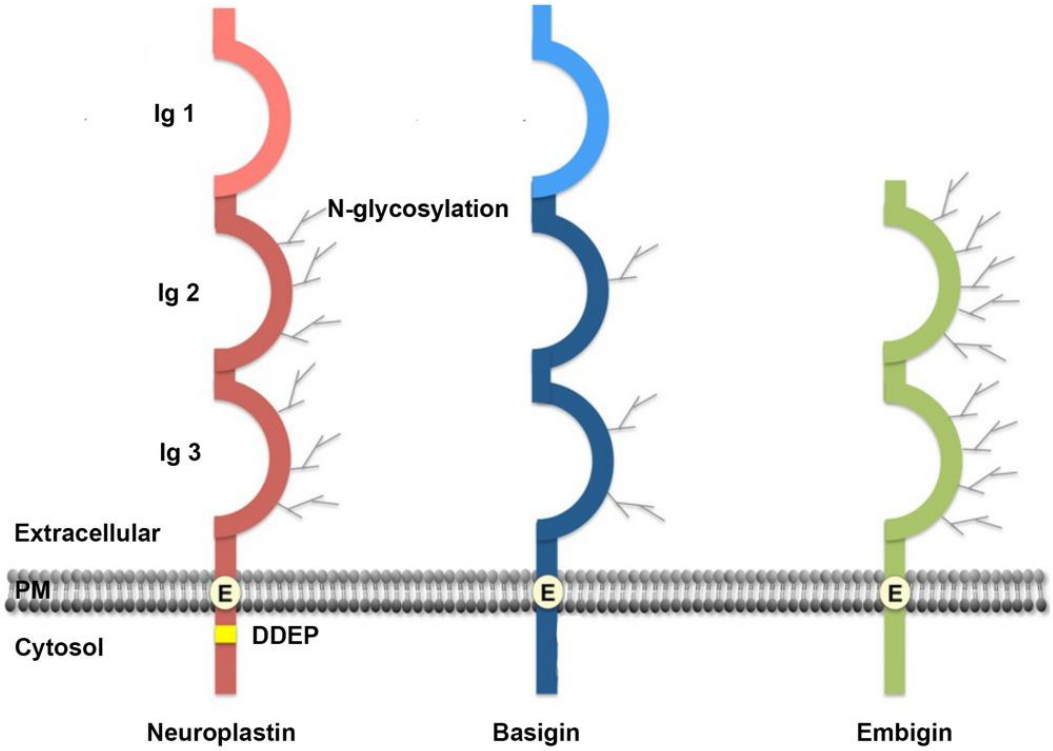

Fig.4. Structure of basigin family members: Neuroplastin, Basigin and Embigin.

All members are single membrane-spanning protein, which typically contain at least two Ig domains carrying N-glycosylation sites. An additional, N-terminal Ig domain (Ig1) is present in the Nptn splice variant Np65 and the Basigin splice variant Bsg-1, which are abundant in brain and the retina, respectively. Alternative splicing also leads to Nptn variants with or without a cytosolic DDEP sequence. The TMDs are highly conserved and include a central glutamate (E) residue (Beesley *et al.,* 2014).

1.6 Neuroplastin as a determinant for synaptic plasticity and memory

The interaction between Nptn and PMCAs gained particular interest, as previous and ongoing studies pointed (a) to a pivotal role of Nptn for the maintenance of LTP in rat brain slices (Smalla *et al.,* 2000) and (b) to a crucial requirement of Nptn for associative memory in mice (Bhattacharya *et al.,* 2017). Np65 significantly enriches in the PSD fraction of CA1 synapses after induction of long-term potentiation (LTP), and the maintenance of LTP was blocked when treated with Np65-specific or pan-Nptn antibodies or by applying a fusion protein comprising all 3 Ig domains of Nptn (Smalla

et al., 2000). These findings implied an involvement of Nptn, in particular of Np65, in long-term synaptic plasticity. Consistent with this idea, Li et al. (2019) reported impaired maintenance of LTP in the CA1 region of mice specifically lacking Np65 (Li *et al.,* 2019). Moreover, behavorial analyses revealed that constitutive $Nptn^{-/-}$ mice (i.e. both Np55 and Np65 deleted) not only display less anxious behavior, altered social interaction and impaired sensorimotor capabilities but also loss of fear-conditioned associative learning as monitored in a two-way active avoidance shuttle box paradigm (Bhattacharya *et al.,* 2017) and deletion of Nptn in glutamatergic neurons, as achieved by using conditional mutants, revealed that Nptn is not essential for associative learning in the same paradigm (Herrera-Molina *et al.,* 2017). Most interestingly, complete retrograde amnesia was observed two months after induction of a pan-neuronal deletion of Nptn by tamoxifen injection into conditional knockout mice expressing CreERT under the control of the PrP promoter ($Nptn^{lox/loxPrpCreERT}$) (Bhattacharya *et al.,* 2017, Weber *et al.,* 2001). An obvious question was, whether the interaction between Nptn and PMCA adds to the role of Nptn in learning and memory. A first assessment by western blot analysis showed a reduction of PMCAs in mouse brain in the absence of Nptn (Bhattacharya *et al.,* 2017). In line with reduced PMCA levels, depletion of Nptn leads to increased free cytosolic calcium ($[Ca^{2+}]_i$) and delayed post-stimulatory Ca^{2+} clearance in neurons and also other cell types (Herrera-Molina *et al.,* 2017, Korthals *et al.,* 2017, Schmidt *et al.,* 2017). Nptn, however, was also reported to interact with other proteins and, as mentioned above, there is ample evidence that Np65 acts as a homophilic, synaptic CAM. In fact, quantitative analyses revealed mismatching of pre- and postsynapses in cultured primary hippocampal neurons that were either Nptn-deficient or treated with a fusion protein to specifically interfere with the Ig1 domain of Np65 (Herrera-Molina *et al.,* 2014). A similar phenotype was observed within synaptic areas of inner hair cells of the cochlea of Nptn-mutant mice (Carrott *et al.,* 2016). Moreover, Nptn was recently shown to promote spinogenesis through its cytoplasmic binding partner TRAF6 (Vemula *et al.,* 2020). Thus, both PMCA-related changes in neuronal Ca^{2+} homeostasis and synaptogenic and adhesion deficits might add to the observed learning and memory phenotypes.

Previously reported interaction partners of Nptn also include the fibroblast growth factor FGFR1, subunits of the $GABA_A$ receptor and the monocarboxylate transporter MCT2 (Owczarek *et al.,* 2010, Sarto-Jackson *et al.,* 2012, Wilson *et al.,* 2013). These interactions might add to inhibitory transmission, energy metabolism and neurite outgrowth, respectively, but the actual impact of Nptn onto these functions in neurons has remained poorly characterized.

Behavorial studies of Np65-specific KO mice as well as single nucleotide polymorphisms in non-coding regions linked to the NPTN gene in humans point to Nptn as a candidate gene for anxiety, schizophrenia and reduced cognitive capabilities. Suggested cellular correlates include reduced neurogenesis and an imbalance between inhibitory and excitatory synapses (Amuti *et al.,* 2016, Desrivieres *et al.,* 2015, Herrera-Molina *et al.,* 2014, Saito *et al.,* 2007). To what extent altered PMCA levels relate to the respective phenotypes or disorders remains elusive.

1.7 Nptn is crucial for hearing

A profound impairment of hearing was deduced for $Nptn^{-/-}$ mice from reduced prepulse inhibition of the so-called startle response (Bhattacharya *et al.,* 2017). Moreover, two independent screens for mouse mutants with severe hearing deficits found Nptn as an essential factor for auditory function (Carrott *et al.,* 2016, Zeng *et al.,* 2016). Both studies focussed on the role of Nptn in the cochlea.

In brief, the mammalian inner ear is formed by the cochlear and vestibular system. The vestibular system is a complex structure required for proprioception and body balance (Casale *et al.,* 2020). Auditory signals are transducted in the cochlea (Fig. 5 A), which harbors the organ of Corti, where inner and outer hair cells (IHCs, OHCs; Fig. 5B) are regularly arranged in one and three rows, respectively, and are surrounded by supporting cells (Fig. 5A). The stereociliar bundles of the hair cells convert sound-evoked mechanical stimuli into electrical signals, which are eventually relayed *via* synapses to the central nervous system (CNS). (Driver and Kelley 2020, Hudspeth 2008). The IHCs signal *via* their ribbon-type synapses to the afferent nerve fibers. The

OHCs amplify and sharpen incoming signals, transmitted by the tectorial membrane, which is a specialized structure of the extracellular matrix (Moser and Starr 2016, Ren and Gillespie 2007). In the studies by Carrott et al., evidence was provided that loss of Np65 at synapses between inner hair cells (IHCs) and afferent fibers (Fig. 5) leads to mismatching of the pre- and postsynaptic compartments and to reduced glutamate release and thus to impaired transmission to the CNS (Carrott *et al.,* 2016). In striking contrast, a role for Np65 in hair cells was largely ruled out in the another study (Zeng *et al.,* 2016). This report showed that loss of Np55 interferes with the coupling of the tectorial membrane to the stereocilia of the OHCs and thus with cochlear amplification. Moreover, an additional role for Np55 downstream from the mechanoelectrical transduction was postulated. The reason for the partial differences between the two studies remained unclear, though unspecific antibody labeling of Np65 was considered (Zeng *et al.,* 2016). Also, it can not be formally ruled out, that the alleles that were used in either study might still give raise to truncated or instable products with residual or even dominant-negative function. Of note, neither study addressed possible effects of Nptn deficiency on calcium homeostasis or PMCA.

Ca^{2+} signaling, however, plays a pivotal role in the hair cells. Ca^{2+} enters into hair cells through both mechano-electrical transduction channels (MET) and voltage-dependent Ca^{2+} channels, whereas Ca^{2+} extrusion is achieved mainly if not exclusively by PMCAs (Fettiplace and Nam 2019, Mammano 2011). The balance between Ca^{2+} influx through METs within the stereocilia of OHCs and its extrusion back into the endolymph by the highly active isoform PMCA2a is highly important as indicated by analyses on a number of missense mutations in both human and murine PMCA2 that lead to deafness (Bortolozzi and Mammano 2018, Preiano *et al.,* 1996, Schultz *et al.,* 2005, Spiden *et al.,* 2008). In contrast to OHCs, IHCs mainly express PMCA1, which is not enriched in stereocilia (Fig. 5). Given the tight interaction between PMCAs and Nptn, it is conceivable that disturbed control of cytosolic Ca^{2+} at least contributes to the hearing loss in Nptn mutant mice.

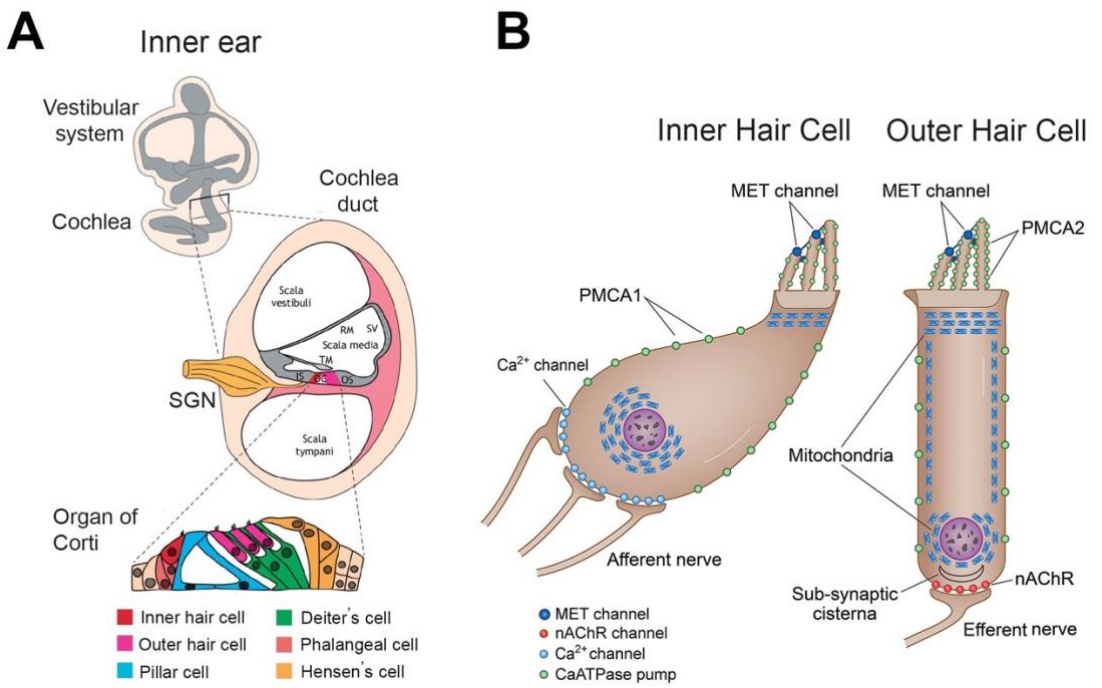

Fig.5. Cellular organization of the cochlea and Ca^{2+} flux in inner and outer hair cells.

(A) Inner ear structure consisting of the vestibular system and the cochlea. The cochlea duct includes the scala vestibuli, media and tympani. The scala media harbors the organ of Corti (OC), flanked by two areas of non-sensory cells, the outer and inner sulcus (OS and IS). The OC comprises outer and inner hair cells and different types of supporting cells (pillar cell, Deiter's cell, phalangeal cell and Hensen's cell). The hair cells have hair bundles which are in contact with the tectorial membrane (TM). The signals from the inner hair cells are projected to the CNS *via* bipolar neurons of the spiral ganglion (SG). (B) Inner and outer hair cells. Ca^{2+} (next to K^{+}) ions enter through mechano-electrical transduction (MET) channels in the hair bundles of both hair cell types, through voltage-dependent Ca^{2+} channels in the basolateral part of the hair cells (mainly IHCs and less so in OHCs) and also through nicotinic acetylcholine receptors (nAChR) stimulated by efferent fibers onto OHCs. Ca^{2+} is extruded from the stereocilia by PMCA2 which is particularly abundant in OHCs, PMCA1 extrudes Ca^{2+} mainly from the IHC soma (Driver and Kelley 2020, Fettiplace and Nam 2019).

2 Hypothesis and Research Goals

This thesis is based on the recent finding that Nptn binds all mammalian PMCA isoforms. Nptn knockout mutants are viable but suffer from hearing loss and display striking learning and memory deficits. These phenotypes would be consistent with impaired PMCA-related disturbance of neuronal Ca^{2+} homeostasis. The main hypothesis of my thesis is therefore: *"Loss of Nptn affects the four PMCA isoforms differently and/ or in a neuron type-dependent manner, thus causing phenotpyes of different severity".* Nptn-mutant mice, primary neuronal cultures and cell lines will be used in combination with molecular, biochemical, Ca^{2+} imaging and immunofluorescent approaches to further elaborate on this hypothesis. Specifically, the following goals will be addressed:

Goal 1: Characterization of the expression of the PMCA paralogs and of Basigin in brains from wild type and different Nptn mutant mice. Quantitative analyses will reveal if PMCA isoforms are affected differently in different brain areas and neuron subtypes; with regard to synaptic versus overall cellular abundance; and when Nptn is constitutively absent or lost after induction. Basigin expression will be quantified as a putative resource for compensation of loss of Nptn. These analyses shall provide insights on the prospective resistance or vulnerability of PMCA-based Ca^{2+} homeostasis to loss of Nptn in various brain areas.

Goal 2: Comparative evaluation of Nptn, Basigin and variants thereof for their capability to bind and stabilize PMCA isoforms and thus to modulate the function of PMCA. A structure-function analysis will be conducted to define subregions in Nptn that promote the stability and surface expression of various PMCAs. Basigin will be included for comparison. Complementing results from goal 1, this part may uncover possible redundancies and isoform-specific features among PMCAs and Nptn/Basigin, respectively.

Goal 3: Validation and characterization of PMCA-related deafness in Nptn$^{-/-}$ mice.

Hearing loss is a hallmark of Nptn mutants but the underlying cellular and molecular mechanisms are controversial and will thus be re-addressed on the basis of constitutive and conditional Nptn null mutants. The putative involvement of reduced PMCA will be evaluated for the first time. The results will broaden the understanding of the auditory phenotype with impact for the validation and interpretation of previously reported amnesia in inducible Nptn mutants.

3 Materials and Methods

3.1 Material

All the employed chemicals, medias, buffers, assays, antibodies and kits applied in this research are listed below.

3.1.1 Commonly used buffers and solutions

Buffers/ Solutions	Composition /Company
10x PBS	1.37 M NaCl, 2.7 M KCl, 14 mM KH_2PO_4, 43 mM Na_2HPO_4, pH 7.2.
2x SDS Loading buffer	125 mM Tris-HCl, pH 6.8, 4% SDS, 20% glycerin, 0.2% bromophenol blue, 10% β-mercaptoethanol.
10x electrophoresis buffer	Bio-Rad (161-0772)
Stripping buffer	Thermoscientific (21059)
10x Blotting buffer	0.25 M Tris-base, 1.92 M glycine, 0.2% SDS (Supplemented with 15% methanol in 1X buffer)
Ponceau S	0.5% Ponceau S, 3% TCA.
10x TBS	200 mM Tris-HCl, 1.5 M NaCl, pH 7.5 (Supplemented with 0.5% Tween 20 in 1X buffer)
4% PFA	Paraformaldehyde dissolved into 1x PBS

3.1.2 Pharmacological agents and reagents

Pharmacological agents/reagents	Company	Cat. No.
D-AP5	TOCRIS	#0106

Tetrodotoxin citrate	TOCRIS	#1069
CNQX disodium salt	TOCRIS	#1045
5(6)-Carboxyeosin	Marker Gene	#M1300
Lipofectamine® 2000	Thermo Scientific	#11668019
Digitonin	SIGMA	#D141

3.1.3 Antibodies

Antibody	Species	Cat. No./Company
anti-Nptn	Sheep	AF7818 R&D
anti-Np65	goat	AF5360 R&D
anti-PanPMCA (5F10)	Mouse	#Ab2825 Abcam
anti-PMCA1	Rabbit	#Ab3528 Abcam
anti-PMCA2	Rabbit	#Ab3529 Abcam
anti-PMCA3	Rabbit	#Ab3530 Abcam
anti-PMCA4	Mouse	#Ab2783 Abcam
anti-β-III-Tubulin	Rabbit	#302 302 SYSY
anti-β-Actin	Mouse	#A5441Thermo Fisher
anti-Basigin	Goat	AF772 R&D
anti-GFP	Mouse	11814460001 Sigma
anti-tRFP	Rabbit	#AB233 Evrogen
anti-Myosin7a	Rabbit	#PTS-25-6790-C050 BD Bioscience
anti-Parvalbumin	mouse	#235 Swant
anti-Calbindin	mouse	#300 Swant
anti-Amphiphysin	Rabbit	#Ab244375 Abcam
anti-BIN1	Rabbit	#51844 CST
anti-EAAT1	Rabbit	#250103 SYSY
anti-PSD95	Rabbit	#342403 SYSY

anti-Vglut 1	Mouse	#135011 SYSY
anti-Vglut 2	Mouse	#135411 SYSY
anti-SNAP25	Rabbit	#111002 SYSY

3.1.4 Commonly used Kits

Kit	Company
uMACS GFP Isolation Kit	uMACS (#130-091-125)
NucleoBond® Xtra Midi EF Kit	Macherry-Nagel
NucleoSpin Gel and PCR clean-up Kit	Macherry-Nagel
BC assay protein quantification Kit	Interchim (#UP40840A)
Cold Fusion™ Cloning Kit	System Biosciences
Chemiluminescent HRP Substrate	Millipore (#WBKLS0500)

3.1.5 Primers used in this research

Construct		Primer sequence
rNp55-RFPT	F	5'-ACTCTAGAGGATCCAGGATGTCGGGCTCGTCGCT-3'
	R	5'-TTCTAGGTCTCGAGTTACTTGTACAGCTCGTCCA-3'
rNp55(TMD)-RFPT	F	5'-TTTATTTTCTGTATCTGCAAGAGGAAGAGGCCAGAT-3'
	R	5'-CCCACTATGAGATAGAGGTGGCTCCGTACCCTGAG-3'
rNp55(ΔCyt)-RFPT	F	5'-TGTTGTGTATGAGAAGCTCGAGATGGTGTCTAAGG-3'
	R	5'-CCTTAGACACCATCTCGAGCTTCTCATACACAACA-3'
rNp55(ΔCytRKR)-RFPT	F	5'-GAGAAGAGGAAGAGGCTCGAGATGGTGTCTAAGGG-3'
	R	5'-CCCTTAGACACCATCTCGAGCCTCTTCCTCTTCTC-3'
rNp55(E232V)-RFPT	F	5'-CTTGGGAATTCTGGCTGTAATCATCATCC-3'
	R	5'-GGATGATGATTACAGCCAGAATTCCCAAG-3'
rNp55(E242A)-RFPT	F	5'-CATTGTTGTGTATGCGAAGAGGAAGAGGC-3'
	R	5'-GCCTCTTCCTCTTCGCATACACAACAATG-3'

rNp55(P255G)-RFPT	F	5'-CTTGCCCCACTTTGGGGTTTCTTGGGAATTCTGGCT-3'
	R	5'-AGCCAGAATTCCCAAGAAACCCCAAAGTGGGGCAAG-3'
rNp55(FL226_7VV)-RFPT	F	5'-GCCCCACTTTGGCCTGTCGTGGGAATTCTGGCTGAA-3'
	R	5'-TTCAGCCAGAATTCCCACGACAGGCCAAAGTGGGGC-3'
rNp55(A231L)-RFPT	F	5'-CCTTTCTTGGGAATTCTGCTTGAAATCATCATCCTT-3'
	R	5'-AAGGATGATGATTTCAAGCAGAATTCCCAAGAAAGG-3'
GCamP5	F	5'-GTTCCTATAGGATCCGGCGCCACC-3'
	R	5'-CCGGATCCTATAGGAACCTTGTACAGCTCGTCCATG-3'
RFPT-GCaMP5	F	5'-ACTCTAGAGGATCCAGGATGGTGTCTAAGGGCGA-3'
	R	5'-CATGTTTTTCTAGGTCTCGAGTCACTTCGCTGTCATC-3'
mBasigin (TMD)-RFPT	F	5'-TTTATTTTCTGTATCTGCAAGAGGCGGAAGCCAGACC-3'
	R	5'-CCCACTATGAGATAGCGGCTCCGCACACGCAGTGA-3'
mBasigin(ΔCytRRK)-RFPT	F	5'-GAGAAGAGGCGGAAGGCTAGCATGGTGTCTAAGGG-3'
	R	5'-CCCTTAGACACCATGCTAGCCTTCCGCCTCTTCTC-3'

3.1.6 Animals

Neuroplastin complete knockout mice $Nptn^{-/-}$ ($Nptn^{tm1.2Mtg}$) and floxed $Nptn^{lox/lox}$ mice with neuron-specific inducible PrCreERT ($Nptn^{lox/loxPrCreERT}$) or with permanent loss of neuroplastin in glutamatergic specific neurons ($Nptn^{lox/loxEmx1Cre}$) were described in previous papers (Bhattacharya *et al.,* 2017, Herrera-Molina *et al.,* 2017). PMCA4 deficient mice $PMCA4^{-/-}$ (Atp2b4, MMRRC stock #36807) and corresponding wild type controls were on a FVB/N background. In all experiments, adult (3 - 4 months old) mice were used, except when stated otherwise.

3.2 Molecular Methods

3.2.1 Polymerase Chain Reaction

10 µl 5x Phusion™ HF buffer (New England Biolabs, NEB), 10 ng template DNA, 20 pMol of each primer, 100 µM deoxynucleotide triphosphate (dNTP), 0.2 units of Phusion™ (NEB) and H_2O were added to final volume of 50 µl into a PCR tube on ice. All the DNA fragments were produced by PCR amplification with a program as below:

I	95°C	5'	Initial denaturation	
II	95°C	45"	Denaturation	
III	60°C	30"	Annealing	32-35 Cycles
IV	70°C	60"	Elongation	
V	72°C	10'	Final elongation	

The PCR products were separated by 1% agarose gel electrophoresis then cut out from the gel under the UV-light and purified using PCR clean-up kit.

3.2.2 Cold Fusion™-based cloning procedures

All cloning procedures were carried out in a ligation-free manner using the cold fusion kit according to the manufacturer's recommendation. For this, vector DNA and fragments shared overlapping sequences of at least 15 bp. 20-200 ng of linearized destination vector (FUGW vector was used in this work), 40-400 ng of PCR inserts, 2 µl of 5x cold master mix and H_2O added to a total volume of 10 µl, were incubated at room temperature and on ice for 5 min and 10 min, respectively. The cold fusion reactions were then transformed into XL10 GOLD E. coli competent cells.

Mutagenized Nptn constructs based on the lentiviral plasmid vector FUGW (addgene plasmid #14883) were generated combining PCR and cold fusion. In brief, overlapping PCR fragments carrying the desired mutation integrated into the primers (see 3.1.5)

were used to replace a wild type $Np55^{DDEP}$ sequence in previously generated FUGW constructs IH31 and IH22 (I. Herbert, U. Thomas), with TagRFPT- or EGFP sequences in frame with the end of the Np55 coding region. All constructs were sequence verified.

3.2.3 Bacterial Transformation

50 µl competent bacteria were added to cold fusion cloning mixtures (or plasmid DNA), followed by a 20 min incubation on ice and a heat shock at 42 °C for 50 seconds. After another 2 min on ice, 250 µl LB medium were added. After shaking for one hour at 37 °C with 400 RPM, 100 µl of the suspension was spread on pre-warmed agar plates containing proper antibiotics.

3.2.4 Plasmid DNA preparation

Single bacterial colonies were used to inoculate cultures in LB medium with corresponding antibiotic overnight. Then plasmid DNA was prepared by using the ® Xtra Midi EF Kit (Macherry-Nagel) according to the manufacturer's instructions.

3.2.5 Cell culture

Human embryonic kidney cells (HEK293-T) were originally purchased from Clontech. Cells were cultured in Dulbecco's modified eagle medium (DMEM) supplied with 10% fetal bovine serum (FBS), 1% penicillin and streptomycin and 1% L-glutamine at 37°C, 5% CO_2 in the incubator.

3.2.6 Hippocampal neurons

Rat hippocampal neurons were used as provided after preparation from 18 d rat embryos (E18) following published protocols (Herrera-Molina *et al.,* 2014). In brief, the cells had been trypsinized for 15 min at 37°C and after stopping trypsin activity with 1X horse serum in DMEM, the cells were dissociated into a single-cell suspension using a glass tube. 50,000 neurons in 1 ml medium per well were seeded in 12-well plates

with cover slips or 300,000 neurons in 2 ml medium per well in 6-well plates. After 1hr, the culture media were replaced with 1 ml or 2 ml Neurobasalmedium (1% B-27 Supplement, 1% Penicillin/streptomycin and 1% L-glutamine). At Day 7, 100 µl or 200 µl of complete medium was added to the cultures.

3.2.7 Transfection

All the cultures were transiently transfected with the plasmids (for 6 well plates, 1.5 µg DNA per well, for 12 well plates, 0.5 µg per well) mixed with Lipofectamine 2000 (#11668-019, Invitrogen) (for 6 wells, 3 µl per well, for 12 wells, 1 µl per well). For HEK cells, transfection was done 24 hours after seeding (for 6 well plates, 300,000 cells per well, for 12 well plates, 20,000 cells per well), and harvested for staining or Western blot analysis 48 hours after transfection. For neuronal cultures, transfection was done on Day 9, the Ca^{2+} imaging was performed on Day 14.

3.2.8 Synaptic junction preparation

The brain tissue was homogenized in a Beckman polycarbonate tube with buffer A (see below; 1 g brain tissue in 10 ml buffer) by using a potter S™ (Kaltenbach & Voigt, Biberach, Germany) at 900 rpm, 12 strokes. After transfer of the homogenate to a 1.5 ml Eppendorf tube, samples were centrifuged at 1000 g for 10 min. The supernatant was transferred to a new tube and centrifuged at 12,000 g for 20 min. The supernatant was carefully decanted and the pellet was resuspended in 1 mM Tris/HCl pH 8.1 with protease inhibitor (1 g pellet in 1.5 ml buffer), incubated for 30 min at 4 ℃ to induce a hypo-osmotic shock and then centrifuged at 32,000 g for 20 min. The pellet was re-homogenized in buffer B (see below). A sucrose density step gradient consisting of 1.0M/1.2M sucrose solution in 5 mM Tris/HCl pH 8.1 was prepared in Beckman ultracentrifuge tubes. 2.5 - 4 ml resuspended samples were loaded on top of the gradients. After spinning samples at 32,000 g for 2 h the synaptic junctions were collected from the 1.0M/1.2M sucrose interphase using a plastic Pasteur pipette. An equal amount of buffer B was mixed with the collected sample and the mixture

centrifuged at 35.000 g for 60 min. Synaptic junctions were in the pellet and ready for Western blot after solubilization with 2x SDS loading buffer.

500 mM HEPES	5.958 g HEPES, pH 7.4, 50 ml ddH_2O
500 mM Tris/HCl	6.057 g Tris, pH 8.1, 100 ml ddH_2O
2 M Sucrose	410,76 g Sucrose, 600 ml ddH_2O
Protease-Inhibitor Cocktail	1 per 50 ml buffer
Protein extraction buffer A	80 ml 2 M sucrose, 5 ml 5 mM HEPES, 415 ml ddH_2O
Protein extraction buffer B	32 ml 2 M sucrose, 2 ml 5 mM Tris/HCl, 166 ml ddH_2O
1.0 M Sucrose	50 ml 2 M sucrose, 1 ml 5 mM Tris/HCl, 49 ml ddH_2O
1.2 M Sucrose	60 ml 2 M sucrose, 1 ml 5 mM Tris/HCl, 39 ml ddH_2O

3.2.9 Measurement of protein concentration by Amido Black

200 µl Amido Black was added to 2µl test samples and incubated for at least 20 min at room temperature with shaking. Samples were then centrifuged at 14000 rpm at RT for 5 min, the pellet was resuspended in 1 ml wash solution, spun again and the procedure was repeated at least 3 times until the buffer appeared colorless. The last pellet was air-dried and dissolved in 300 µl 0.1 M NaOH and the OD was measured at 620 nm against 0.1 M NaOH.

Wash solution	900 ml methanol, 100 ml acetic acid
Amido Black	14.4 g Amido Black, 1 l wash solution

3.2.10 Co-immunoprecipitation

After transfection, HEK cells were incubated with with 100 µl lysis buffer (1% Triton X-100 or 1 % digitonin in 50 mM Tris/HCl, pH 8.0, protease inhibitor) for 10 min and then

the cell lysates were harvested using a scraper and transferred to 1.5 ml tubes. 10-20 µl of cell lysates were used as input control. The rest was incubated with anti-GFP antibody-coated magnetic beads at 4 ℃ for 2 h. The procedures were performed according to the manufacturer's instructions (µMACS GFP isolation kit). The eluted samples were boiled and were then ready for Western blot analysis.

3.2.11 Western blot

For HEK cells and neurons, the cells were harvested with lysis buffer (1% Triton X-100 in 50 mM Tris/HCl, pH 8.0 protease inhibitor), spun down at 12,000g for 20 min and the supernatant was used for analysis. For brain and cochlea lysates, tissues were homogenized in 50 mM Tris-HCl buffer (pH 8.0) with protease inhibitor cocktail. The samples were centrifuged at 1000 g for 10 min. The supernatant was collected and centrifuged again at 12,000 g for 20 min. The supernatant was carefully decanted and the pellet was resuspended in 1% Triton X-100 in 50 mM Tris/HCl, pH 8.0, including protease inhibitor. All samples were boiled with 2X SDS loading buffer for 5 min, separated by SDS polyacrylamide gel electrophoresis and then electrotransfered (Constant 200 mA for 90 mins) onto nitrocellulose membrane (Cytiva, Amersham™ Protran™ 0.45µm NC). After blocking with blocking buffer (5% non-fat milk in TBS containing 0.1% of Tween 20), blots were probed overnight at 4°C in fresh blocking buffer with primary antibodies overnight at the following concentrations: sheep anti-Nptn (pan-Np55/65; 1:5000), goat anti-Np65 (1:5000) , mouse anti-GFP (1:5000), rabbit anti-RFP (1:5000), mouse anti-PanPMCA (1:5000), rabbit anti-PMCA1/2/3 (1:5000), mouse anti-PMCA4 (1:5000), rabbit anti-β III-Tubulin (1:5000), mouse anti-β-Actin (1:5000), goat anti-Basigin (1:5000), rabbit anti-Amphiphysin (1:1000), rabbit anti-BIN1 (1:1000), rabbit anti-EAAT1 (1:1000), rabbit anti-PSD95 (1:1000), mouse anti-vGlut1 (1:1000), mouse anti-vGlut2 (1:1000) and rabbit anti-SNAP25 (1:1000). After washing 3 times with TBST, secondary antibodies conjugated to horseradish peroxidase were applied at 1:5000 for 1 h at room temperature. After washing with TBS containing 0.5% of Tween 20, the membrane was visualized by ECL solution

using Intas ECL system (Intas Chemocam ECL Imaging). ECL-blots were evaluated by using sequence exposure (10 seconds per scan, 10 times). The signals on the blots were quantified by using Fiji imageJ (version 2.0)

3.2.12 Immunocytochemistry

24 h after transfection, HEK cells were briefly washed with cold PBS, and then fixed with cold methanol for 3 min, followed by washing 5 times with cold PBS and blocking with 10% horse serum and 0.1 % Triton X 100 in PBS for 1h. Hippocampal neurons were fixed with 4% PFA for 10 min instead. The cells were incubated with appropriate combinations of rabbit anti-RFPT (1:1000), mouse anti-GFP (1:1000), mouse anti-PMCAs (1: 500), sheep anti-Nptn (1:500), and goat anti-basigin (1: 500) antibodies overnight at 4℃. For detection species-specific secondary antibodies conjugated with Alexa-488, Cy3 or Cy5 were used at 1:1000, then washed with PBS and briefly with water. The coverslips carrying the cells were mounted on glass slides with fluoromount g DAPI (Southern biotech, USA) and were visualized using a Leica SP5 confocal microscope.

3.2.13 Immunohistochemistry

Mice were anesthetized with isoflurane and transcardially perfused with PBS followed by 4% PFA. The brain was dissected and post-fixed in 4% PFA overnight, serially infiltrated with 15% and 30% sucrose for 24 h each. Coronal or sagittal sections 30 µm thick were sliced by using a cryostat at -19℃. For cochlea stainings, the organ was prepared after brain removal from the inner ear. After post-fixation with 4% PFA, decalcification was performed by incubation in 0.1 M EDTA in PBS for 48 hours and the organ of Corti was isolated and processed for staining.

Following blocking with 20% horse serum in PBS for 1 h, primary antibodies were incubated with: sheep anti-Nptn and goat anti-Np65 (1:500), mouse anti-pan-PMCA (1:1000), rabbit anti-PMCA1 and rabbit anti-PMCA2 (1:500), rabbit anti-β-III Tubulin (TUJ) (1:1000), rabbit anti-Myosin7a (1:1000), mouse anti-Parvalbumin (1:500), and

mouse anti-Calbindin (1:500). Secondary antibodies and markers were Cy3-conjugated anti-sheep, Cy5-conjugated anti-rabbit or -goat, Alexa Fluor-488 anti-mouse or -rabbit (1:1000), phalloidin-iFluor 488 green (1:1000). After washing with PBS and briefly with water, the sections were mounted on glass slides with fluoromount g DAPI (Southern Biotech) and were visualized using a Leica SP5 confocal microscope.

3.2.14 Electrophysiology - Surgical procedure and recording

Adult mice (2-month-old $Nptn^{-/-}$, n=6; 5-month-old $Nptn^{-/-}$, n=3; 2-month-old $Nptn^{+/+}$, n=6; 5-month-old $Nptn^{+/+}$, n=7) were proceed as described in detail previously (Happel *et al.,* 2010). Briefly, animals were anesthetized with (0.007 ml/g) of 20% Ketavet (Zoetis), 5% xylazine (BayerVital), and 75% isotonic sodium chloride solution (Berlin Chemie) by intraperitoneal injection.

The mouse auditory cortex (AC) region was identified by tonotopic mapping based on the vascularization pattern, and a 32-channel single-shank recording electrode was implanted (Neuronexus A1x32-50-413; channel impedances between 500-800 kΩ) perpendicular to the AC surface.

Local field potentials (LFPs) were recorded in response to pure tones (duration 100 ms, interstimulus interval 800 ms, 50 repetitions per tone, 1 kHz – 32 kHz) at 75 dB SPL and during a pause condition which displays no sound presentation and also a condensed click (Saldeitis *et al.,* 2014) at 75 dB SPL. All the parameters were controlled *via* Matlab (2007), the stimuli were converted into an analog signal by a data acquisition card (NI PCI-BNC2110, National Instruments, Germany), rooted and amplified through a controllable attenuator (gPAH, Guger, Technologies, Austria) and an audio amplifier (Thomas Tech Amp75), respectively. Tones were played in an acoustic far field environment of 1 m distance between the mouse and speaker (Tannoy arena KI-8710-23).

LFPs were recorded for 2 hours to allow cortical activity to be stable after implantation. For final data analysis, the sets of stimulus repetitions with stabilized responses were

selected. Recorded signals were firstly pre-amplified (500X) and filtered by PBX2 preamplifier between 3 and 170 Hz, and then digitized at 1 kHz with a multichannel-recording system.

Current source density (CSD) analysis

Based on pure tone-evoked local field potentials (LFPs), the current-source density (one-dimension) profile was acquired from the second spatial derivative of the laminar LFP (Mitzdorf 1985):

$$-CSD \approx \frac{\delta^2 \emptyset(z)}{\delta z^2} = \frac{\emptyset(z + n\Delta z) - 2\emptyset z + \emptyset(z - n\Delta z)}{(n\Delta z)^2}$$

Here Ø stands for the field potential, z stands for the cortical laminae, Δz stands for the inter-channel distance and n stands for the differential grid. LFPs were smoothed using a weighted average of 7 channels (Hamming window, spatial filter kernel size of 300 µm) before CSD calculation. And based on the CSD profiles, different cortical layers could be identified by the early granular sink components, which reflect the thalamocortical input into cortical later III-IV. Cortical layers I/II, and V/VI were assigned accordingly (Happel *et al.,* 2010).

3.2.15 Auditory brainstem response (ABR)

Adult mice were anesthetized by intraperitoneal injection as described for the CSD measurement. Auditory recording was performed in a single-walled, sound-attenuated and electrically shielded chamber (Industrial Acoustics, Germany). The tone stimulus was performed using Tucker-Davis-Technologies (TDT, USA) System 3 hardware and digitally generated by a real-time processor (RX8, 100k samples/s). Stimuli were passed through a programmable attenuator (PA5) and amplified (AMP84; Thomas Wulf Elektronik) and then delivered by a free-field speaker (MF1) located in front (4 cm) of the animal's head. Levels of stimulus were firstly calibrated to dB pSPL using a

probe microphone (46 BE $^{1}/_{4}$"; G.R.A.S.) and conditioning amplifier (Nexus 2690, B&K). For recordings, subcutaneous electrodes were placed in the posterior midline of the neck (active), the snout (reference), and the back (ground) of the mouse. ABRs were recorded in response to different stimulation levels (90 db to 30 db). And the ABR threshold was defined as the lowest stimulation level that evoked a reproducible response according to visual criteria. Thresholds were tested up to a maximum stimulus level of 90 dB.

3.2.16 Ca^{2+} imaging

Rat hippocampal neurons were transfected with either RFPT, Nptn, or basigin encoded with GCamP5 plasmids at day 9. The Ca^{2+} imaging was performed at day 14. The coverslips were inserted into an imaging chamber which contains recording buffer. The electrical stimulation (20 pulses of 1 msec duration each at 20Hz) was performed with a S48 stimulator (Astro-Med, Inc., West Warwick, RI, USA). During the stimulation, all the neurons on the cover slips are activated and the recording lasted 24 seconds and was performed using a fluorescence microscope under 63x magnification (ZEISS, visitron systems, Germany). The fluorescent proteins were excited at 488 or 551 nm and their emission was acquired at 510 or 584nm. TTX (0.2 µM) or D-AP5 (50 µM) and CNQX (10 µM) were applied into the recording buffer to prevent the spontaneous neuronal firing. 10 µM carboxyeosin was used as PMCA inhibitor. For the data analysis, the images were first quantified using Fiji ImageJ (version 2) and the curve was generated using Clampfit (version 10, Molecular devices), where also the decay time, resting time and peak amplititude were calculated.

2 x Tyrodes buffer	5 mM KCl, 50 mM HEPES, 60 mM Glucose
Recoding buffer	119 mM NaCl, 1x Tyrodes buffer, 2 mM $MgCl_2$ and $CaCl_2$, ddH_2O

3.2.17 Quantification of cochlear cells

The quantification of cells was performed as described (Perny *et al.,* 2016). Briefly, for the hair cell analysis, whole mount preparations of cochlea were labeled with antibodies identifying hair cells (Myosin 7a). 300-400 HCs were analyzed for each cochlea area (apical, middle, and basal turns). The total number of hair cells was normalized to the length of the basilar membrane and the cell number per 100 µm was calculated. For spiral ganglion neuron (SGN) counting, the density of SGNs was analyzed by counting both TUJ and DAPI positive cells in the midmodilar plane (apical, middle and basal turns). Three nonconsecutive sections were selected from a total of 20 sections for analysis. The number of SGNs from each region was divided by the area of corresponding Rosenthal's canal.

3.3 Statistical analysis

For quantification of cells, analysis of variance with Dunnett's multiple comparisons test was performed using Prism (version 9, GraphPad Software). For ABR, Statview (SAS Institute, Inc., Cary, NC) was used for analysis of variance, post hoc analysis (Scheffé or Fisher's protected least significant difference), repeated-measures analysis of variance, and t-tests. For densitometric analysis of western blots, statistical analysis was performed using Student's t-test. For Ca^{2+} imaging, a Mann Whitney test was used for different groups comparison, and a Wilcoxon matched pairs test for the inner group comparison.

3.4 Ethical Statement

Animal experiments were planned within this project. Animals for cell culture and tissue preparation are housed under standard conditions with food and water ad libitum on a reversed 12:12 light/dark cycle. All gene technology procedures were performed in S1 facilities in accordance with institutional, state, and government regulations and approved by an ethics committee.

4 Results

4.1 Differential effects on PMCA isoform expression in Nptn$^{-/-}$ mice brain

Following the identification of PMCAs as close interaction partners of Nptn, a first assessment of total PMCA levels in membrane fractions from mouse brains pointed to a significant reduction in Nptn KO *versus* wild type controls (Bhattacharya *et al.,* 2017). In the present study, I analyzed in depth the effects of Nptn deficiency on PMCA levels. For this, I performed quantitative western blot analyses, by using a pan-PMCA antibody to determine the total amount of PMCAs but also using antibodies for the assessment of the four different PMCA isoforms individually. The approach was further diversified by separately addressing hippocampus, cortex and cerebellum. Three biological replicates of both homogenates and synaptic junctional membranes preparations (SJ) from the respective areas were prepared and analyzed side-by-side. Moreover, the blots were probed for Nptn and I also evaluated possible effects on Basigin levels in the absence of Nptn.

Hippocampus (Fig. 6A-C, Table 1). Compared to homogenates and SJ from hippocampus of Nptn$^{+/+}$ controls, the total amount of PMCAs (detected by a pan-PMCA antibody) was found to be reduced by about 50% and 30%, respectively, in Nptn$^{-/-}$ mice. However, the levels of the four PMCA isoforms were differentially affected. Specifically, PMCA2 was unchanged in homogenates and only reduced by about 12% in SJ. This contrasted with considerable reduction of PMCA1 (~30% and 50% reduction in homogenate and SJ, respectively) and PMCA3 (>45% reduction in both homogenates and SJ) and with even more severe loss of PMCA4 (~85% and >70% reduction in homogenate and SJ respectively).

Cortex (Fig. 6D-F, Table 1). Compared to controls, the total amount of PMCAs in Nptn$^{-/-}$ cortex homogenates and SJ was reduced by about 67% and 39%, respectively. PMCA1, 2 and 3 roughly followed this profile, with reductions of ~70 to 80% in

homogenates and ~25 to 55% in SJ. PMCA4 again was dramatically reduced in both homogenates and SJ (by ~85% in both). While reductions of PMCA1, 2, and 3 were generally less pronounced in SJ than in homogenates, this difference was most pronounced for PMCA2.

Cerebellum (Fig. 6G-I, Table 1). Compared to the controls, the cerebellum of Nptn$^{-/-}$ mice displayed a significant reduction of total PMCA in homogenates and SJ by about 40% and 34%, respectively, i.e. similar to Nptn-deficient hippocampus. In contrast to hippocampus, PMCA2 was more severely reduced while PMCA4 was less affected in cerebellum (PMCA1 reduced by ~70%/ 44% PMCA2 by ~30%/ 46%, PMCA3 by ~48% / 47% and PMCA4 by ~55%/ 58% in homogenates/ SJ).

Assessment of Nptn did not only confirm the genotypes of the various samples but also revealed differences concerning the relative abundance of Np55 and Np65 in Nptn$^{+/+}$ brain areas. Both splice variants were abundant in hippocampal and cortical homogenates and in synaptic junctions of hippocampus (Fig. 6A-C) whereas Np65 was clearly more prominent than Np55 in synaptic junctions from the cortex (Fig. 6D-F). Consistent with transcriptional data (Langnaese et al., 1998), Np55 was by far the predominant variant in the cerebellum (Fig. 6G-I).

Interestingly, I found that compared to Nptn$^{+/+}$ controls, Basigin was up-regulated at least two times (hippocampus, Fig. 6A-C; Table 1) and reached a maximal increase in cerebellar homogenates and SJ to ~540% and 720%, respectively (Fig. 6G-I; Table 1). In wild type and Nptn$^{-/-}$ samples, Basigin was represented by a single band with an apparent molecular weight of ~50 kDa, most likely representing the 2 Ig domain variant, corresponding to Np55.

The quantitative western blot analysis thus revealed differential effects of Nptn deficiency on PMCAs in different brain areas and their synaptic junctions. Profound up-regulation of Basigin, as the closest paralog of Nptn, might allow for partial compensation of loss of Nptn.

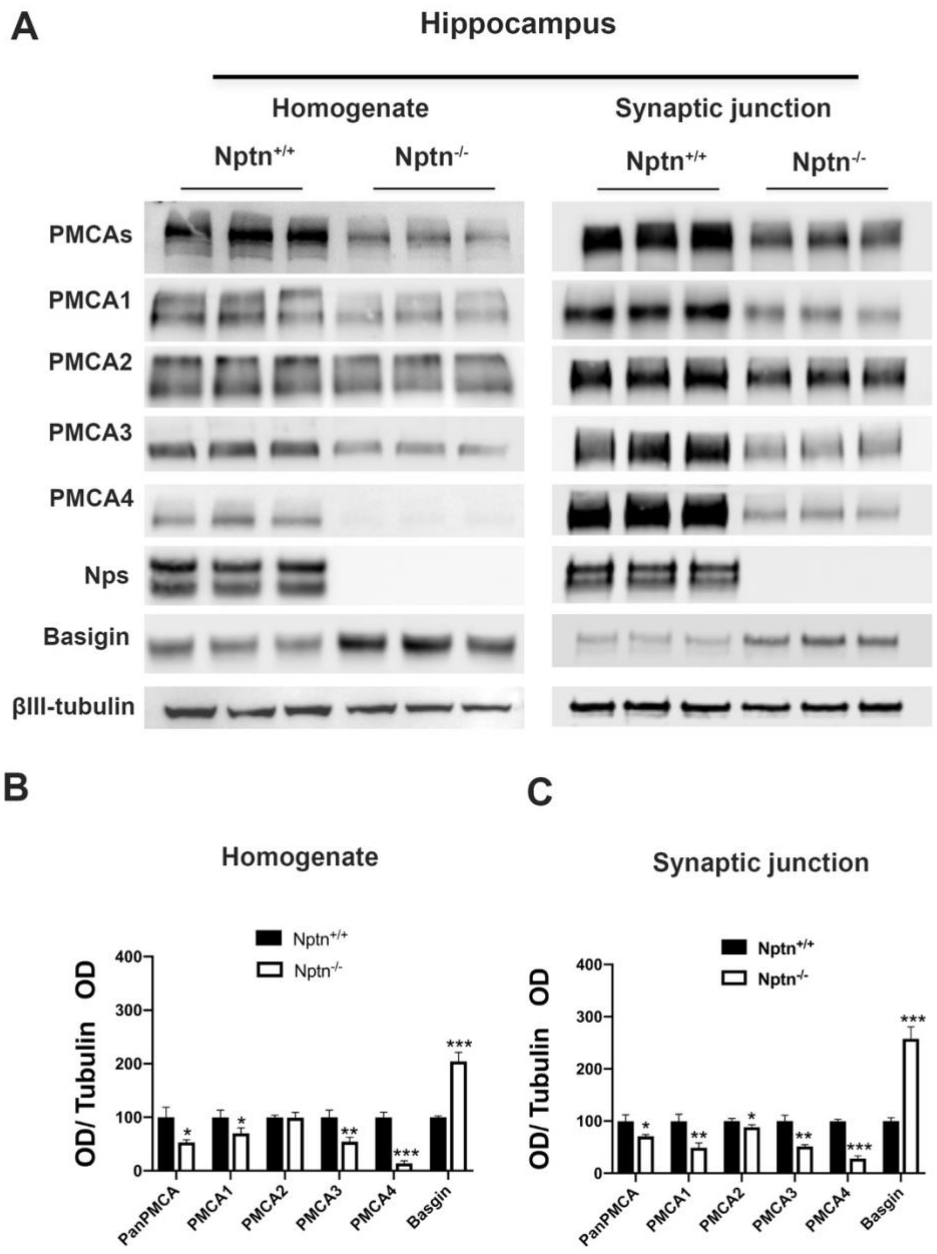

For figure legend see page 44

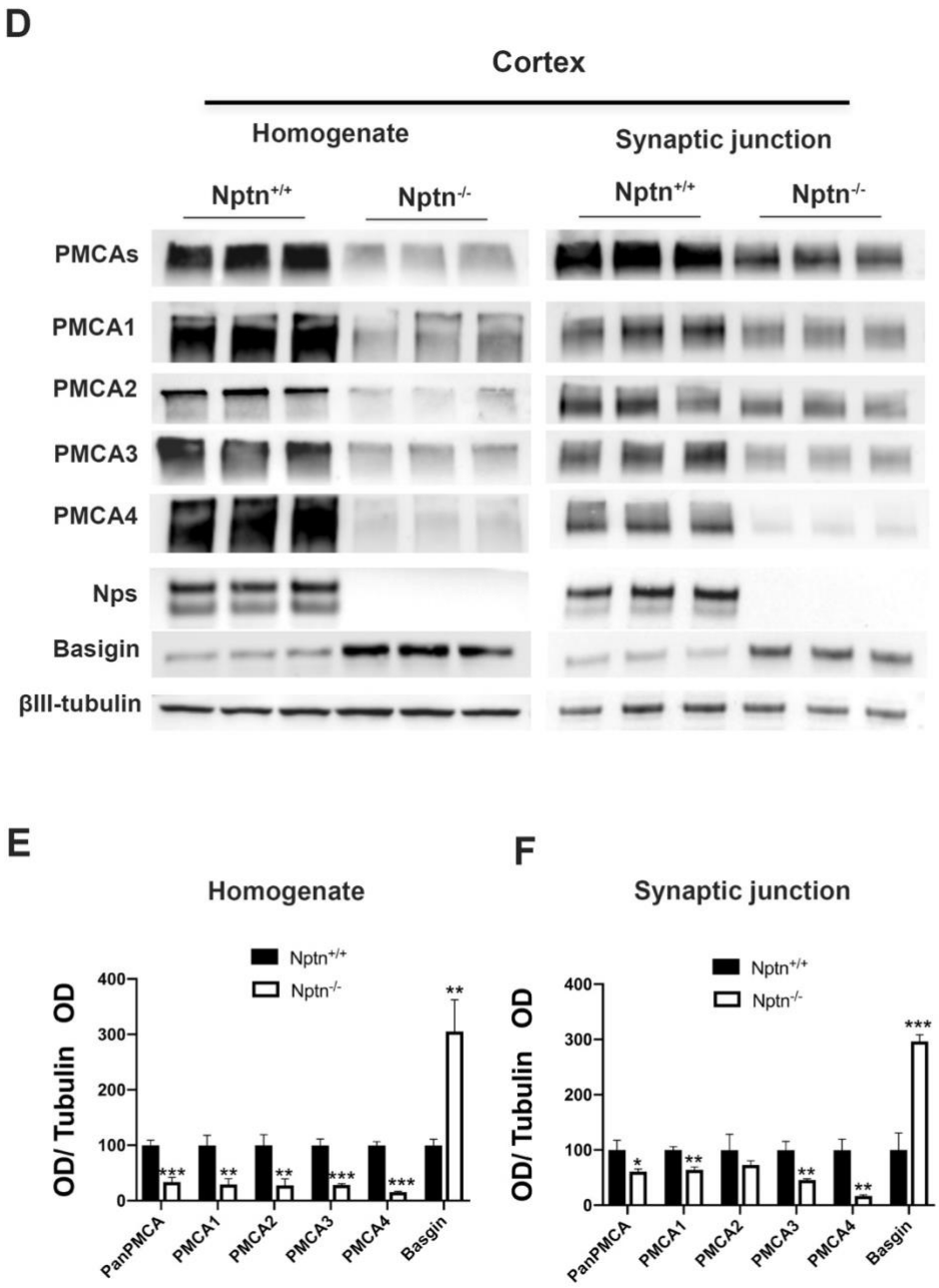

For figure legend see page 44

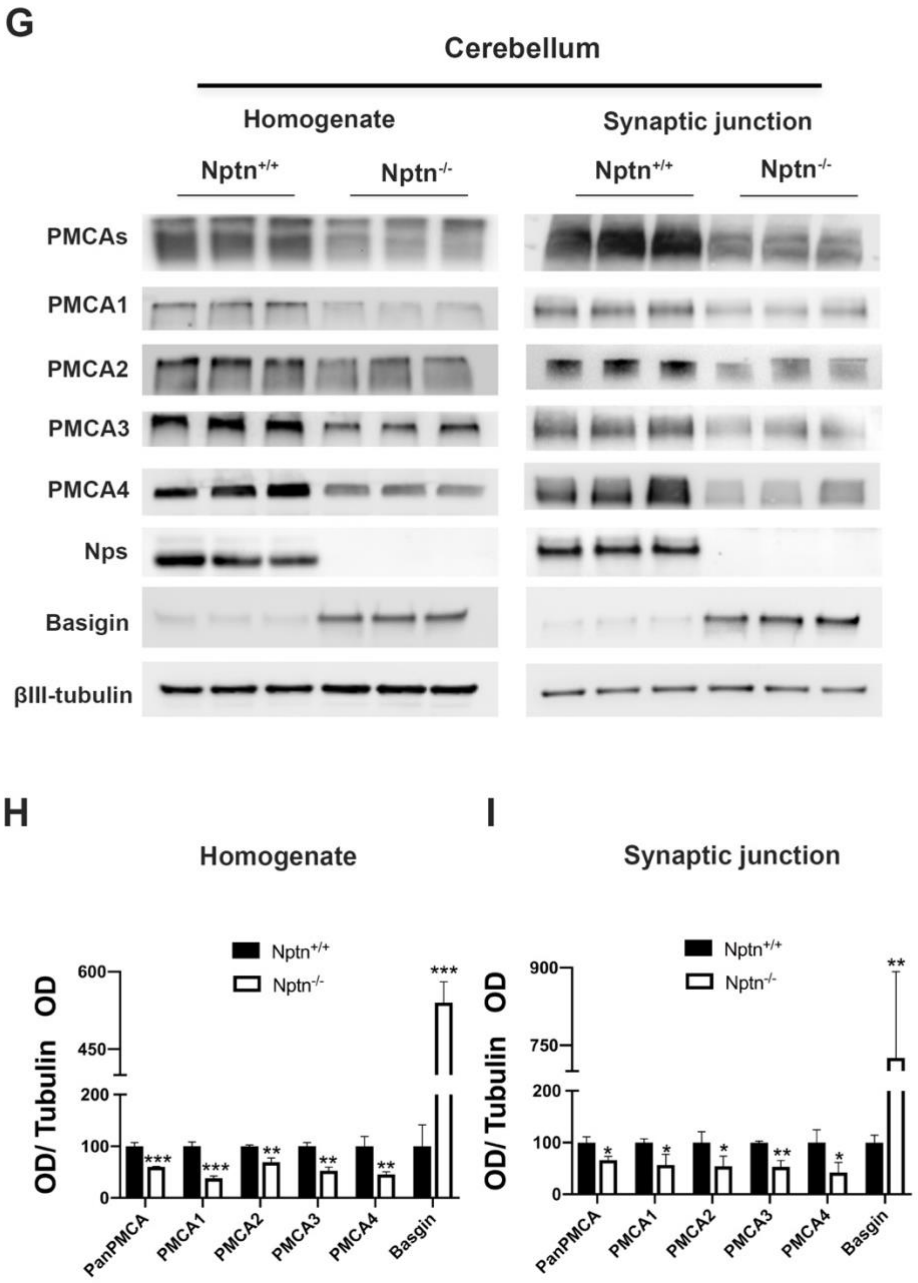

Figure 6: Western blot analysis of PMCA isoforms, Basigin and Nptn expression in the hippocampus (A-C), cortex (D-F) and cerebellum (G-I) of Nptn$^{+/+}$ and Nptn$^{-/-}$ mice

Brains from Nptn$^{+/+}$ and Nptn$^{-/-}$ mice (3 mice per genotype) were dissected and synaptic junctional membranes were as described in section 3.2.8. Homogenate (Homo, A，D，G left) and Synaptic junctions (SJ, A, D, G right) were probed with antibodies against total PMCA, the different PMCA isoforms, Nptn and Basigin, Anti-βIII-tubulin was used as a loading control. (B, C, E, F, H and I) Quantitative analyses on the basis of OD values are shown in (A, D and G). The means of anti-βIII-normalized control values were set to 100%, all data are represented as mean ± SD with *P < 0.05, **P < 0.01, ***P < 0.001 unpaired Student t-test.

Table 1

PMCA and Basigin levels in Nptn$^{-/-}$ brain areas in % of Nptn$^{+/+}$ control levels

	Hippocampus		Cortex		Cerebellum	
	Homo	SJ	Homo	SJ	Homo	SJ
PMCAs	53.05±5.22	70.86±3.28	33.68±8.43	60.99±4.41	60.17±0.98	66.23±7.12
PMCA1	70.23±10.0	49.21±9.09	29.61±10.1	64.27±4.75	29.61±10.1	56.78±20.7
PMCA2	99.03±9.76	88.43±4.27	27.85±11.5	72.80±11.5	69.20±7.93	54.33±19.1
PMCA3	54.46±7.95	51.34±3.45	28.40±1.97	45.86±1.95	52.57±7.04	53.14±12.5
PMCA4	14.09±4.86	28.22±5.29	15.36±1.50	16.89±1.94	45.29±5.43	42.05±19.3
Basigin	204.7±16.4	257.8±22.9	305.4±57.1	296.6±11.98	540.3±40.1	725.9±166.5

(Mean ± S.D. of OD measurements for different PMCA isoforms and basigin in Nptn$^{-/-}$ brain areas expressed as percent of Nptn$^{+/+}$ control)

The expression of Nptn and Basigin in the cerebellum of wild type and Nptn$^{-/-}$ mice was also addressed by immunohistochemical analysis. Suitable antibodies against either protein were derived from sheep and goat, respectively, and thus do not allow for double-labeling as respective secondary antibodies hardly discriminate between antibodies from these species. Anti-Nptn and anti-Basigin stainings were therefore performed separately including antibodies against Calbindin to label Purkinje cells. Consistent with the western blot data, Basigin-specific immunoreactivity was strongly increased in cerebellar slices of Nptn$^{-/-}$ mice (Fig. 7), and thereby displayed a staining pattern that closely resembled that for Neuroplastin in Nptn$^{+/+}$ slices.

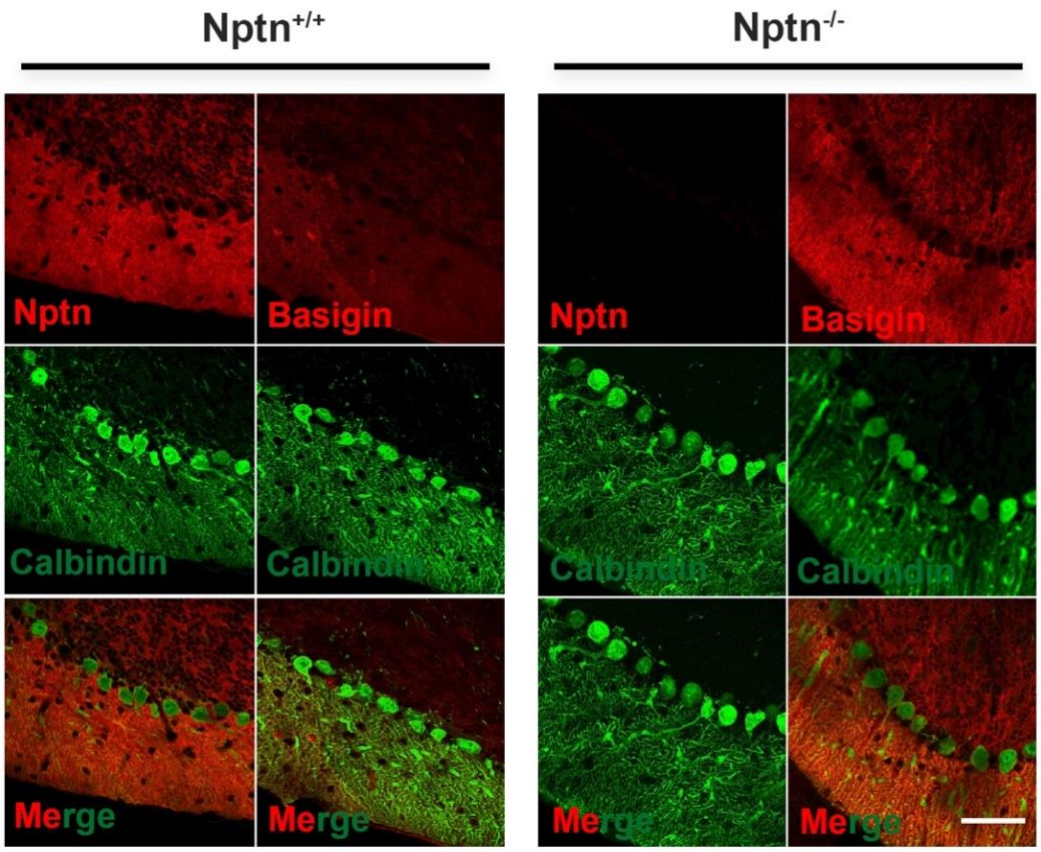

Figure 7: Nptn and Basigin in the molecular layer of mouse cerebellum.
Confocal image stacks taken from slices of Nptn$^{+/+}$ and Nptn$^{-/-}$, fluorescently labeled with antibodies against Nptn, Basigin and Calbindin as a marker for Purkinje cells. Note the strong upregulation of Basigin in Nptn$^{-/-}$. Scale bar = 50 µm

4.2 Effect of Nptn loss in excitatory neurons on overall PMCA, Nptn and Basigin in hippocampus and cortex

Neuroplastin is expressed in glutamatergic and GABAergic neurons (Herrera-Molina *et al.,* 2017, Herrera-Molina *et al.,* 2014). In order to assess whether loss of Nptn in excitatory, i.e. mostly glutamatergic neurons results in significant changes in the overall levels of PMCAs and Basigin, I employed conditional Nptn KO mice bred to Emx1Cre mice (Gorski *et al.,* 2002) in order to obtain Nptn$^{lox/loxEmx1Cre}$ animals (Herrera-Molina *et al.,* 2017), in which Nptn is lost in excitatory neurons of the developing forebrain. Crude membrane extractions from hippocampus and cortex of respective mice and controls were subjected to western blot analyses. Nptn was indeed found to be reduced by ~86%

and ~79% in hippocampus and cortex, respectively (Table 2), confirming the efficacy of the Cre-mediated KO (Fig. 8 A-C). Assessment of total PMCA levels by the pan-PMCA antibody revealed a statistically significant reduction in the hippocampus of $Nptn^{lox/loxEmx1Cre}$ animals by ~30% (Table 2) i.e. less severe than in the hippocampus of constitutive KO mice (compare Fig. 8B to Fig. 6B). This may easily be explained by little if any change of PMCAs in inhibitory neurons. Similarly, cortex samples displayed a strong reduction of PMCAs upon Emx1Cre-mediated KO (level of PMCAs reduced by ~57%, Table 2), but again slightly less severe than in cortex homogenates of constitutive KO mice (Fig. 8C, compare to Fig. 6E). Considerable upregulation of Basigin was evident for both hippocampus and cortex of $Nptn^{loxl/oxEmx1Cre}$ mice. For hippocampus, Basigin upregulation even exceeded the respective value determined for $Nptn^{-/-}$ (~263% versus 204%, Table 1 and 2), whereas Basigin levels were increased to a lesser extent in cortex samples of $Nptn^{lox/loxEmx1Cre}$ versus $Nptn^{-/-}$ mice (150% versus 305%, Table 1 and 2). Collectively, this assessment implies that the observed reduction of PMCAs due to loss of Nptn in all neurons of the hippocampus and cortex (Fig. 6A - I) represents a composite effect of reduced PMCA levels in excitatory and inhibitory neurons. Upregulation of Basigin appears to be particularly pronounced in excitatory neurons of the hippocampus and coincides with a relatively moderate reduction of total PMCA levels.

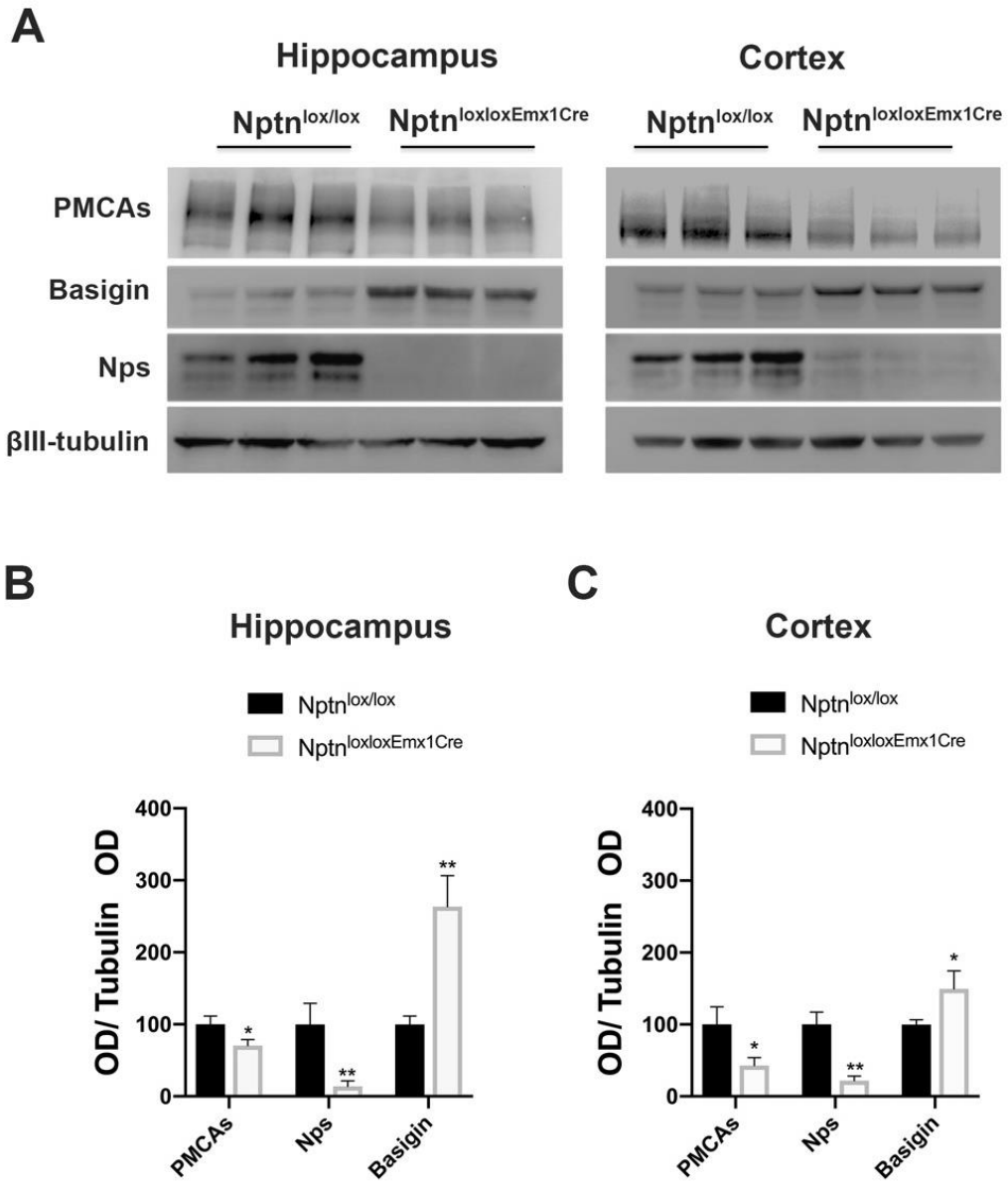

Figure 8 Western blot analysis of PMCAs, Basigin and Nptn in Nptn^{loxloxEmx1Cre} and Nptn$^{lox/lox}$ brain areas.

Crude membrane fractions from hippocampus (A left) and cortex (A right) of Nptn$^{lox/lox}$ controls and Nptn^{loxloxEmx1Cre} mice (3 mice per genotype) were probed with antibodies against total PMCA, Basigin and Nptn. Anti- β III-tubulin was used as a loading control. Respective densitometric intensity quantifications are shown in (B) and (C) with means of β III-tubulin-normalized control values set to 100%. Data are represented as mean ± SD with *P < 0.05, **P < 0.01, unpaired Student t-test.

Table 2

Nptn, PMCA and Basigin levels in Nptn$^{lox/loxEmx1Cre}$ brain areas (% of controls)

	Hippocampus (Homo)	Cortex (Homo)
PMCA	70.43±8.49	42.84±11.05
Basigin	263.5±43.04	149.4±25.03
Nptn	13.77±7.67	21.82±6.43

(Mean ± S.D. of OD measurements for PMCA and basigin in Nptn$^{lox/loxEmx1Cre}$ brain areas expressed as percent of Nptn$^{lox/lox}$ control)

4.3 Effect of induced loss of Nptn on hippocampal and cortical PMCA and Basigin levels

Constitutive loss of Nptn resulted in significant reduction of PMCAs although PMCA2, depending on the brain area, appeared to be less affected than other isofoms in various instances (Fig. 6). It is conceivable, however, that these changes in the levels of PMCAs are, at least partially, affected by compensatory, long-term developmental adjustments. Therefore, and because of the observed retrograde amnesia after induced loss of Nptn (Bhattacharya *et al.,* 2017), I wondered how PMCA levels might be affected when Nptn was removed after normal development of the brain. For this, I used the mouse model (Nptn$^{\Delta lox/loxPr\text{-}CreERT}$) established by Bhatthacharya et al. (2017), in which pan-neuronal deletion of Nptn was induced at the adult stage by intraperitoneal injection of tamoxifen. 8 weeks after injection, crude membrane fractions from cortex and hippocampus of these and of control mice were collected for western blot analysis. At this time point, Nptn was already strongly reduced by 82% and 92% in hippocampal and cortex samples of the respective mice (Fig. 9A-C). Like in Nptn$^{-/-}$ mice, all PMCA isoforms were strongly reduced in cortex (Fig. 9C, and table 3, total PMCAs reduced by 45% and 40%, PMCA1 by 49% and 43%, PMCA2 by 33% and 68%, PMCA3 by 57% and 65%, PMCA4 by 71% and 90% in cortex and hippocampus, respectively). A noticeable difference to the constitutive KO, however,

was observed for hippocampus, where in the induced KO not only PMCA1, 3 and 4 but also PMCA2 was significantly reduced (compare Fig. 6A-C to Fig. 9A-C). This suggests that the inducible, i.e. more acute KO might lead to more severe disturbances in Ca^{2+} homeostasis in hippocampal neurons than the constitutive deletion of Nptn. Basigin was again found to be strongly increased to 198% and 204% of controls in hippocampus and cortex respectively, though to a slightly lesser degree when compared to the constitutive KO. Taken together, these observations demonstrate that Nptn is required to maintain the level of all PMCA isoforms in adult mice, and that Basigin upregulation as a possible means to partially compensate for loss of Nptn can still occur in a mature state of the brain.

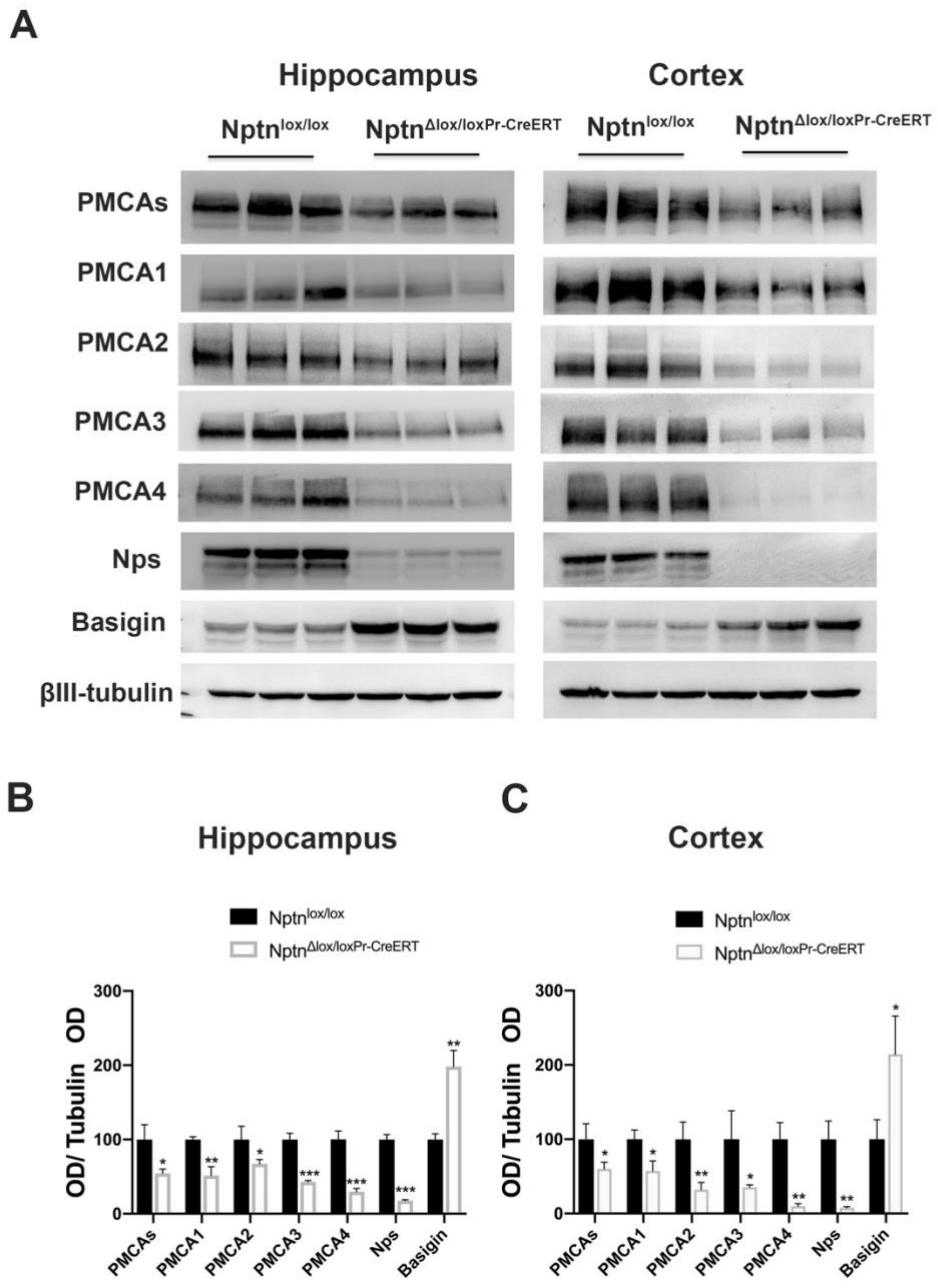

Figure 9: Western blot analysis of PMCA，Basigin and Nptn expression in the hippocampus and cortex of Nptn$^{\Delta lox/loxPr\text{-}CreERT}$ mice.

Crude membrane fractions from hippocampus (A left) and cortex (A right) from three control mice (Nptn$^{lox/lox}$) and three Nptn$^{\Delta lox/loxPr\text{-}CreERT}$ mice were analyzed by using antibodies against total PMCA, PMCA isoforms 1-4, Nptn and Basigin. Anti-βIII tubulin was used to normalize loaded amounts. Intensity quantification of the Western blots are shown in (B) and (C). Means of β III-normalized control values were set to 100%, all data are represented as mean ± SD with *P < 0.05, **P < 0.01, unpaired Student t-test.

Table 3

Levels of Nptn, PMCA and Basigin in Nptn$^{\Delta lox/loxPr\text{-}CreERT}$ brain areas (% of controls)

	Hippocampus (Homo)	Cortex (Homo)
PMCAs	**54.44±5.61**	**60.24±8.81**
PMCA1	**51.47±11.9**	**57.48±13.3**
PMCA2	**67.18±5.89**	**32.18±9.81**
PMCA3	**42.8±2.01**	**35.42±3.31**
PMCA4	**29.56±4.65**	**9.76±3.69**
Basigin	**198±21.88**	**214.4±51.5**
Nptn	**17.52±1.29**	**7.62±1.67**

(Mean ± S.D. of OD measurements for PMCA isoforms, basigin and Nptn in Nptn$^{\Delta lox/loxPr\text{-}CreERT}$ brain areas expressed as percent of Nptn$^{lox/lox}$ control)

4.4 Expression of potential Nptn interaction partners in Nptn KO brains

While mass spectrometry had revealed PMCAs as prime interaction partners of Nptn, additional proteins were identified as potential interaction partners. Amphiphysin, as mentioned in the introduction, emerged from the same approach as the PMCAs. In addition, some 30 synaptic interaction partners were detected in another screen, where Triton X-100 was used as a detergent (K.H. Smalla and T. Kaehne, personal communication; Conny Leistner, 2016) and in which Nptn KO mice were again used as controls to exclude non-specific hits. Some of the candidates were selected for western blot analysis to assess possible changes in expression levels in Nptn$^{-/-}$ forebrain homogenate and synaptic junction samples. As ongoing work by C. Montenegro at the LIN implies a role for Nptn in the synaptic vesicle cycle (Montenegro et al., in prep.), a focus was placed on such proteins that might be involved in neurotransmitter release and uptake as well as in synaptic vesicle endocytosis. BIN-1 (myc box-dependent interacting protein 1, also known as Amphiphysin-2), though not identified in the screen, was included because of its similarity to Amphiphysin.

Additional, screen-derived candidates for testing included excitatory amino acid transporter 1 (EAAT1), vesicular glutamate transporters 1 and 2 (VGLUT1 and VGLUT2) and the synaptosomal-associated protein 25 (SNAP25), an important player in the fusion of synaptic vesicles to the plasma membrane. Finally, postsynaptic density protein 95 (PSD-95), though not identified in this particular screen, was included as a major scaffold protein of the postsynapse and as a previously identified interaction partner of PMCAs. As shown in Fig. 10 A-C, none of these proteins displayed a significant change in expression levels in either homogenates or SJ fractions.

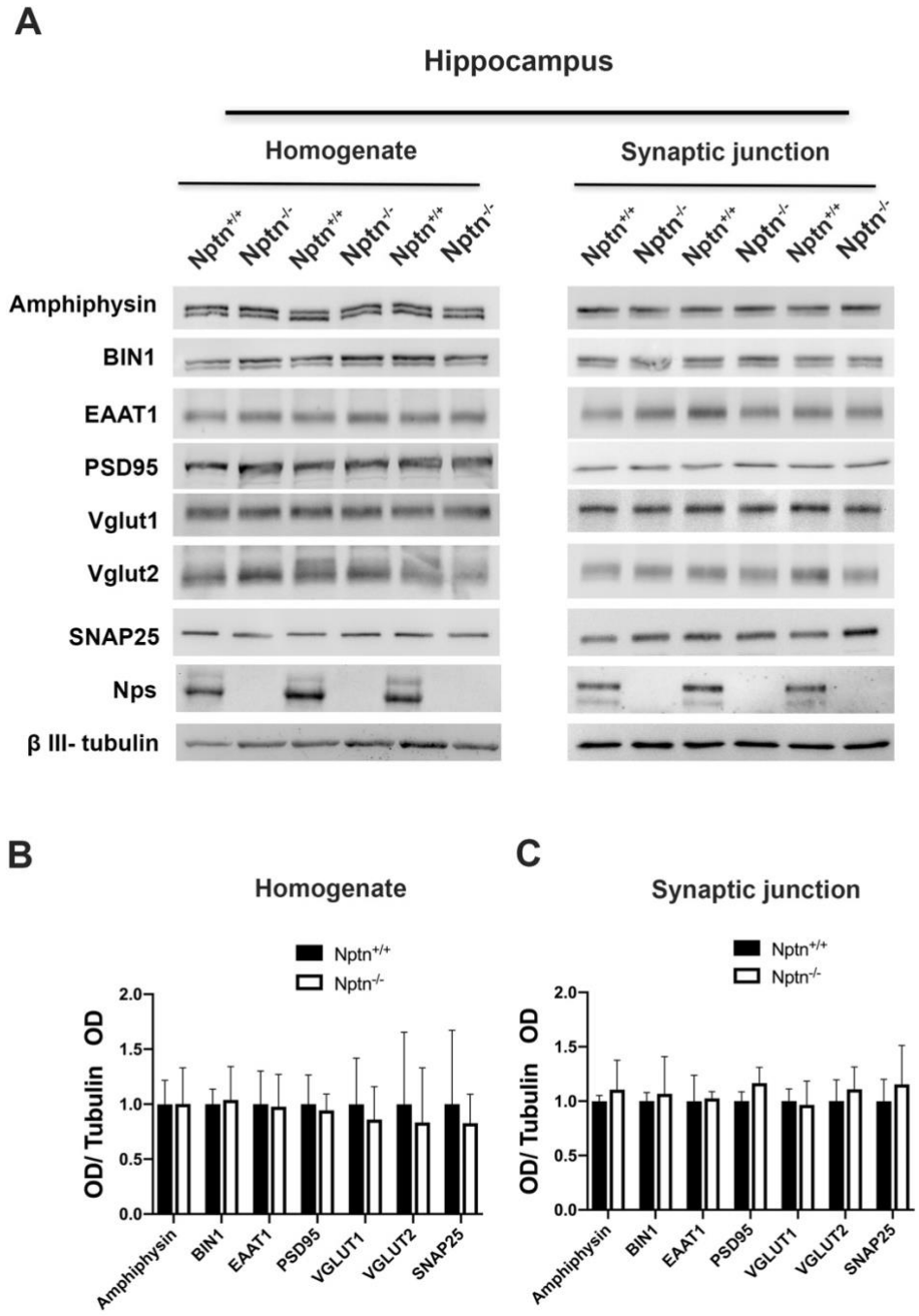

Figure 10: Western blot analysis of potential interaction partners in Nptn$^{+/+}$ and Nptn$^{-/-}$ mice.

Homogenates (A left) and synaptic junctions (A right) were prepared from mouse forebrains (3 mice per genotype) and were probed with antibodies against Amphiphysin, BIN1, EAAT1, Vglut1, Vglut2, SNAP25 and Nptn. Anti-βIII-tubulin served as a loading control. (B) and (C) show intensity quantifications with mean βIII-normalized values of the control samples set to 1. All the data represent mean ± SD with *P < 0.05, **P < 0.01 unpaired Student t-test.

Among all PMCA isoforms PMCA4 was most dramatically reduced in the hippocampus and cortex of Nptn$^{-/-}$ mice. If competition between the four PMCA isoforms for Nptn in wild type and for upregulated Basigin in the absence of Nptn plays a role for their differential expression levels, then the absence of one isoform might affect the levels of the others. Moreover, the competition might also have some influence on Nptn or Basigin. Therefore, I made use of available PMCA4 KO mice to evaluate them for possible effects on the levels of the other PMCA isoforms, Nptn and Basigin in hippocampus and cortex. Western blot analyses confirmed complete loss of PMCA4 and quantification revealed that total PMCA levels as well as PMCA1 and 2 were unchanged in PMCA4$^{-/-}$ hippocampus. PMCA3, however, was increased by ~46%. This may explain the unchanged levels of total PMCA. Nptn and Basigin remained unaffected (Fig 11A left, B, Table 4). In cortex, loss of PMCA4 resulted in a significant reduction of total PMCA levels by ~29%, while none of the remaining isoforms displayed any significant change in expression. Interestingly, both Nptn and Basigin were significantly reduced by ~36% and ~58%, respectively, suggesting that the dependency between PMCAs on one hand and Nptn and Basigin on the other might be bidirectional (Fig 11A right, C, Table 4). It is therefore possible that in the cortex the synthesis of PMCA1, 2 and 3 might be limiting to compensation for the loss of PMCA4 and to the stabilization of Nptn and Basigin.

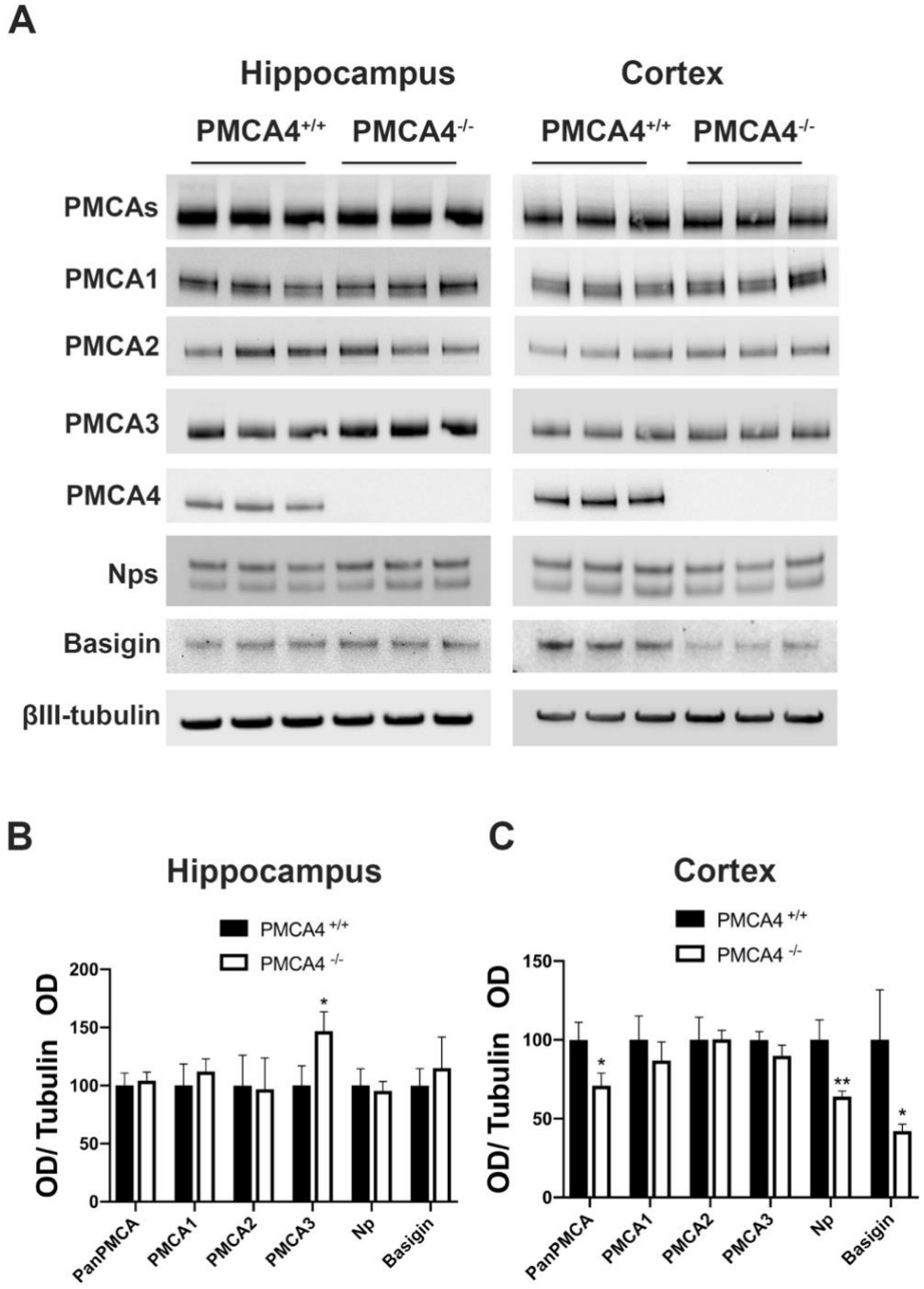

Figure 11: PMCA，Basigin and Nptn expression in the hippocampus and cortex of PMCA4$^{+/+}$ and PMCA4$^{-/-}$ mice.

Mouse hippocamous and cortex were dissected and crude membranes were extracted as the methods mention above. (A) All the brain samples were probed with Nptn, basigin, βIII-tubulin and different PMCA isoforms antibodies, β III-tubulin served as a loading control (3 mice per genotype). (B and C) intensity quantification of the Western blots in (A). All the data are shown as mean ± SD with *P < 0.05, **P < 0.01 unpaired Student t-test.

Table 4

Levels of Nptn, PMCA and Basigin in PMCA4$^{-/-}$ brain areas (% of controls)

	Hippocampus (Homo)	Cortex (Homo)
PMCAs	104.3±7.236	70.89±8.027
PMCA1	112.2±10.83	86.98±11.64
PMCA2	96.79±27.04	100.3±5.767
PMCA3	146.7±16.71	89.92±6.685
Basigin	115.2±26.63	42.22±4.289
Nptn	95.49±7.963	64.11±3.481

(Mean ± S.D. of OD measurements for PMCA isoforms, basigin and Nptn in PMCA4$^{-/-}$ brain areas expressed as percent of PMCA4$^{+/+}$ control)

4.5 Neuroplastin and Basigin both promote PMCA expression levels

As detailed above, PMCA levels were significantly reduced in the Nptn-deficient brain and the four PMCA isoforms were differently affected. At the same time, Basigin was found to be strongly increased, suggesting that it may contribute to maintain some of the remaining PMCA expression, possibly in an isoform-specific manner. To elaborate on this, I investigated, whether over-expression of Nptn and Basigin would affect levels of endogenous or co-expressed PMCA in HEK cells to a similar degree. Specifically, constructs encoding C-terminally TagRFPT-tagged versions of rat Np55, mouse Basigin or human Basigin were transfected into HEK cells either alone or in combination with GFP-tagged PMCA2b and PMCA4b. A TagRFPT encoding plasmid was used as a control. 48 hours after transfection, cells were lysed and subjected to western blot analysis. Anti-RFP detection revealed comparable expression levels for the respective proteins (Fig. 12A-C). Compared to the TagRFPT control, expression of tagged Nptn and of both tagged mouse and human Basigin resulted in a significant increase of endogenous PMCA levels. Likewise, expression levels of GFP-tagged

PMCA 2b and PMCA4b were clearly increased as compared to the control group (Fig. 12D-F). Notably, Basigin appeared to be as efficient in stabilizing PMCA levels as Nptn, supporting the idea of a compensatory role of upregulated Basigin in Nptn mutant mice.

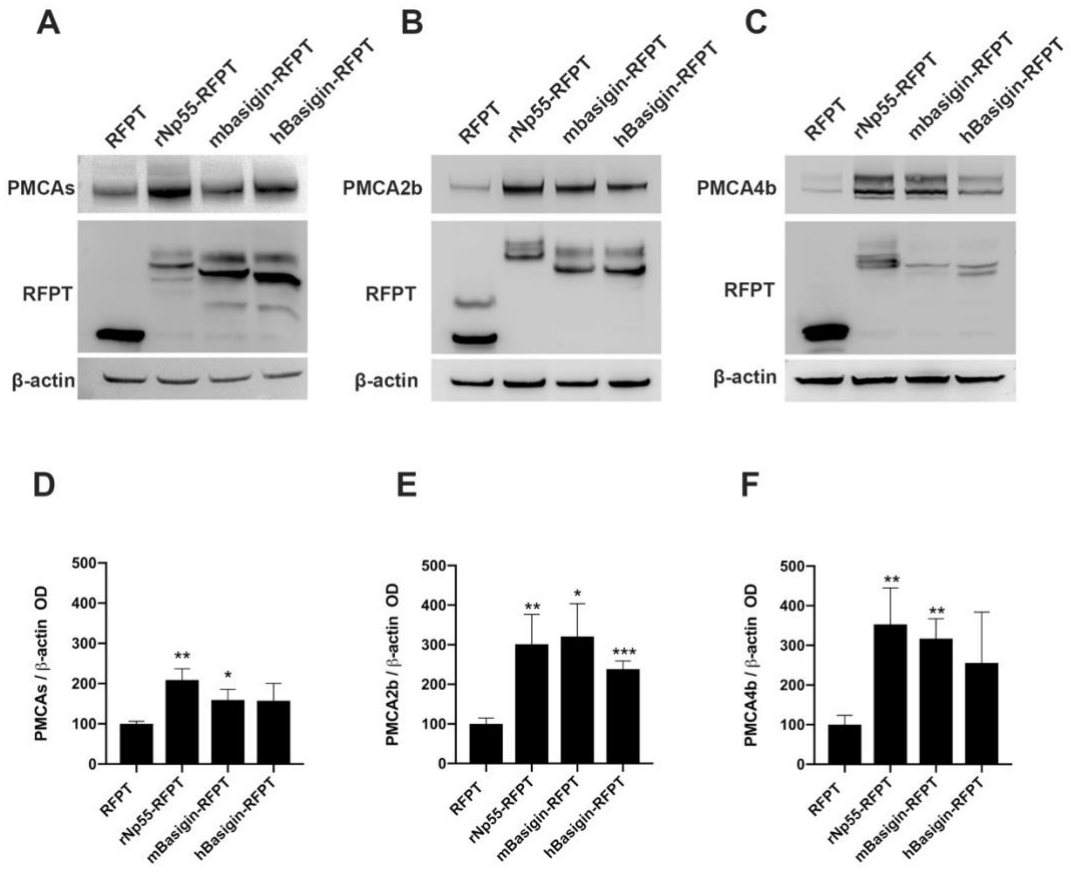

Figure 12: Np55 and Basigin promote PMCA expression in HEK cells.
HEKs cell lysates were analyzed by western blot (A) after single transfection with TagRFPT, rNp55-TagRFPT, mBasigin-TagRFPT and hBasigin-TagRFPT, or after co-transfection with EGFP-PMCA2b-GFP (B) or EGFP-PMCA4b-GFP(C). For single transfections, endogenous PMCA levels were detected by the pan-PMCA antibody, whereas for co-transfections the levels of the respective EGFP-PMCA isoforms were detected by an anti-GFP antibody (B, C). TagRFPT and TagRFPT-tagged Np55 and Basigin variants were detected by anti-RFP antibody. Anti- β actin was used as a loading control. All blots are representative for three independent experiments. (D-F) Quantification of western blots. All OD values represent mean ± SD with *P < 0.05, **P < 0.01, ***P < 0.001 unpaired Student t-test and the means of Anti- β actin-normalized TagRFPT-controls set to 100%.

4.6 Characterization of the interaction between Nptn and PMCA2b

A very close physical interaction between Nptn and PMCAs was first inferred from the aforementioned mass spectrometric analyses of Np65-specific immunoprecipitates from synaptic junctional preparations. Biochemical analyses on immune cells, in which only Np55 is expressed, revealed that this shorter splice variant is also associated with PMCA (Korthals *et al.,* 2017). To further characterize the interaction between Nptn and PMCAs, specifically PMCA2b, I generated expression constructs encoding mutated variants of Np55 and tested them for their ability to associate with EGFP-tagged PMCA2b upon co-expression in HEK cells. The respective variants were either expressed without a tag or tagged C-terminally with TagRFPT. Three principal variants were used in a first set of experiments: Np55 wild type control (including the cytoplasmic DDEP motif); Np55[TMD^{CD2}] in which the TMD of Np55 was replaced by the TMD of another Ig domain protein, CD2; and Np55-Δcyt in which the complete cytoplasmic domain was deleted right after the membrane-proximal lysine residue (Fig 13A; see also Fig 14A). 48 h after transfection, cells were harvested and extracted with either 1% Triton-X100 (Fig 13B) or 1% Digitonin (Fig 13C). Extracts were subjected to immunoprecipitation with anti-GFP antibody-coated magnetic beads. Subsequent western blot analysis of the input controls revealed that EGFP-PMCA2b expression levels were clearly elevated by co-expressed Np55 or Np55-Δcyt, whereas co-expressed Np55[TMD^{CD2}] had little if any stabilizing effect on EGFP-PMCA2b (Fig. 13B and C). For both detergents, western blot analysis of the immunoprecipitates revealed an association of EGFP-PMCA2b with both Np55 and Np55-Δcyt. Interestingly, EGFP-PMCA2b was found associated with Np55[TMD^{CD2}] in Triton-extracts but not in Digitonin-extracts (Fig. 13B and C, bottom panels). The latter shows that the TMD of Nptn is crucial for the interaction with PMCA2b. Triton-X100 might not be stringent enough to prevent non-specific interactions between transmembrane segments and/ or sequences in Np55 other than the TMD add to the interaction with EGFP-PMCA2b

in a Digitonin-sensitive manner (see below). To further elaborate on this, I inspected HEK cells and primary hippocampal neurons cells co-transfected with EGFP-PMCA2b and TagRFPT-tagged Np55 variants by confocal microscopy (Fig. 13D and E). Strong co-localization at the plasma membrane and intracellularly was observed for Np55-TagRFPT and EGFP-PMCA2 in both HEK cells and neurons (Fig. 13D, E, left panels). Np55-Δcyt-TagRFPT, assessed in HEK cells only, perfectly co-localized with EGFP-PMCA2b (Fig. 13D right panel). In striking contrast, EGFP-PMCA2b and TagRFPT-tagged Np55[TMD^{CD2}] displayed very little co-localization in both types of cells (Fig. 13D, E, right panel). While Np55[TMD^{CD2}]-TagRFPT was mainly detectable on the plasma membrane, the bulk of EGFP-PMCA2b remained enriched intracellularly. These findings strongly suggest that the TMD of Nptn is required to target PMCA to the plasma membrane in both HEK cells and hippocampal neurons. They also imply that the co-immunoprecipitation of EGFP-PMCA2b and Np55[TMD^{CD2}] observed after Triton-X100 extraction (Fig. 13B) most likely resulted from non-specific association of the overexpressed proteins.

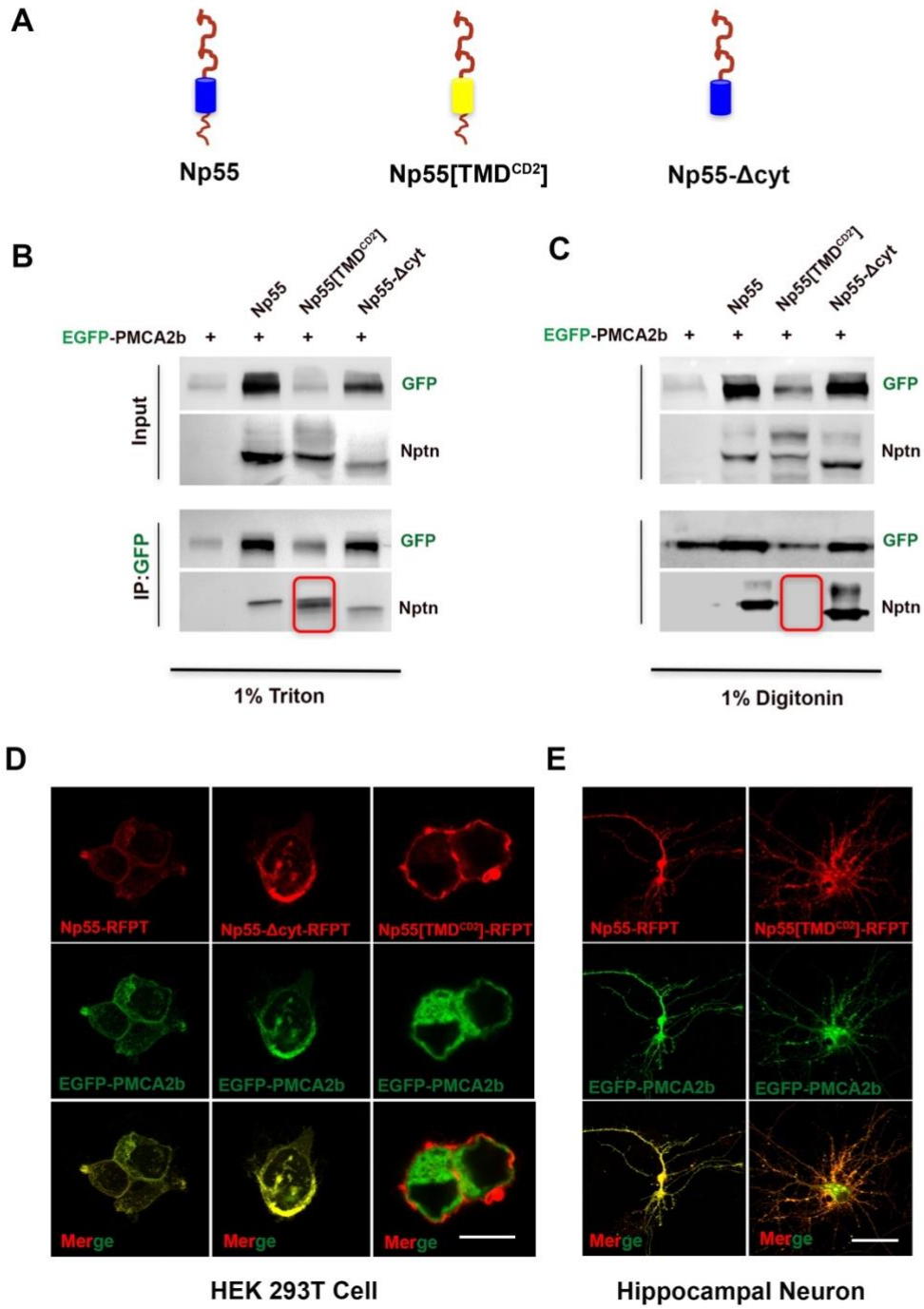

Figure 13: The TMD of Nptn specifies the interaction with PMCA2b

(A) Schematic illustration of Np55 variants including wild type, the TMD-swapping variant Np55[TMD^{CD2}] and the truncated Np55-Δcyt variant. TMDs are symbolized as blue or yellow cylinders. (B, C) Western blot analysis of input controls and anti-GFP-specific IPs derived from crude membrane fractions of HEK cells transfected with EGFP-PMCA2b and Nptn constructs as indicated and solubilized with either Triton-X100 (B) or digitonin (C). Note the appearance of Np55[TMD^{CD2}] in the IPs in (B) but not in (C) (boxed areas). Blots are representative for three independent experiments. (D, E) Representative confocal microscopic images of HEK cells (D)

and hippocampal neurons (E) co-transfected with EGFP-tagged PMCA2b and variants of RFPT-tagged Np55 as indicated. Note the poor plasma membrane targeting of EGFP-PMCA2b in HEK cells co-expressing Np55[TMD^{CD2}]-TagRFPT (D, right panel) compared to the other two combinations (D, left and middle panels). Scale bar = 50µm in D and 45µm in E.

Sequence comparisons showed that Nptn and Basigin share the highest degree of identity within and around the transmembrane sequence (Fig. 14A). As both proteins can stabilize PMCA levels, and since the above results demonstrate a pivotal role of the TMD of Nptn for the interaction with PMCA, it may be expected that the TMD of Basigin is also crucial for its interaction with PMCA. This was indeed confirmed in another set of co-transfection/ co-immunoprecipitation experiments (see below, Fig. 15B) and it implies that amino acid residues specifying the interaction with PMCAs are conserved between the TMDs of Nptn and Basigin. Following this idea, I generated constructs for TagRFPT-tagged Nptn variants with amino acid changes in the TMD. Specifically, proline at position 225 (numbering referring to rat Np55), potentially a helix-breaking residue, was changed to glycine (P225G) and a glutamate residue in the center of the TMD, which is highly conserved across phyla and also present in the more distant family member Embigin was changed into valine (E232V). Likewise, a glutamate residue presumably localized at the interface between membrane and cytosol was changed into alanine (E244A). In adition a tandem of large hydrophobic residues, phenylalanine 226 and leucine 227 was changed into a pair of valines (F226V, L227V) and the small aliphatic alanine preceding E232 was changed into a large aliphatic leucine (A231L). These constructs were co-expressed with EGFP-PMCA2b in HEK cells and tested for co-immunoprecipation with the latter by using 1% digitonin in the lysis buffer, including non-mutated Np55-TagRFPT as a control. All constructs gave rise to similar levels of expression (Fig. 14B, upper panel) and all variants were found to co-immunoprecipitate with EGFP-PMCA2b to virtually the same extent (Fig. 14B, bottom panel). Consistently, the levels of EGFP-PMCA2b were very similar in all samples, implying that its expression was promoted by all variants. To rule out that the TagRFPT tag at the C-terminus of the Nptn variants contributes to some unspecific association with EGFP-PMCA2b, a control experiment was performed,

in which Np55[TMD^{CD2}]-TagRFPT was included. Just as Np55[TMD^{CD2}], the respective TagRFPT-tagged variant neither promoted the elevation EGFP-PMCA2b expression (Fig. 14C, upper panel) nor did it co-immunoprecipitate with EGFP-PMCA2b (Fig. 14C, bottom panel). However, compared to the non-tagged wild type variant of Np55, Np55-TagRFPT was consistently found to co-immunoprecipate more efficiently with EGFP-PMCA2b (Fig. 14C, bottom panel), suggesting that TagRFPT might indeed strengthen the interaction, possibly by dimerization, which in turn might promote cis-homophilic interaction of Nptn.

In summary, none of the tested amino acid residues of the TMD, including the central glutamate residue E232, was found to be essential for the interaction with PMCA2b nor did any of the changes lead to dominant effects that would substantially reduce or increase the interaction or the ability to promote EGFP-PMCA2b levels. While these experiments were in progress, Gong et al. (2018) published a cryo-EM study, in which they identified residues within the TMD of Nptn that interface with the transmembrane region of PMCA1 and indeed these are different from those tested in this work.

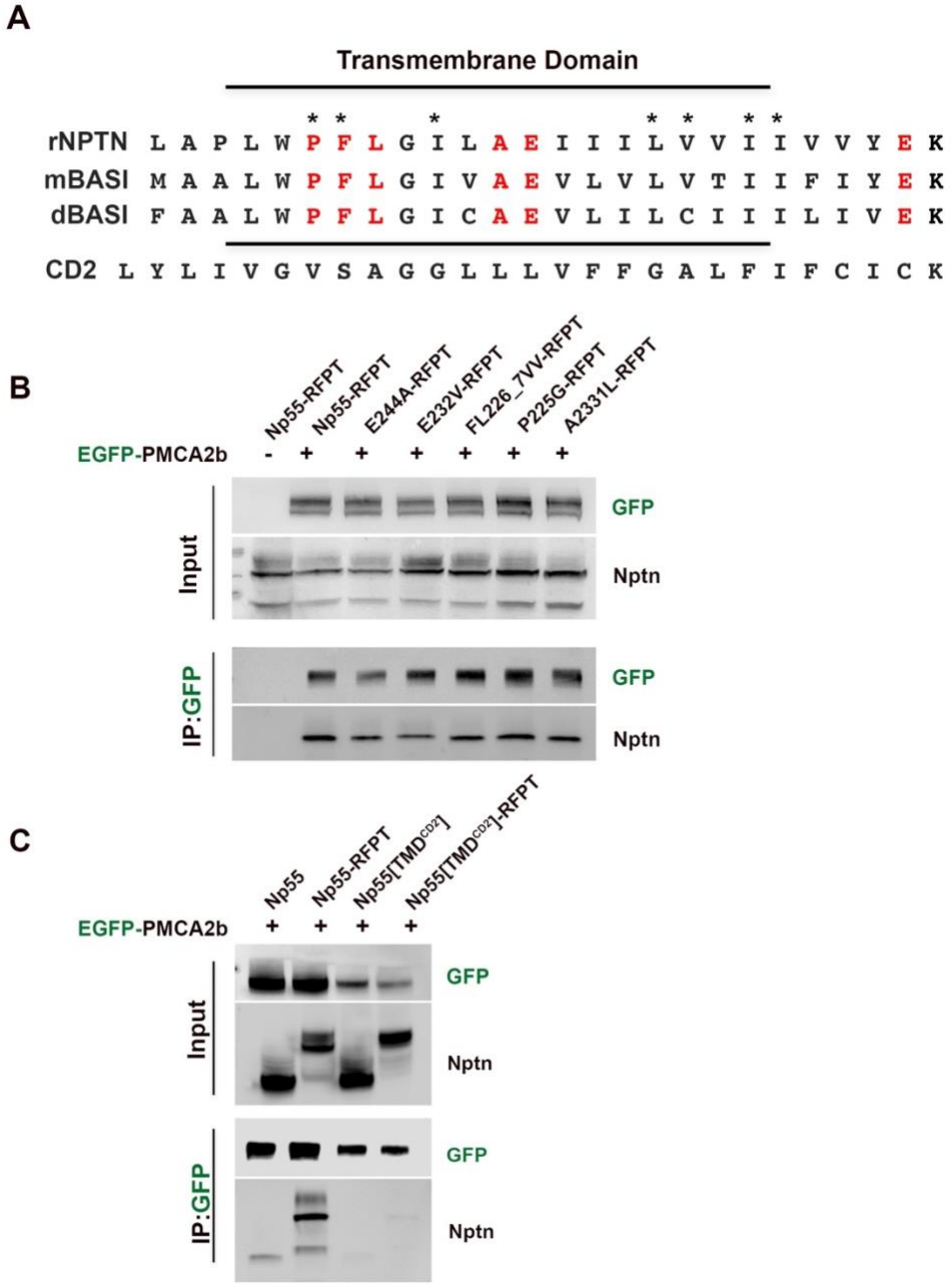

Figure 14: Mutational analysis of the TMD of Nptn and its interaction with PMCA2b
(A) Alignment of highly conserved TMD sequences of Basigin and Nptn from various species (d = drosophila, m = mouse, r = rat). The TMD sequence of CD2 is shown for comparison. Residues that were altered in this study are shown in red whereas those later identified by Gong et al. (2018) to interface with PMCA1 are labelled with a star. (B) Western blot analysis of input controls and anti-GFP-specific IPs derived from crude membrane fractions of HEK cells transfected with EGFP-PMCA2b and Nptn constructs as indicated, solubilized with digitonin (C)Control experiment with HEK cells co-transfected with EGFP-PMCA2b and tagged or non-tagged Np55 or Np55[TMD^{CD2}]. Representative blots come from three independent experiments.

4.7 Assesment of Ca^{2+} sensitivity of Np-PMCA and Basigin-PMCA interactions

The activity of PMCAs is regulated by cytosolic Ca^{2+}, specifically by Ca^{2+}/calmodulin binding to their cytoplasmic tail. Wondering whether Ca^{2+} might also affect the interaction between PMCA and Nptn or Basigin, I performed immunoprecipitation experiments on HEK cells expressing EGFP-PMCA2b and/ or TagRFP-tagged Np55 (Fig. 15A) or Basigin (Fig. 15B) and used lysis buffer containing either no Ca^{2+} (i.e. 1 mM EDTA) or 1 mM Ca^{2+}. Variants with the TMD replaced by the TMD of CD2 were included for both Np55 and Basigin to assess a possible, TMD-independent impact of Ca^{2+}, e.g. *via* the cytoplasmic domains. As expected, the TMD of Basigin was required to interact with PMCA (Fig. 15B). The results shown in Fig 15A and B, however, do not reveal Ca^{2+} effects on the interaction between Np55 or Basigin with PMCA.

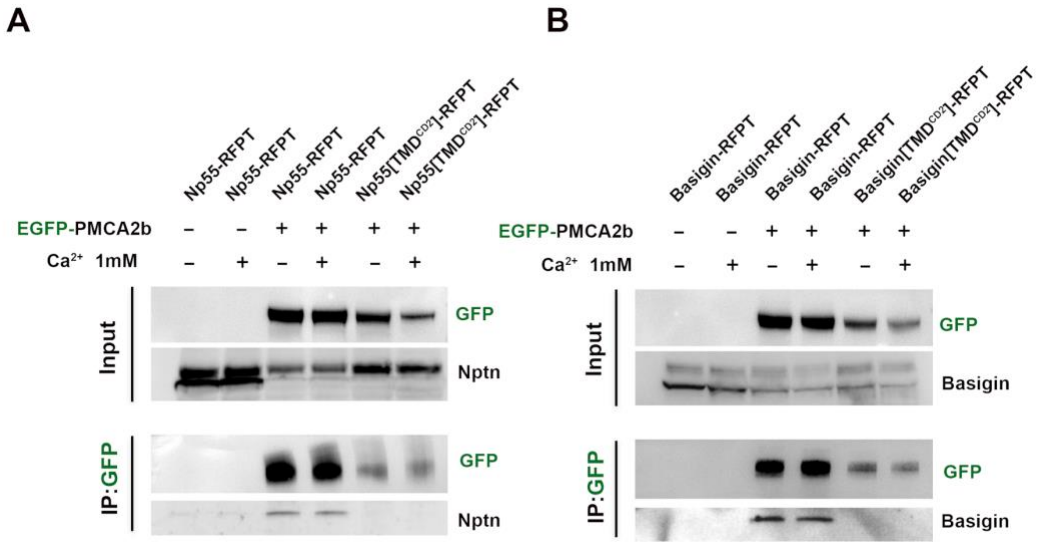

Figure 15: Characterization of the effect of Ca^{2+} on Np/Basigin-PMCAs complexes.

HEK cells were transfected with EGFP-tagged PMCA2b and TagRFPT-tagged Np55 and mutants (A) or TagRFPT-tagged Basigin and mutants (B). Co-IP was carried out with either 1 mM or 0 mM Ca^{2+} in the lysis buffer. Note that the presence or absence of Ca^{2+} at this step had no effect on the immunoprecipitation of Np55 or Basigin (bottom of lanes 3 and 4 in A, B). All the results were obtained from three independent experiments.

4.8 Heterodimerization of Nptn and Basigin

Nptn and Basigin can both associate with PMCA and both Nptn and Basigin can form homodimers (Smalla *et al.,* 2000, Yoshida *et al.,* 2000). Moreover, analyses on Nptn-PMCA complexes imply a 2:2 stoichiometry (Schmidt et al., 2017; Korthals et al., 2017; K.H. Smalla and T. Kaehne, pers. communication). This raises the question whether Nptn and Basigin can heterodimerize in a complex with PMCA. Although Basigin was not found in the proteomic analysis of synaptic Np65-immunoprecipitates (Leistner, 2016; P. Klemmer, K.H. Smalla and T. Kaehne, unpublished), this could be explained by the low level of Basigin in synaptic junctions or by disruption of the interaction by the detergent. Therefore, I tested whether the two proteins form complexes when co-expressed in HEK cells. For this, I used C-terminally EGFP-tagged Np55 variants, including the aforementioned wild type version $Np55^{DDEP}$, $Np55[TMD^{CD2}]$ and Np55-Δcyt as well as a variant lacking the extracellular Ig domains (Np55-ΔIgs; Fig. 16A) and co-expressed them with non-tagged mBasigin. Co-immunoprecipitations were performed using Triton X-100 (Fig 16B, left) or digitonin (Fig 16B, right) as detergents. All Np55 variants could bind to mBasigin and in contrast to the findings with Np55 and PMCA (Fig. 13B) no principle difference was observed between Triton- or digitonin-treated samples. This suggests that Nptn and Basigin can form heterodimers. The only region common to all 4 Np55 variants is the small extracellular region (TVLRVRSHLA) that usually is between the TMD and the Ig domains which might therefore be crucial for the interaction with Basigin.

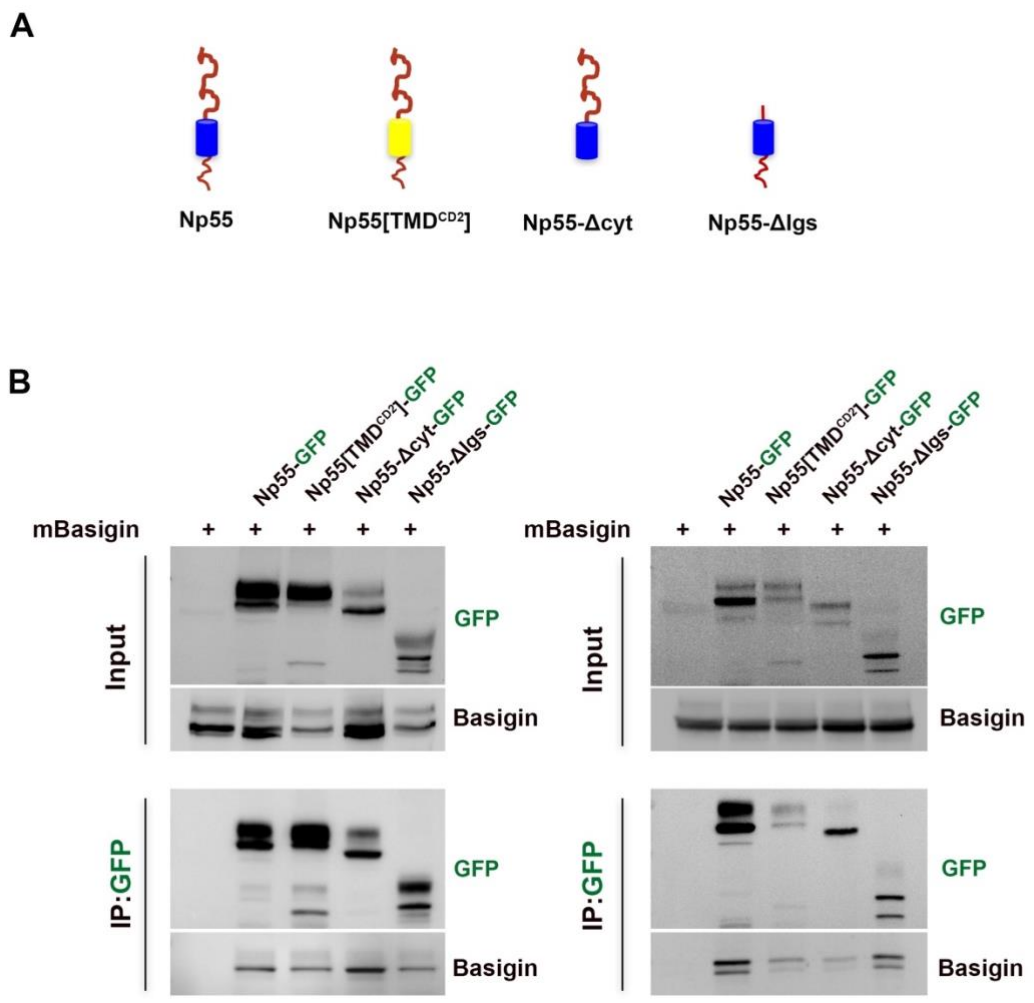

Figure 16: Heterodimerization between Nptn and Basigin.
HEK cells were transfected with GFP-tagged Np55 or one of three different mutants therof (A) and with mBasigin without tag. After 48 hours, cells were harvested using Triton-X100 (B, left) or digitonin (B, right). The blots are representative for three independent experiments.

In the course of these experiments I noticed that EGFP-tagged human Basigin when co-expressed with Np55-Δcyt almost completely disappeared. This was further analyzed by transfecting Np55-EGFP, mBasigin-EGFP and hBasigin-EGFP with or without non-tagged Np55 and Np55-Δcyt. The results showed that the intracellular domain of Nptn was required to stabilize both EGFP-tagged hBasigin and Np55. In contrast, mBasigin was stably expressed in the presence of Np55-Δcyt (Fig 17A and B). This observation might point to a protective role of the cytosolic domain of Np55 in homo- or heterodimers. It remains obscure, however, why mBasigin in contrast to

hBasigin and Np55 appears to be independent of such protection, as rNp55 and hBasigin share only two residues in their cytoplasmic domains that are not shared between mBasigin and hBasigin or rNp55 (Fig. 17C).

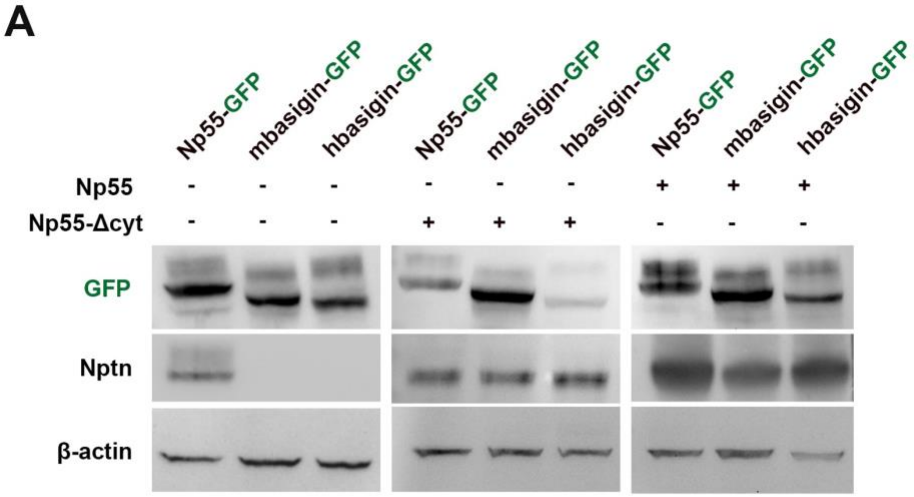

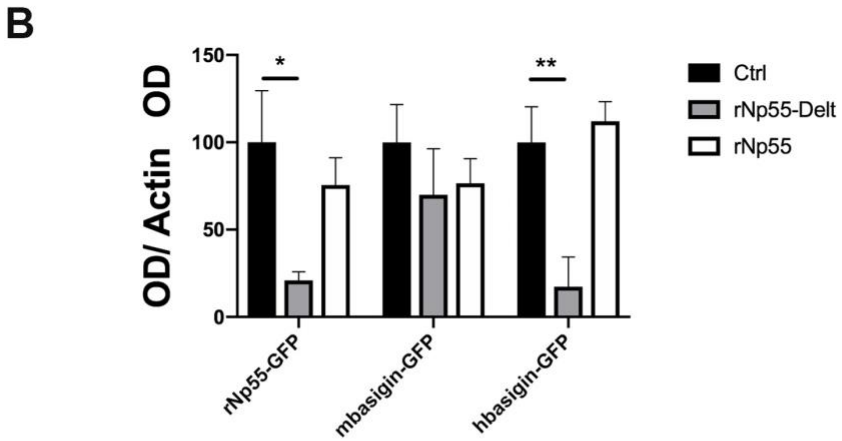

C

```
rNPTN55  KRKRPDEVPDDDEP-AGPMKTNSTN-NHKDKNLR
  mBASI  KRRKPDQTLDEDDPGAAPLKGSGTHMNDKDKNVRQRNAT
  hBASI  KRRKPEDVLDDDDAGSAPLKSSGQHQNDKGKNVRQRNSS
```

Figure 17: The cytosolic tail of Np55 modulates the level of hBasigin and Np55 but not of mBasigin.

(A) GFP-tagged Np55, hBasigin, mBasign were co-transfected with Np55 and Np55-Δcyt. 48 hours later, cells were harvested and analyzed by western blot with anti-actin as a loading control. Note that in the presence of Np55-Δcyt (middle panel), Np55-EGFP and hBasigin-EGFP were reduced as compared to respective lanes in the left and right panels (B) Intensity quantification of the western blots with the OD values obtained from three independent experiments. (C) Alignment of cytosolic domain sequences of rNp55 and Basigin from mouse

and human. Residues that are identical exclusively between rNp55 and mBasigin are in blue, those between rNp55 and hBasigin in red and those between mBasigin and hBasigin in green. All data were assessed by the mean ± SD with *P < 0.05, **P < 0.01 unpaired Student t-test.

4.9 Assessment of a possible gain-of-function

The biochemical assays show a pivotal role for Nptn in promoting stable expression of PMCAs. Moreover, Ca^{2+} measurements in Nptn-deficient immune cells and neurons revealed elevated levels of baseline cytosolic Ca^{2+} ($[Ca^{2+}]_i$) and delayed Ca^{2+} clearance after stimulation (Herrera-Molina *et al.,* 2017, Korthals *et al.,* 2017, Schmidt *et al.,* 2017). However, it remained unclear, if increased levels of Nptn or Basigin would affect PMCA-dependent control of Ca^{2+} homeostasis in neurons. To address this, we aimed at generating Ca^{2+} reporter constructs, which would allow for normalization to the level of Nptn or Basigin overexpression in the transfected neurons. For this I used a viral peptide sequence known as P2A that mediates a ribosome-skipping event, i.e. fails to form one specific peptide bond within the P2A sequence during translation (Daniels *et al.,* 2014, Szymczak *et al.,* 2004). This way two proteins are encoded by one transcript. I generated three such P2A constructs: 1. TagRFPT-P2A-GCamP5G (control); 2. Np55-TagRFPT-P2A-GCamP5G; and 3. Basigin-TagRFPT-P2A-GCamP5G (Fig 18A). I first expressed the control and Np55 constructs in HEK cells and analyzed the products by western blotting. The blots in Fig. 18B show that TagRFPT and TagRFPT-tagged Nptn variants were indeed well separated from GCamP5G. They also show that TagRFPT and the tagged Nptn variants when expressed from the P2A constructs reached very similar levels as their counterparts expressed from the conventional constructs and that the wild type Np55-TagRFPT version was able to elevate the levels of endogenous PMCA.

The constructs were used to transfect rat hippocampal neurons at DIV9. Ca^{2+} imaging was performed on dendritic branches at DIV14 and in the presence of TTX or CNQX/AP5 to prevent spontaneous Ca^{2+} signals. Individual recordings lasted for a total of 24 s. After 5 s of baseline recording, a train of 20 stimuli (1 ms each) was presented at 20 Hz to neuronal cultures on a coverslip (see the methods of Ca^{2+}

imaging for further details). This protocol allowed to trigger single Ca^{2+} spikes. The TagRFPT-normalized GCamP5 signals were used to determine the baseline and peak levels, and decay times were defined as the time between peak and a 90% decline from the peak, as exemplified in Fig18C.

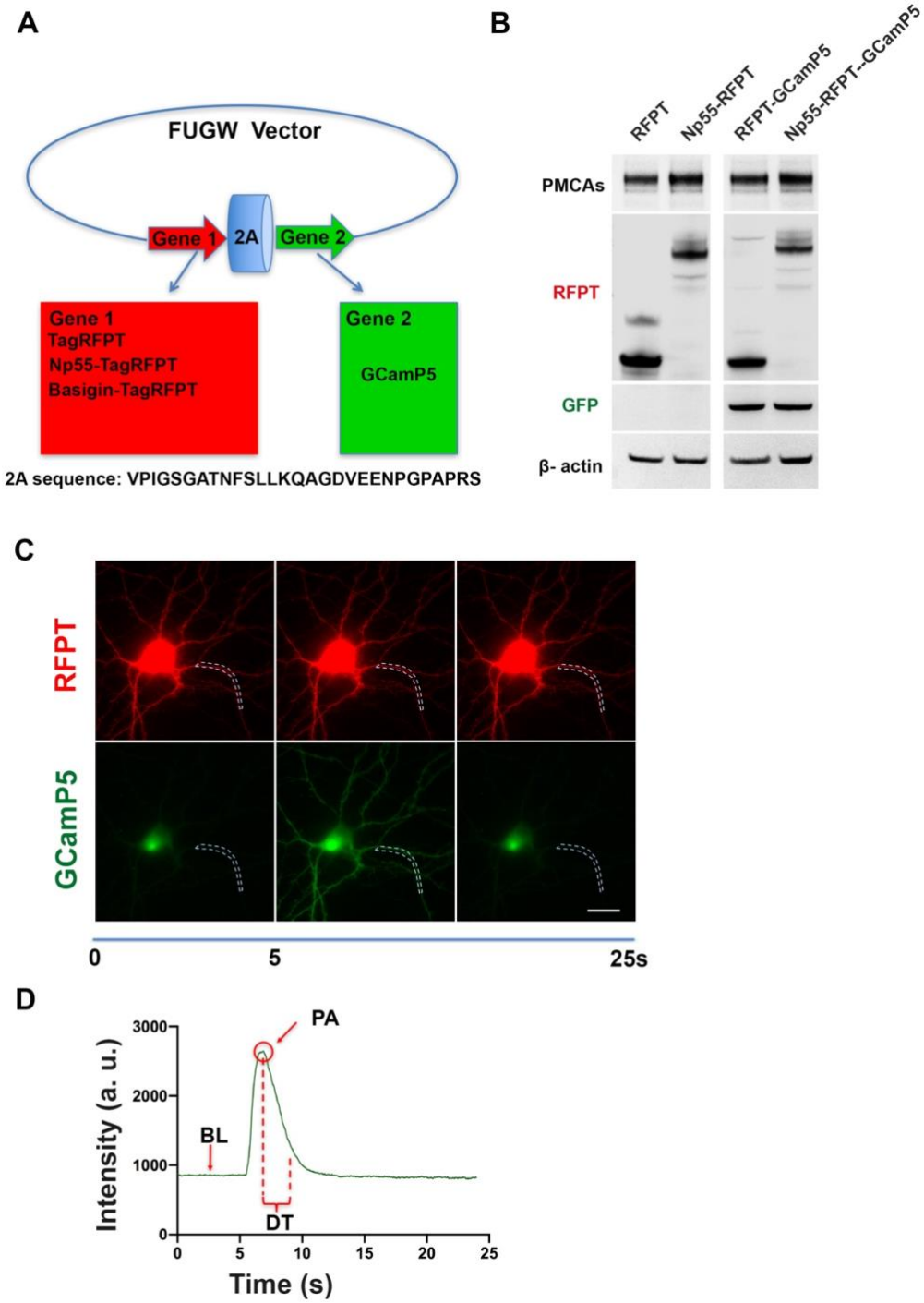

Figure 18: Design and evaluation of Np55-TagRFPT-P2A-GCamP5G and control constructs.

(A) Schematic representation of P2A constructs, which were generated on a FUGW lentiviral plasmid backbone. The 29 aa P2A sequence is shown and the ribosome skipping occurs between residues G24 and P25 (B) Western blot analysis on HEK cell lysates after transfection with conventional constructs (left) and with P2A constructs as indicated (right). TagRFPT and TagRFPT-tagged Nptn were detected by anti-RFP, GCamP5G was detected by anti-GFP and probing with anti- β actin served as a loading control. (C) Principle of monitoring Ca^{2+} in DIV14 hippocampal neurons. Left: a TagRFPT-positive control neuron was stimulated after 5 s of baseline Ca^{2+} recording. GCamP5-signals were typically recorded on 3 to 4 dendritic regions on the same neuron. The stippled line marks on such region. (D) For baseline measurements (BL) and peak amplitudes ($F-F_o$; PA), GCamP5G fluorescence was normalized to TagRFPT fluorescence. Decay times (DT) were determined for stimulated Ca^{2+} signals based on GCaMP5G signals only. The decay time was determined as the period between PA and 10% PA. Scale bar = 20 µm.

In a first set of experiments the neurons were transfected with RFPT-GCamP5 or Np55-RFPT-GCamP5 and spontaneous activities were blocked by TTX (0.2 µM) to prevent action potentials. Five minutes after a first stimulation and measurement, the PMCA inhibitor carboxyeosin (CE, 10 µM) was added for 10 minutes, and then excessive CE was washed out. Another stimulation and measurement was performed 10 minutes later (Fig. 19A). Interestingly, transfection with Np55-TagRFPT-GCamP5 did not affect Ca^{2+} baseline levels compared to the control (Fig. 19B). Peak levels were also not significantly different (Fig. 19C). In contrast, the decay times showed a mild but statistically significant decrease when Np55-TagRFPT was expressed (Fig. 19D). As expected, after addition of CE, decay times were increased in TagRFPT-expressing control hippocampal neurons (Fig. 19D). Decay times in Np55-TagRFPT-expressing neurons were also increased significantly after CE, but did not reach the level of CE-treated controls (Fig. 19D). This strongly suggests that Np55-TagRFPT enhanced extrusion of Ca^{2+} in a PMCA-dependent manner.

In another set of experiments, TTX was replaced by combined AP5 and CNQX to block both NMDA- and AMPA-type glutamate receptors, and thereby excitatory synaptic transmission between the neurons. With this treatment, Np55-TagRFPT again did not affect baseline $[Ca^{2+}]_i$ (Fig. 19E) nor peak levels (Fig. 19F) in comparison to controls. Moreover, in contrast to the TTX-treated neurons, Ca^{2+} extrusion was not facilitated

compared to the control group (Fig.19G). Furthermore, CE did not significantly change decay times in controls or Np55-TagRFPT-expressing controls (Fig. 19G). Surprisingly, CE had no effect in neither the controls nor the Np55-TagRFPT transfected cells.

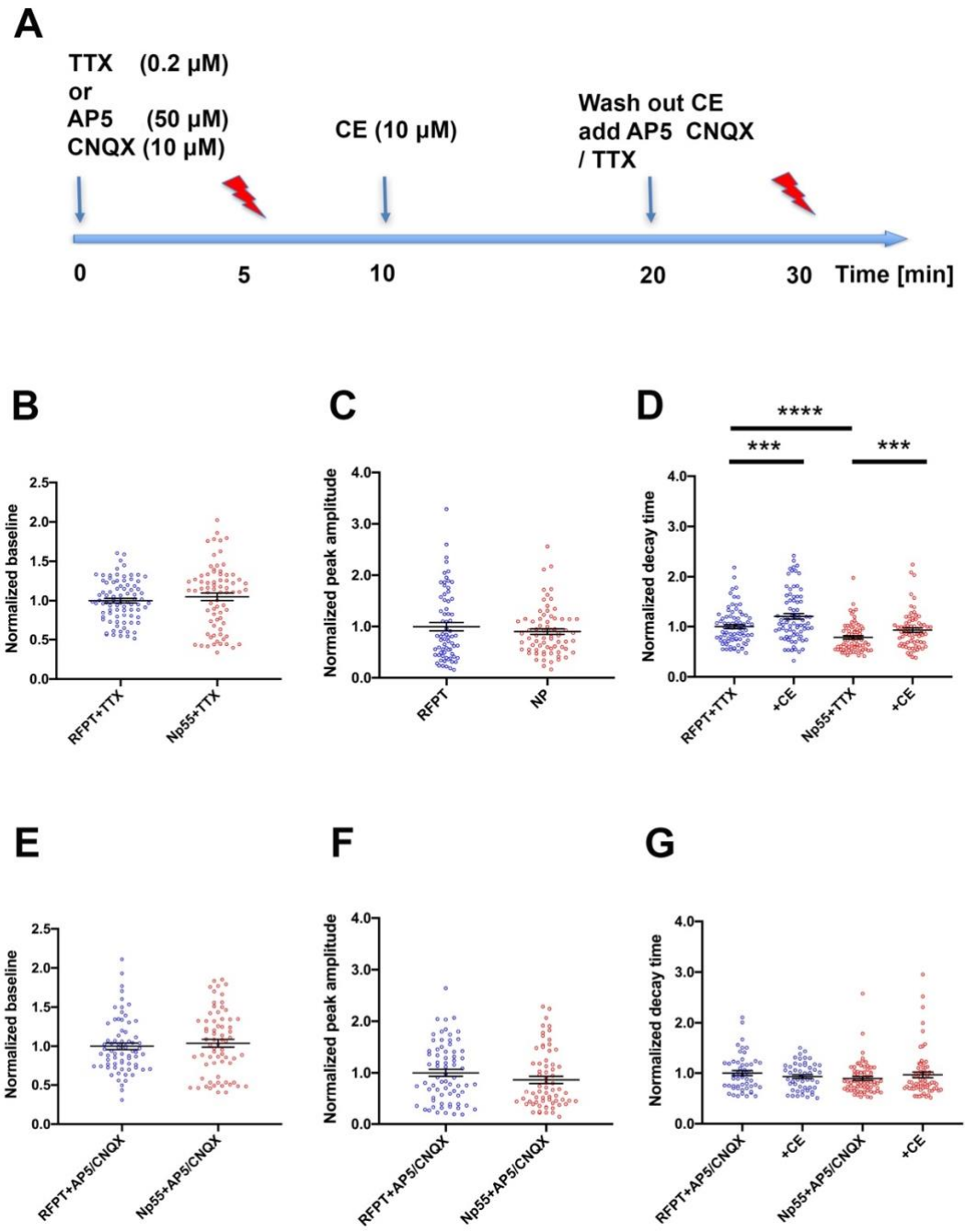

Figure 19: Ca^{2+} imaging in DIV14 hippocampal neurons expressing TagRFPT or Np55-TagRFPT

(A) Time course of drug supply and stimulation/ imaging. TTX, AP5 and CNQX, and CE were added at indicated concentrations and time points to inhibit neuronal activity and PMCAs, respectively. Arrows mark stimulation trains as described in the text. Washout of CE was necessary as the drug strongly interferes with GCamP5 imaging. (B-G) Dot plots of Ca^{2+} measurements in the presence of TTX (B-D) or AP5 and CNQX (E-G). (B, E) TagRFPT-normalized Ca^{2+} baseline levels. (C, F) TagRFPT-normalized Ca^{2+}peak levels. (D, G) Decay times in the presence of activity inhibitors without or with CE. Data were normalized to the mean value of the control in each of 3 independent experiments and then pooled. Each experiment includes measurements of a total of 12 to 16 branches from 4 to 5 neurons of each group. Dot blots are shown with mean ± SEM with *P < 0.05, **P < 0.01, ***P < 0.001. Mann Whitney test was used for groups comparisons, and a Wilcoxon mateched pairs test within group comparisons.

These results show that increased levels of Nptn promote Ca^{2+} extrusion in dendrites of stimulated hippocampal neurons, and this effect was abolished, when glutamate receptors were blocked. To evaluate whether Basign could promote the function of PMCA and thus compensate for loss of Nptn, I repeated the above experiments using Basigin-TagRFPT-P2A-GCamP5G instead of the respective Np55 construct. As shown in Fig. 20, the outcome was almost the same as for Np55-TagRFPT. Expression of Basigin-TagRFPT did not affect baseline or peak levels (Fig. 20A, B, D, E). Importantly, like Np55-TagRFPT, Basigin-TagRFPT significantly decreased decay times and this effect was partially reverted when CE was applied (Fig. 20C). Again, this effect was only observed in the presence of TTX (Fig. 20C) but not in the presence of AP5 plus CNQX (Fig. 20F).

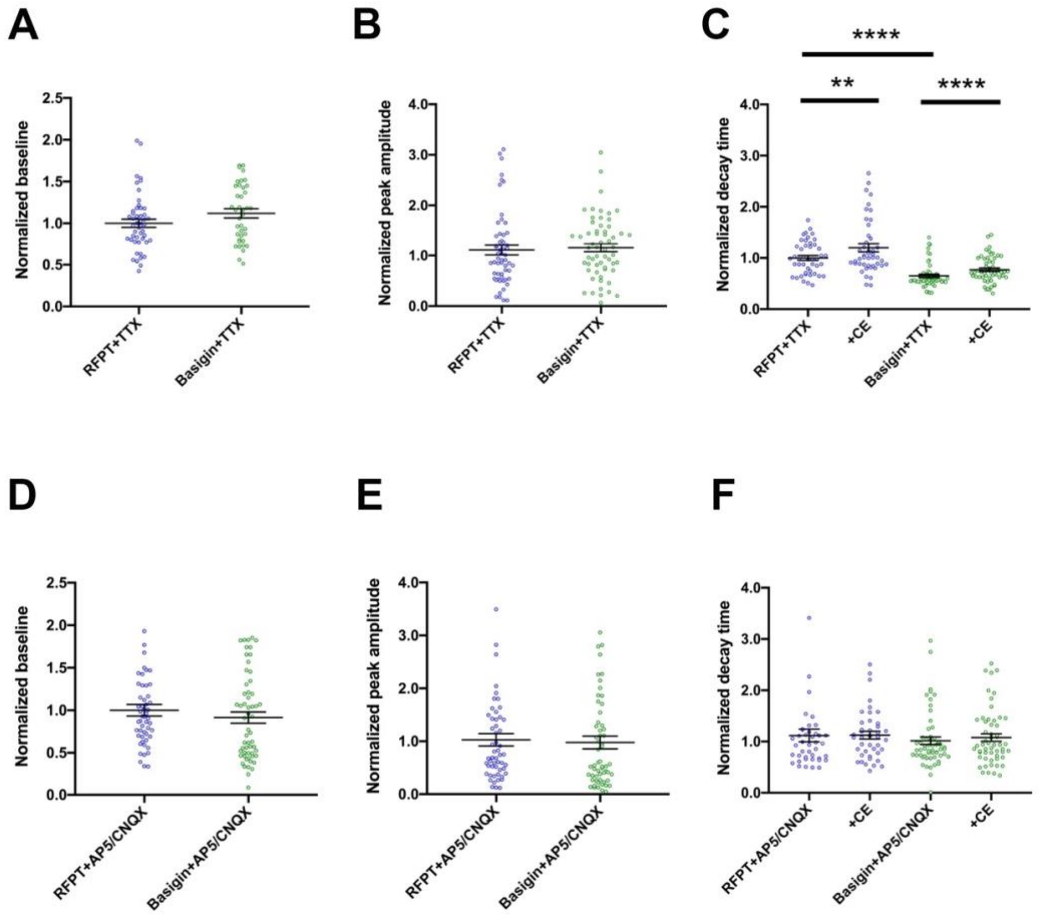

Figure 20: Ca^{2+} imaging in DIV14 hippocampal neurons expressing TagRFPT or Basigin-TagRFPT.

(A-F) Dot plots of Ca^{2+} measurements in the presence of TTX (A-C) or AP5 and CNQX (D-F). (A, D) TagRFPT-normalized Ca^{2+} baseline levels. (B, E) TagRFPT-normalized Ca^{2+} peak levels. (C, F) Decay times in the presence of acitivity inhibitors without or with CE. Data were normalized to the mean value of the control group in each of 3 independent experiments and then pooled. Each experiment includes measurements of a total of 12 to 16 branches from 5 neurons of each group. Dot blots are shown with mean ± SEM with $*P < 0.05$, $**P < 0.01$, $***P < 0.001$. Mann Whitney test was used for groups comparison, and a Wilcoxon mateched pairs test for within group comparisons.

4.10 Prolonged network silencing affects expression levels of Basigin, but not Nptn and PMCA

The strong up-regulation of Basigin in the absence of Nptn but also the changes of

Nptn expression in the developing and aging brain (Langnaese *et al.,* 1997, Marzban *et al.,* 2003, Schmidt *et al.,* 2017) suggested that long term changes in activity might affect the levels of these proteins and thus of PMCAs. To test this, I silenced DIV21 rat cortical neurons by pharmacological manipulations for 2 days and evaluated Nptn, Basigin and PMCAs by quantitative western blot analysis. The synaptic activity was blocked by adding the NMDA- and AMPA-receptor antagonists D-AP5 (10 µM) and CNQX (50 µM) (Fig. 21A) The propagation of action potentials were suppressed by TTX, these treatments have been shown not to affect the cells' survival (Lazarevic *et al.,* 2011). In tendency, following these treatments, the total expression levels of Nptn, PMCAs and Basigin were lower, but a statistically significant reduction was only observed for Basigin after treatment with D-AP5 and CNQX (Fig. 21 B, C).

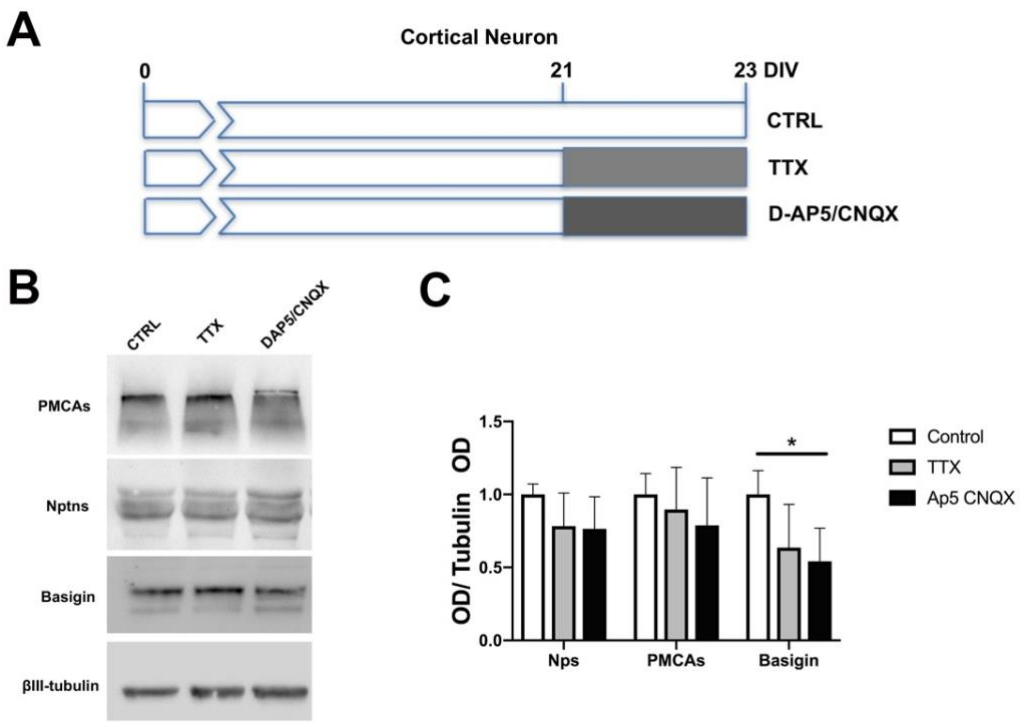

Figure 21: Expression levels of Nptn, Basigin and PMCAs upon neuronal network modulation.

(A) Timing of the pharmacological treatment for the experiment. Rat cortical neurons were exposed to TTX or D-AP5/CNQX to silence the neuronal network activity at DIV 21 and two days later the neurons were collected for western blot analysis. (B) Representative Western blots for PMCAs, Nptn, Basigin and β III tubulin. (C) Quantification of the blots, the OD values

were normalized to the value of βIII tubulin. All the values were obtained from four independent experiments. The results were analyzed by unpaired Student t-test. Data are mean ± SEM with *P < 0.05.

4.11 Nptn$^{-/-}$ mice are deaf

Both constitutive and induced, pan-neuronal knock out of Nptn leads to severe impairment in learning and memory (Bhattacharya *et al.,* 2017). The widespread expression of Nptn, in particular Np55, also implies a possible involvement of Nptn in sensory perception. In fact, while an essential function for Nptn in the retina has been ruled out (Carrott *et al.,* 2016), severe hearing deficits were reported for Nptn null mutants (Bhattacharya *et al.,* 2017) and Nptn alleles have been identified in independent screens for mutations that cause deafness in mice (Carrott *et al.,* 2016, Zeng *et al.,* 2016). Interestingly, the latter studies suggested different mechanisms underlying this phenotype. Carrott et al. (2016) proposed a pivotal role for Np65 at synapses between inner hair cells (IHCs) and afferent spiral ganglion neurons (SGNs). Zeng et al. (2016) assigned the crucial role for Nptn within the inner ear to Np55 in outer hair cells (OHCs). Moreover, both studies did not consider the impact of Nptn on PMCA expression. We therefore revisited the role of Nptn in the auditory system using Nptn null mutants as well as conditional and inducible Nptn-KO mice.

Multichannel electrophysiological recordings followed by current source density (CSD) analyses were used to investigate the response of the auditory cortex (AC) to pure tone and click stimulation in anaesthetized animals (Happel *et al.,* 2010, Saldeitis *et al.,* 2014) (Fig. 22A). In both young (2-month-old) and adult (5-month-old) control mice, a typical canonical CSD pattern of sensory evoked processing with thalamocortical input of layers III/IV and sink activity across layers I/II and V/VI layers was displayed. These click responses were significantly different from cortical activity during pause conditions without acoustic stimulation (Fig. 22A, left). In Nptn$^{-/-}$ mice of respective age, click stimulation virtually did not evoke responses different from activity profiles during pause condition (Fig. 22A, right). Since, however, parallel recordings within the AC of Nptn$^{-/-}$ mice did not reveal significant changes in basal neurotransmission (data

acquired by Dr. Yuanxiang Pingan at LIN; (Lin *et al.,* 2021), one can conclude that the main cause for severe hearing deficits lies upstream of cortical processing. I therefore tested 2-months-old control and Nptn$^{-/-}$ mice for responsiveness in the auditory periphery. Monitoring auditory brain stem responses (Willott, 2006) (ABR) revealed that the hearing threshold was 90 dB (n = 3) for 4-month-old Nptn$^{-/-}$ as compared to wild type littermates with 30 to 40 dB (n = 3) (Fig. 22B). These results revealed deafness in Nptn KO mice ($p < 0.0001$). I also determined the ABR in 3-month-old Nptn$^{lox/loxEmx1Cre}$ mice and found that the hearing threshold is very similar to wild type (4-month-old). This suggests that Nptn is not required in central glutamatergic neurons for hearing capacitiy.

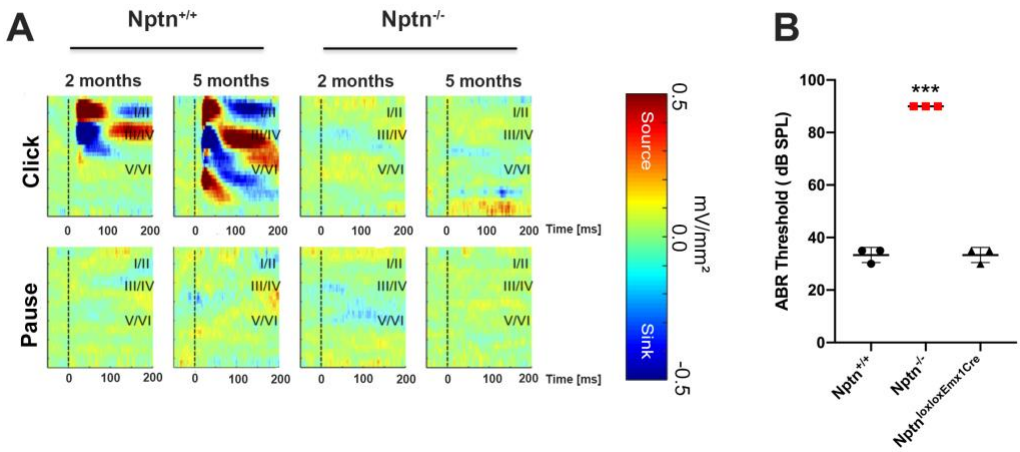

Figure 22: Tone-evoked cortical processing (CSD analysis) and auditory brainstem responses in Nptn$^{+/+}$ and Nptn$^{-/-}$ mice.

(A) Top row: click-evoked CSD responses in 2- and 5-month-old Nptn$^{+/+}$ (left) and Nptn$^{-/-}$ (right) mice. Activity evoked by thalamocortical input was only observed in the WT mice. Bottom row: representative CSD patterns in pause conditions. All cortical layers (I/II, III/IV and V/VI) of the auditory cortex are displayed. (Nptn$^{+/+}$, 2 months, n= 6; 5 months, n=7,) and Nptn$^{-/-}$ (2 months, n = 6; 5 months, n= 3). (B) ABR measurement of Nptn$^{+/+}$, Nptn$^{-/-}$ (red circles) and Nptn$^{lox/loxEmx1Cre}$ mice (blue triangles) (n=3 per group; 1-way ANOVA, $F_{(2,6)} = 480.5$; *** $p \leq 0.0001$). Thresholds in Nptn$^{-/-}$ mice reached our criterion for deafness (>85dB; In collaboration with Max Happel and Michael Brunk).

4.12 Severe reduction of PMCAs in Nptn$^{-/-}$ hair cells

In many neuron types, Ca^{2+} ions can be extruded across the plasma membrane by PMCAs and by sodium-calcium exchangers (NCX) and the relative contribution of either module may vary between neuron types (Lisek *et al.,* 2018). In cochlear hair cells, expression of NCX is questionable (Fettiplace and Nam 2019) and these cells may therefore be expected to be particularly dependent on PMCAs. PMCA1 and 2 have previously been shown to be differentially expressed in inner and outer hair cells (Fettiplace and Nam 2019). I first evaluated the expression of Nptn relative to these PMCA isoforms in the organ of Corti of wild type mice. For this, I performed quadruple fluorescent labeling of cochlear whole mount preparations (4-5 month-old mouse) including DAPI to label nuclei, phalloidin to label actin bundles, antibodies against Nptn and antibodies against PMCA1 (Figure 23A, a-d) or PMCA2 (Figure 23B, a-d). Confocal imaging revealed that Nptn is expressed in both OHCs and IHCs (Fig 23Ab, 23Bb). In IHCs it was localized mainly to the plasma membrane around the cell bodies, where it co-localized with PMCA1 (Fig 23A, b-d). In contrast, in OHCs Nptn was enriched in the stereocilia (Fig. 23b and b'), where also PMCA2 is highly enriched (Fig. 23c', d'). Nptn thus reflects the subcellular localization of the predominant PMCA isoform in either type of hair cell.

The same labeling cocktail was also applied to cochlear whole mounts from Nptn$^{-/-}$ mice (Fig. 23A, e-h, 18B, e-h). Absence of Nptn immunolabeling confirmed the specificity of the antibody (Fig. 18A, f and 18B, f'). PMCA1 immunofluorescence was reduced substantially but not completely absent in IHCs (Fig. 23A, g and h). PMCA2 immunofluorescence was virtually lost in the Nptn$^{-/-}$ OHCs (Fig. 23B, g' and h').

Assessment of Nptn and PMCAs in cochlear preparations of Nptn$^{lox/loxEmx1Cre}$ mice did not reveal differences when compared to wild type (Fig 23A, i-l; Fig 23B, l' and l'). Thus, although IHCs are glutamatergic, they remain unaffected by the Emx1Cre-induced knock out of Nptn.

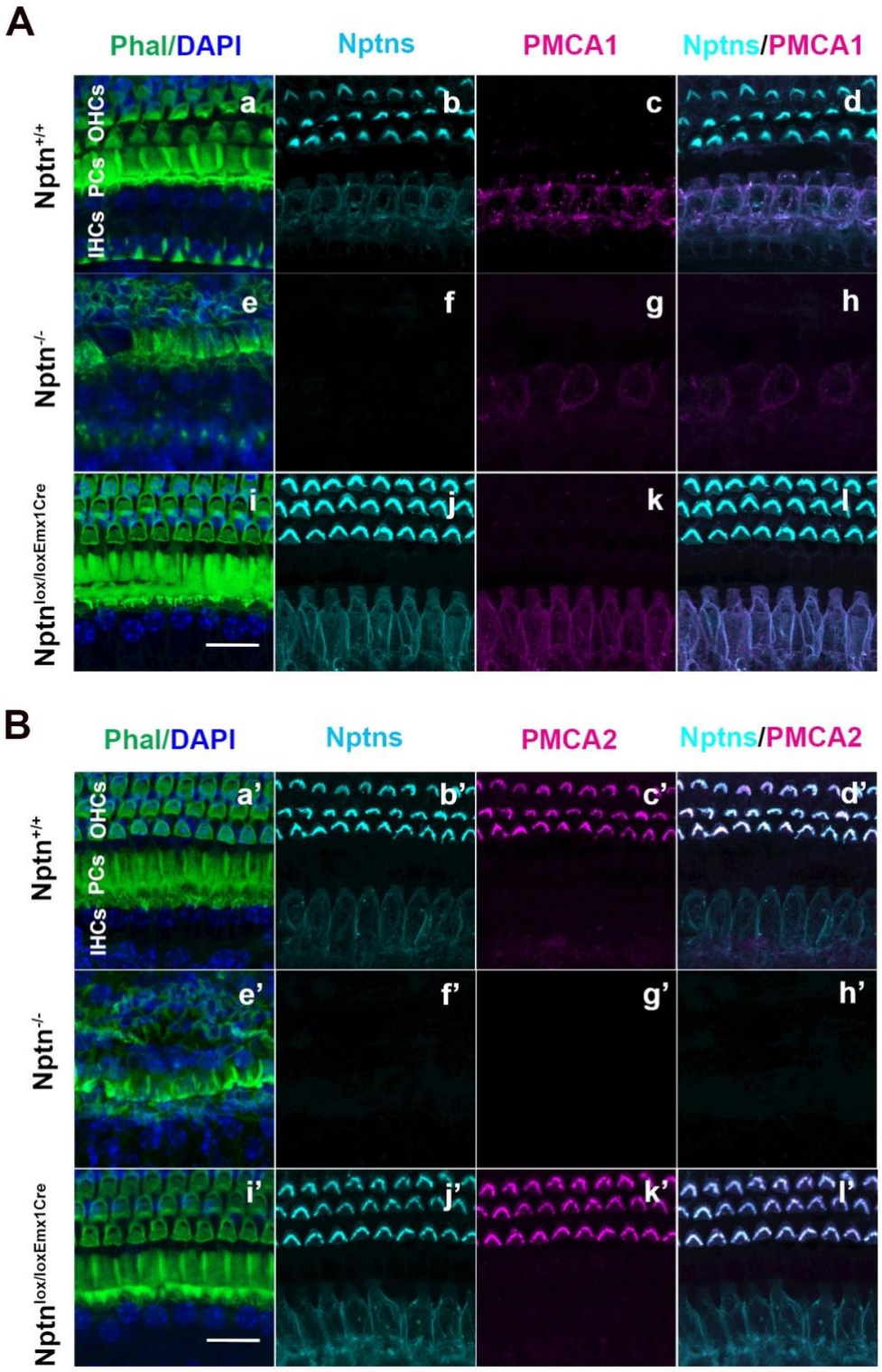

Fig. 23 Nptn and PMCA in cochlear hair cells of wild type and Nptn-mutant mice. Cochlea whole mounts from Nptn$^{+/+}$, Nptn$^{-/-}$ and Nptn$^{lox/loxEmx1Cre}$ mice were stained with Phalloidin (Phal), DAPI, and with antibodies against Nptns and PMCA1(A) or PMCA2 (B). Neuroplastin was detected at the plasma membrane around IHC bodies (Ab, j) and at the stereocilia of OHCs (Bb, j) where it co-localized with PMCA1 (Ac, d, k, l) and PMCA2 (Bc, d, k.,

l), respectively. The pillar cells (PCs), which separate IHCs and OHCs show little if any expression of Nptn and PMCAs. Note the differential expression of PMCA1 and PMCA2. Scale bar= 25 µm.

4.13 Absence of Np65 immunoreactivity in the cochlea

Previous studies presented controversial results concerning the expression and role of Np65 in the cochlea (Carrott *et al.,* 2016, Zeng *et al.,* 2016). The exclusive potential of Np65 to form homophilic adhesion complexes across the synaptic cleft might be crucial for proper synapse formation between IHCs and afferent neurons (Beesley *et al.,* 2014, Carrott *et al.,* 2016, Herrera-Molina *et al.,* 2014). I therefore used a Np65-specific antibody for staining on mid-modiolar sections and whole mounts of the cochlea. As depicted in Fig. 19A and B, this antibody failed to detect Np65 in both IHCs and OHCs. The same antibody when applied to AC preparations resulted in robust labeling that was specific, as it was not observed in samples from both $Nptn^{-/-}$ and $Nptn^{lox/loxEmx1Cre}$ mice (Fig. 24C; Herrera-Molina *et al.,* 2017). I also performed western blot analyses on mouse inner ear samples, which, in addition to the cochlea contain the vestibular system and at least part of the efferent and afferent nerves (Fig. 24D). In these samples, a distinct, Np65-specific signal was detectable (Fig. 24E). It is therefore possible that the Np65-specific epitope is masked in cochlear whole mount preparations, (precluding detection by immunolabeling in situ) or that the signal is derived from non-cochlear parts of the inner ear samples.

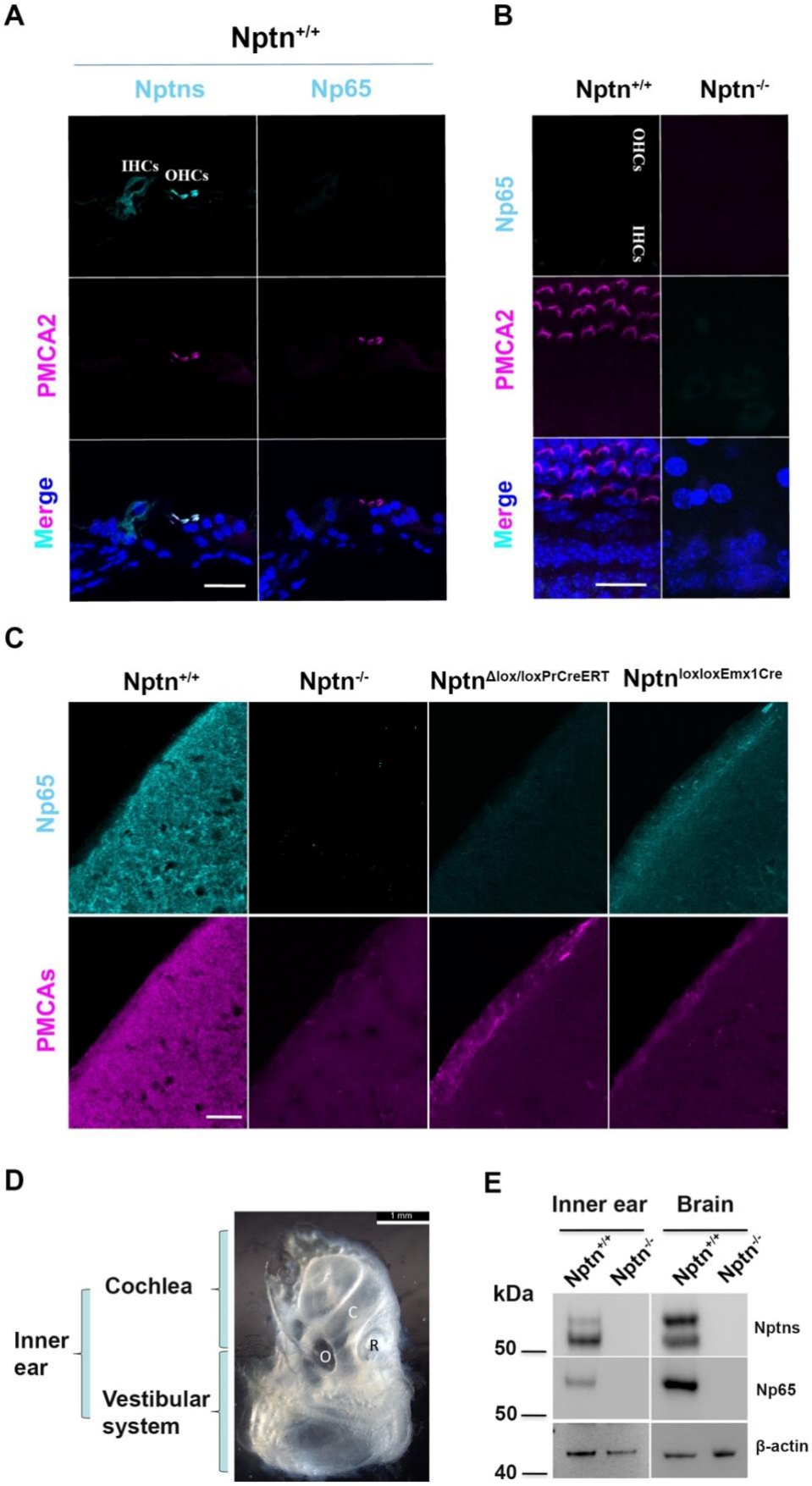
A
Nptn+/+
Nptns
Np65
IHCs
OHCs
PMCA2
Merge
B
Nptn+/+
Nptn-/-
Np65
OHCs
IHCs
PMCA2
Merge
C
Nptn+/+
Nptn-/-
NptnΔlox/loxPrCreERT
NptnloxloxEmx1Cre
Np65
PMCAs
D
Inner ear
Cochlea
Vestibular system
1 mm
C
R
O
E
Inner ear
Brain
Nptn+/+
Nptn-/-
Nptn+/+
Nptn-/-
kDa
50
50
40
Nptns
Np65
β-actin

Fig. 24 Np65 is not dectable in cochlear hair cells

(A) Mid-modiolar cochlea sections form wild type mice were stained with DAPI, and antibodies against PMCA2 and against Nptn (Np55 + Np65; left panel) or Np65 alone (right panel). Note immunoreactivity for Nptn but not Np65. Scale bar = 30 µm. (B) Cochlear whole mounts of $Nptn^{+/+}$ and $Nptn^{-/-}$ mice were labeled with DAPI, antibodies against PMCA2, and antibodies specific for Np65. Np65 could not be detected in inner (IHC) or outer hair cells (OHC). Scale bar = 20µm. (C) Section from the auditory cortex of $Nptn^{+/+}$, $Nptn^{-/-}$, $Nptn^{lox/loxEmx1Cre}$ and $Nptn^{\Delta lox/loxPrCreERT}$ mice, stained with anti-Np65 and anti-pan-PMCA. (D) Dissected inner ear of mouse, oriented such that the cochlea (C) with the round and oval windows (R, O) are on top of vestibular system; image is modified from (Kuhn *et al.,* 2012). Scale bar = 100µm. (E) Western blot analysis of expression of Nptn and Np65 in the inner ear and brain. Note the detection of a Np65-specifc band in the inner ear sample.

4.14 Nptn is required for survival of hair cells and spiral ganglion neurons

While the immunofluorescent staining revealed profound loss of PMCAs in $Nptn^{-/-}$ deficient cochlea, the simultaneous DAPI and phalloidin labeling pointed to severe effects on cochlear morphology in $Nptn^{-/-}$ mice (Fig 23Ae, Be). This could mean that the loss of PMCA1 and PMCA2 could, at least in part, be due to the loss of hair cells. To further elaborate on this, I aimed at quantifying the number of hair cells in the organ of Corti in control and mutant conditions. To this end I included an antibody against myosin VIIa to label both OHCs and IHCs in the cochlea of 4- to 5-month-old mice (Fig. 25A). Both myosin VIIa and DAPI positive hair cells were counted from the apical to the basal part of the organ of Corti in whole mount preparations. The results showed that, compared to wild type, the number of both OHCs and IHCs were dramatically reduced in all areas (apex, middle, base) of the organ of Corti in $Nptn^{-/-}$ mice (Fig. 25B). In contrast, $Nptn^{loxloxEmx1Cre}$ mice displayed no significant difference to controls (Fig. 25B), which is in an agreement with normal ABR and unchanged Nptn levels in the hair cells of this genotype. These results suggest that loss of Neuroplastin could lead to the degeneration of hair cells in the adult mice and further affect the hearing capacity.

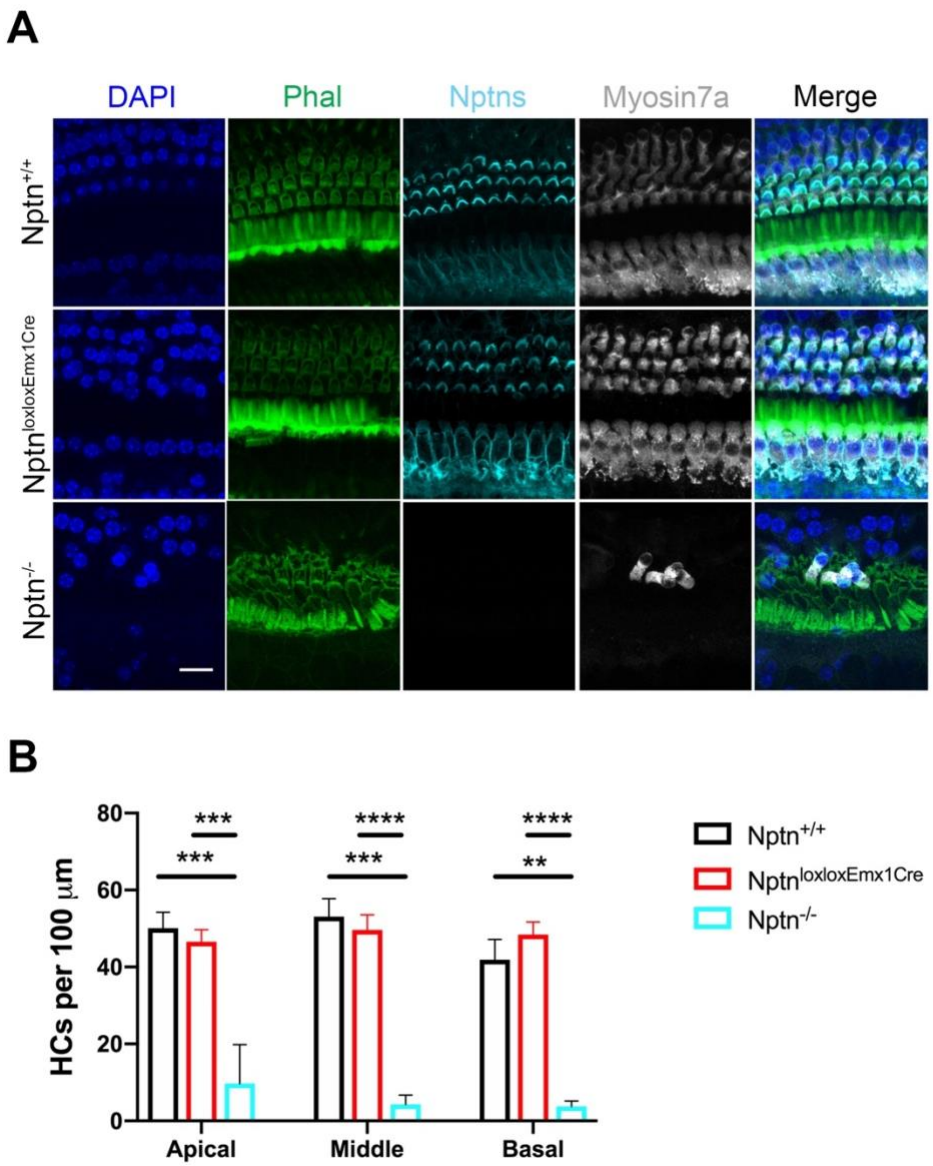

Fig.25. Quantitative immunfluorescent analysis of cochlear hair cells in adult mice
(A) Cochlea whole mounts from Nptn$^{+/+}$, Nptn$^{-/-}$ and Nptn$^{lox/loxEmx1Cre}$ mice were labelled with Phalloidin (Phal), DAPI, anti-Nptn and anti-myosin VIIa. Representative confocal images of the middle turn of the cochlear of 4- to 5-month-old mice are shown. (B). Quantification of cochlear hair cells as identified by myosin VIIa-positive labeling in the apical, middle and basal areas of cochlea. (Nptn$^{+/+}$, n=3; Nptn$^{lox/loxEmx1Cre}$, n=4; Nptn$^{-/-}$, n=5). All data were assessed by 1-way ANOVA with Dunnett’s multiple comparisons test, * p⩽0.05; ** p⩽0.01; *** p⩽0.001; **** p ⩽0.0001. Scale bar = 15 μm.

For further characterization of cellular deficits in the cochlea that might add to the hearing loss in Nptn$^{-/-}$, I assessed the density of spiral ganglion neurons (SGNs), which

innervate the hair cells *via* efferent fibers. Anti-Nptn staining revealed robust expression of Nptn in these cells, which was abolished in SGN of Nptn$^{-/-}$ but not of Nptn$^{lox/loxEmx1Cre}$ mice (Fig. 26A). Again, I performed quantitative immunofluorescent analyses along the different, i.e the apical, middle and basal parts of the cochlea. Specifically, I focused onto the SGN cell bodies in the so-called Rosenthal canal in the cochlea of 4- to 5-month-old Nptn$^{+/+}$, Nptn$^{-/-}$ and Nptn$^{lox/loxEmx1Cre}$ mice. A neuron-specific anti-β-III tubulin antibody (TuJ) was included to distinguish SGN from other, DAPI-positive cell types in the area (Fig. 26A). A significantly decreased cell density of SGN was observed in the middle and basal parts of the cochlea of Nptn$^{-/-}$ versus Nptn$^{+/+}$ and Nptn$^{lox/loxEmx1Cre}$ mice (Fig. 26B). Reduction of SGN density in the apical area did not reach statistical significance (Fig. 26B).

Although loss of Nptn causes a significant reduction of SGN density in at least the middle part and at the base of the cochlea it can hardly account for the complete hearing loss. The analysis further showed that Nptn persists in the SGNs of Nptn$^{lox/loxEmx1Cre}$ mice, meaning that impairment of this cell type is not to be considered for the interpretation of behavioral phenotypes associated with this conditional Nptn knockout.

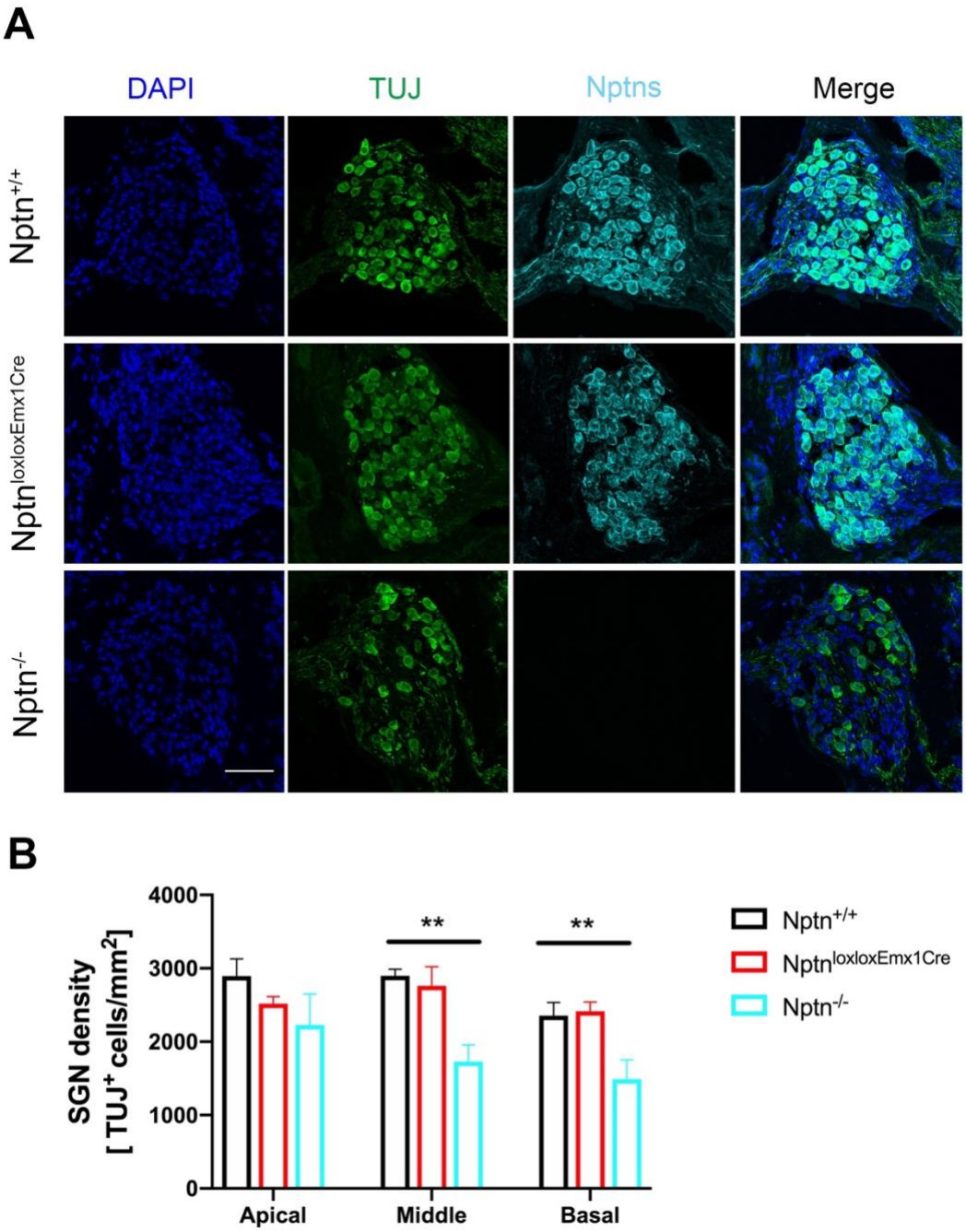

Fig.26. Analysis of cell density of spiral ganglion neurons (SGNs)

(A) Cochlea sections from 4- to 5-month-old $Nptn^{+/+}$, $Nptn^{-/-}$ and $Nptn^{lox/loxEmx1Cre}$ mice were labelled with DAPI, anti-β-III Tubulin (TUJ) and anti-Nptn. Representative confocal images depict cells within the Rosenthal canal at the middle cochlear turn. SGNs are identified as TUJ-positive cells. (B). Quantification of the density of SGNs. The density of SGNs in the middle and basal but not in the apical area were significantly reduced in $Nptn^{-/-}$ (n=4) but not in $Nptn^{lox/loxEmx1Cre}$ (n=3) in comparison to $Nptn^{+/+}$ (n=3). All data were assessed by the mean ± SEM with 1-way ANOVA with Dunnett's multiple comparisons test, * $p \leqslant 0.05$; ** $p \leqslant 0.01$; *** $p \leqslant 0.001$; **** $p \leqslant 0.0001$. Scale bar = 50 µm.

4.15 Loss of PMCA2 precedes outer hair cell loss

The severely reduced number of hair cells in the cochlea of adult Nptn$^{-/-}$ mice could be the result of failed development or of an ongoing degeneration of the cells. To discriminate between these possibilities, I pursued a qualitative assessment of IHCs and OHCs in the cochlea of young control and Nptn$^{-/-}$ animals (P18). In addition to DAPI and antibodies against Nptn and PMCA1 or PMCA2, an antibody against parvalbumin was used to outline the morphology of hair cells (the anti-myosin VIIa antibody could not be applied together with the anti-PMCA antibodies). Strikingly, at this young age, IHCs of Nptn$^{-/-}$ mice still displayed PMCA1 levels similar to wild type and rather normal morphology (Fig. 27A). In OHCs, however, PMCA2 was aready strongly reduced in the stereocilia, while the laminar arrangement of the OHCs appeared to be moderately affected (Fig. 27B). The stereocilia were still largely present (see below). These observations argue for a degenerative process in the cochlea of Nptn$^{-/-}$ animals. PMCA2 expression in OHCs relies on Nptn from early onwards, whereas PMCA1 in IHCs could persist to a considerable extent. This finding contrasted with observations in the CNS, where in the absence of Nptn, PMCA2 was often less affected than PMCA1 (e.g. Fig. 6).

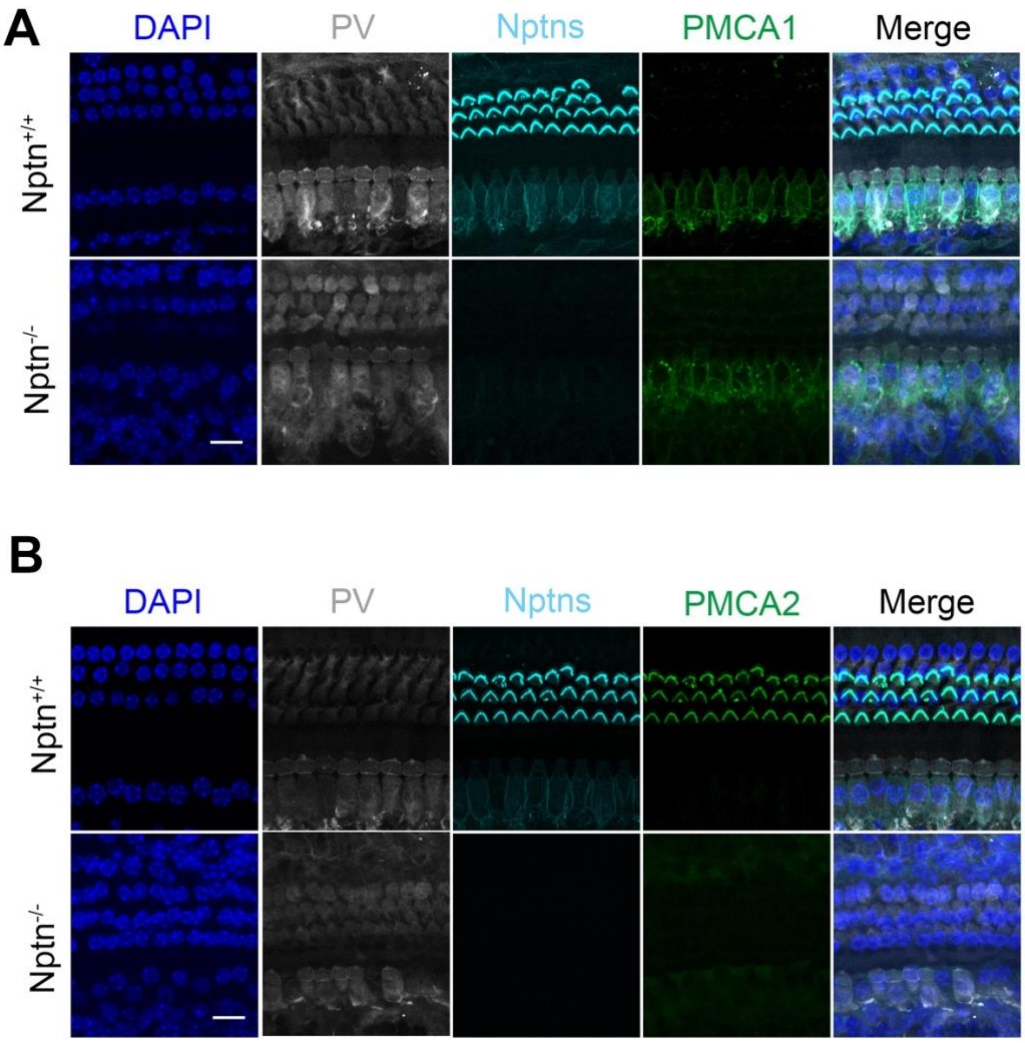

Fig.27. Analysis of hair cells of the cochlea in P18 mice

Cochlea whole mounts from Nptn$^{+/+}$ and Nptn$^{-/-}$ P18 mice were labelled with DAPI, anti-parvalbumin (PV), anti-Nptn and anti-PMCA1 (A) or anti-PMCA2 (B). Representative confocal images from the middle turn of the cochlea are displayed. Both outer and inner hair cells were labeled with PV in Nptn$^{+/+}$ and Nptn$^{-/-}$ mice, Note, PMCA1 was no changed but PMCA2 was completly lost in Nptn$^{-/-}$ in P18 mice. Scale bar = 15 µm.

4.16 Basigin is upregulated in Nptn-deficient hair cells

Considering that differential up-regulation of Basigin might account for this finding, I stained P18 cochlear whole mounts with DAPI, anti-parvalbumin and anti-Basigin. As is evident from Fig. 28, Basigin was expressed at low levels in IHCs and hardly detectable in OHCs (and their stereocilia) in wild type cochlea. Loss of Nptn resulted in marked up-regulation of Basigin in IHCs but also in OHCs with a striking enrichment

in the stereocilia. It therefore remains unresolved, as to whether Basigin upregulation is qualitatively and/ or quantitatively insufficient to restore wild type levels of PMCA2 in OHCs.

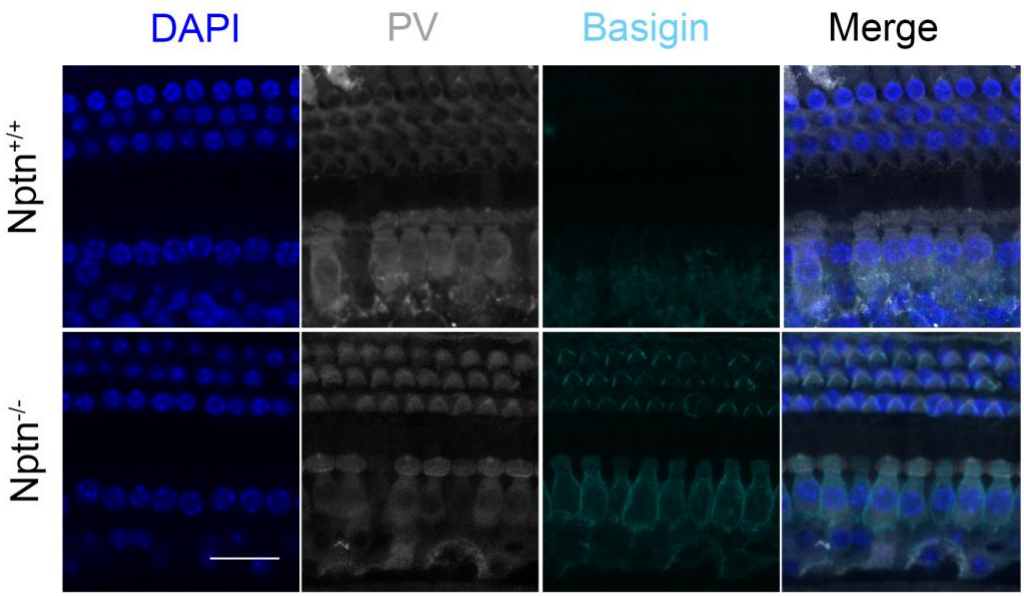

Fig.28. Analysis of Basigin in hair cells of the cochlea in P18 mice
Cochlea whole mounts from Nptn$^{+/+}$ and Nptn$^{-/-}$ in P18 mice were labelled with DAPI, anti-parvalbumin (PV), and anti-Basigin. Representative confocal images from the middle turn of the cochlea are displayed. Note that the upregulated Basigin in the Nptn$^{-/-}$ sample follows the distribution of Nptn and PMCAs normally observed for Nptn and PMCAs in wild type, including the enrichment in the stereocilia of OHCs.

4.17 Nptn is required to maintain hearing capability

Hearing loss is typically associated with aging. To assess, whether Nptn function is required for maintaining acoustic sensitivity in the auditory system of adult mice, I used ≥ 3-month-old Nptn$^{\Delta lox/loxPrCreERT}$ mice to induce neuronal loss of Nptn by tamoxifen injection. Using Nptn$^{lox/lox}$ mice as controls, ABR threshold measurements were performed before and 3 and 6 weeks after injection. ABR thresholds in control animals were in between 30 and 40 dB at all time points. In contrast, thresholds in Nptn$^{\Delta lox/loxPrCreERT}$ mice increased from ~40 dB prior to induction to above 78.75 ± 6.29 dB and 83.75 ± 6.29 dB at 3 and 6 weeks post-induction, respectively (Fig. 29A). Notably, there were obvious ABR threshold differences between individual, tamoxifen-

induced Nptn mutant mice. In order to test whether these differences reflect varying degrees of Nptn reduction, I subjected cochlea whole mounts from the respective mice to immunofluorescent analyses (Fig. 29B). Interestingly, the number of OHCs displaying low to non-detectable Nptn immunofluorescence increased with the ABR threshold measured for the respective animal, i.e. the ABR threshold strongly correlated inversely (R^2 = 0.9814) with the number of Nptn-positive OHCs (Fig. 29B, C).

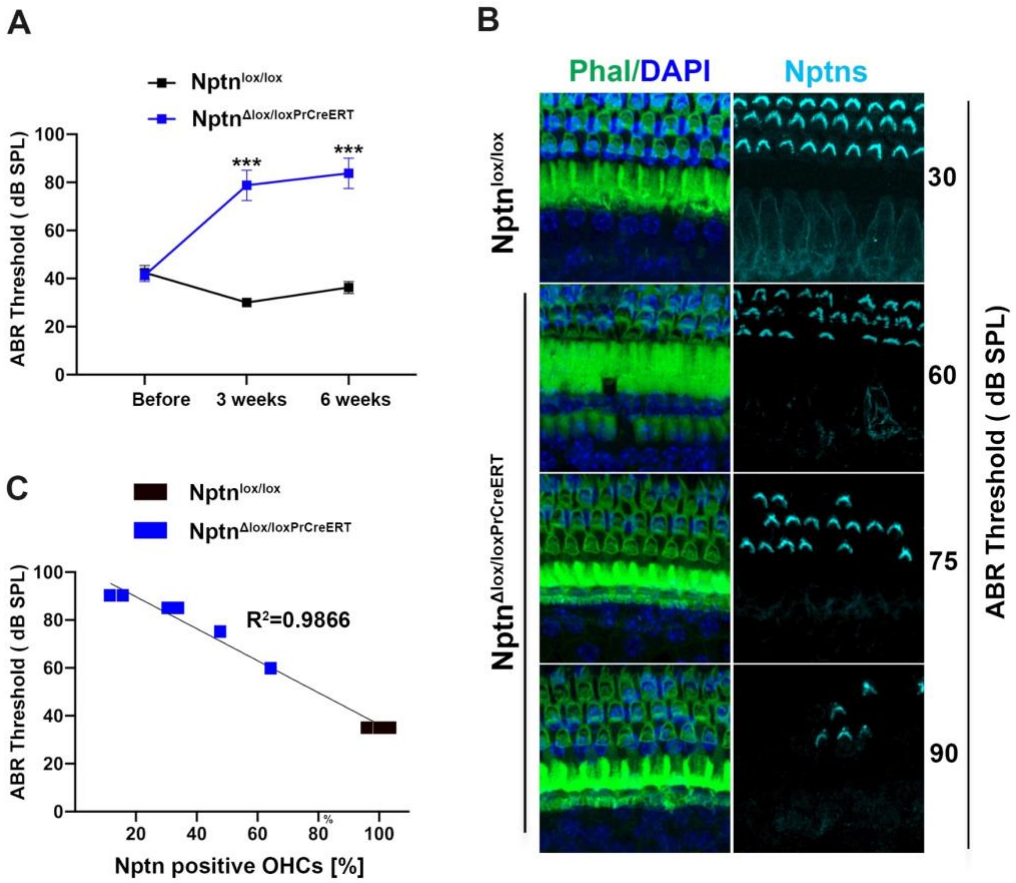

Fig.29 Hearing impairment after ablation of Nptn in adult mice.

(A) ABR measurements in 3-month-old Nptn$^{\Delta lox/loxPrCreERT}$ (n = 4) and Nptn$^{lox/lox}$ (n = 4) mice before, and 3 weeks and 6 weeks after injection of tamoxifen. The data are presented as means ± SD (1- way ANOVA, *** $p \leqslant 0.001$). (B) Cochlear whole mounts of Nptn$^{lox/lox}$ mice and Nptn$^{\Delta lox/loxPrCreERT}$ mice with different ABR thresholds after induction (indicated on the right) were labeled with phalloidin-iFluor 488 green (Phal), DAPI, and an antibody against Nptn. Mice with higher ABR threshold showed fewer IHCs and OHCs with clearly detectable levels of Nptn. Scale bar = 15 µm. (C) Inverse correlation between the percentage of OHC expressing Nptn and ABR thresholds analyzed in Nptn$^{\Delta lox/loxPrCreERT}$ (n=6) and Nptn$^{lox/lox}$ mice (n=3).

While the number of Nptn-expressing hair cells was clearly reduced 3 and 6 weeks after KO induction, the DAPI- and phalloidin-staining often appeared still quite normal (Fig 29B). To determine, whether hair cell degeneration follows loss of Nptn with delay, I turned to mice 8 weeks after the induction of Nptn KO and analyzed the number of hair cells by quantitative immunofluorescent analysis as above described for $Nptn^{-/-}$ and $Nptn^{lox/loxEmx1Cre}$ mice. Compared to controls, DAPI-, phalloidin- and myosin VIIa labeling revealed clear disturbance of the arrangement of OHCs in the induced KOs (Fig. 30A). Counting of myosin VIIa-positive hair cells revealed a substantial reduction in the apical and middle part of the organ of Corti and to a somewhat lesser extent in the basal part (Fig 30C). Given that PrCreERT-based inducible KOs are considered to be pan-neuronal, one might expect that loss in Nptn in SGN contributes to hearing loss observed as early as 3 weeks after tamoxifen injection. Surprisingly, however, immunofluorescent labelings revealed that even 8 weeks after KO induction, Nptn expression persisted in the SGNs (Fig 30B). In line with this observation the density of SGNs remained unaffected (Fig 30D). Collectively these data show that Nptn depletion solely in the hair cells accounts for substantial hearing loss early onwards.

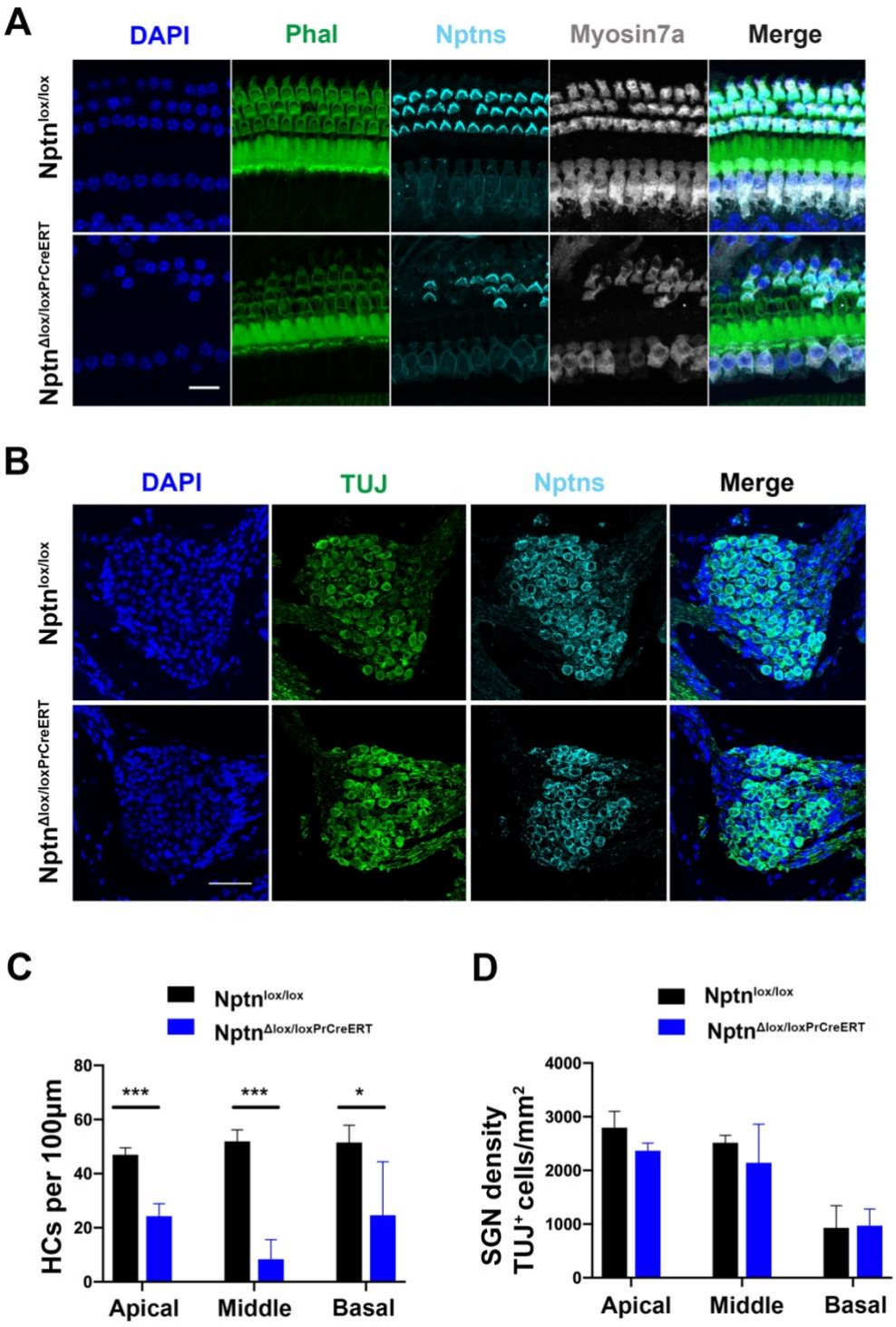

Fig. 30 Hair cell degeneration and maintenance of SGN in Nptn$^{\Delta lox/loxPrCreERT}$ after ablation of Nptn in adult mice

(A) Representative confocal images of the middle turn of the Organ of Corti of Nptn$^{lox/lox}$ and Nptn$^{\Delta lox/loxPrCreERT}$ mice labeled with phalloidin-iFluor 488 green (Phal), DAPI, and antibodies against Nptns and against myosin VIIa, revealing loss of hair cells in Nptn$^{\Delta lox/loxPrCreERT}$ mice. Scale bar = 15 µm. (B) Representative immunostainings of the middle area of the Rosenthal's

canal of $Nptn^{lox/lox}$ and $Nptn^{\Delta lox/loxPrCreERT}$ mice labeled with DAPI and antibodies against Nptn and against β-III Tubulin (TUJ). SGN still express Nptn. Scale bar = 50 µm. (C) Quantification of hair cells identified by Myosin7a in $Nptn^{lox/lox}$ and $Nptn^{\Delta lox/loxPrCreERT}$ mice. The number of hair cells in the apical, middle, and basal areas of the cochlea is significantly reduced in $Nptn^{\Delta lox/loxPrCreERT}$ (n=3) in comparison to $Nptn^{lox/lox}$ (n=4) mice (1-way ANOVA with Dunnett's multiple comparisons test, *$p \leqslant 0.05$; ** $p \leqslant 0.01$; *** $p \leqslant 0.001$). (D) Quantification of SGN identified by β-III tubulin in $Nptn^{lox/lox}$ and $Nptn^{\Delta lox/loxPrCreERT}$ mice. In $Nptn^{\Delta lox/loxPrCreERT}$, SGN still express neuroplastin after induction. The number of SGN in the apical, middle, and basal areas of the cochlea is not affected $Nptn^{\Delta lox/loxPrCreERT}$ (n=4) in comparison to $Nptn^{lox/lox}$ mice (n=3) (1-way ANOVA with Dunnett's multiple comparisons test).

5 Discussion

Neuroplastin is an important player in learning and memory and is also essential for hearing (Bhattacharya *et al.,* 2017, Carrott *et al.,* 2016, Zeng *et al.,* 2016). The molecular interactions and mechanisms underlying these functions remained poorly understood. Earlier studies by Smalla et al. (2000), however, strongly suggested that the long form of Neuroplastin, Np65, would act as a synaptic CAM through homophilic binding by its outermost Ig domain (Ig1). Problems with synapse formation or stability were indeed reported for hippocampal neurons and for IHCs in the cochlea when Nptn was missing (Carrott *et al.,* 2016, Herrera-Molina *et al.,* 2014). In the CA1 region of the hippocampus of Nptn$^{-/-}$ mice, excitatory (but not inhibitory) synapses were diminished (Herrera-Molina *et al.,* 2014)and such deficits may contribute to the observed behavioral and memory impairments. Nptn, however, has also been identified as a close interaction partner of PMCAs (Herrera-Molina R, et al., 2017; Korthals et al., 2017; Schmidt et al., 2017) suggesting that loss of Nptn may also affect brain functions at the level of PMCA-dependent Ca^{2+} regulation. In *Drosophila*, depletion of the single Basigin/Nptn homolog at glutamatergic synapses leads to dramatic reduction of the single PMCA isoform (U. Thomas, pers. communication). In line with this, previous studies on *dBasigin/Nptn* mutants showed severely increased synaptic activity (Besse *et al.,* 2007). In vertebrates the situation is more complex because (i) there are four PMCA isoforms and (ii) Nptn has a close paralog, Basigin. In fact, double-knockdown of Nptn and Basigin was shown to dramatically reduce total PMCAs in cultured hippocampal and cortical neurons (Schmidt *et al.,* 2017), i.e. similar to the situation in *dBasigin/Nptn* mutants. However, for a better assessment of PMCA-related effects of Nptn-deficiency alone, in particular on learning and memory and on hearing, it is necessary to address the levels of each PMCA isoform in different brain regions and the inner ear, respectively.

In this study, I first characterized the expression of the four PMCA isoforms and of Nptn and Basigin in wild type and various Nptn-mutant conditions, focussing on brain regions

which are involved in learning and memory, and motor control, respectively. Although all PMCA isoforms can be expected to tightly interact with Nptn, the effect of Nptn deficiency on the various isoforms was surprisingly variable. There were also considerable differences between brain regions, and between homogenates and synaptic junctions. For Nptn$^{-/-}$, the reduction of total PMCA in homogenates of Nptn was in the range from 40% (cerebellum) to 67% (cortex) compared to wild type and for individual isoforms it ranged from unchanged (PMCA2 in hippocampus) to 86% reduction (PMCA4 in hippocampus). In general, PMCA4 was most severely reduced and PMCA2 was the least affected. Transcript levels of at least PMCA1, 2 and 4 (PMCA3 not tested) remain normal in the absence of Nptn (Herrera-Molina *et al.,* 2017, Korthals *et al.,* 2017), which implies that post-transcriptional mechanisms are crucial for the differential effects. Most importantly, Basigin, which is normally expressed at rather low levels in the brain, was shown to be strongly increased in the present study and also by Schmidt et al. (2017). This, together with the almost complete loss of all PMCAs in cultured Nptn-Basigin double knockdown neurons (Schmidt *et al.,* 2017) strongly argues for a compensatory role of Basigin that helps to maintain roughly 50% of the total PMCA level in all studied brain areas of Nptn-deficient mice. One explanation for the differential effects on the PMCA isoforms might be that Basigin binds and stabilizes some PMCA isoforms (e.g. PMCA2) more than others (e.g. PMCA4). Np55 appeared to be more effetive than Basigin in promoting the expression of endogeneous PMCA (presumably PMCA1 and/or PMCA4) in HEK cells (Fig.12 A). and the fact that in wild type brains, PMCAs almost exclusively associate with Nptn Schmidt et al. (2017) suggests that Nptn generally has a higher affinity for all PMCAs than Basigin. Basigin (CD147), however, has been identified as a tight interaction partner of PMCA4 in T cells (Supper *et al.,* 2016) and Basigin clearly promoted the expression of both co-expressed PMCA2b and PMCA4b in HEK cells (Fig.12 B-C). While such co-overexpression approaches were suitable to assess the principle capacity of Nptn or Basigin (and variants of them) to support PMCA expression they are difficult to interprete with regard to actual affinities. Triple transfections might be used to test, whether in the presence of two PMCA isoforms, Basigin or Nptn

preferentially support the expression of one or the other.

What could be the basis for increased Basigin levels in the absence of Nptn? Since Nptn-depletion leads to increased $[Ca^{2+}]_i$, Ca^{2+}-dependent signaling that would lead to increased expression of Basigin appears to be an attractive hypothesis. In fact, Ca^{2+}-dependent up-regulation of Basigin has been observed in cultured keratinocytes (Sakaguchi *et al.,* 2016). However, quantitative RT-PCR by Schmidt et al. (2017) and by myself (not shown) on Nptn knock-out brain tissue did not reveal striking up-regulation of Basigin mRNA. Alternatively, Basigin synthesis might be up-regulated at the level of protein synthesis. Another explanation is that Basigin simply becomes stabilized by PMCAs, which become available if Nptn is absent. In this scenario no signaling has to be postulated. It is supported by work in *Drosophila*, where knockdown of PMCA strongly diminishes *d*Basigin/Nptn (U. Thomas, pers. communication; (Liao, 2018) and it is also consistent with the reduced levels of both Nptn and Basigin in the cortex of PMCA4$^{-/-}$ mice (Fig. 11). Importantly, it also implies that Basigin, which is produced in excess in wild type (and gets degraded) limits the degree to which PMCAs can be maintained in the Nptn mutants. The various PMCA isoforms and splice variants would have to compete for Basigin and thus the expression level of one isoform/ splice variant would affect the rescue of the others, thereby leading to the region-specific changes in PMCA isoform levels as shown in this work. Further consistent with such competition, I found that in the hippocampus of PMCA4$^{-/-}$ mice, PMCA3 was increased so that the total PMCA levels but also the Basigin and Nptn levels remained unchanged (Fig. 11). In the cortex of PMCA4$^{-/-}$ mice, however, the remaining isoforms remained unaltered, thus leading to reduced levels of total PMCA, Neuroplastin and Basigin. It seems likely that the availability of PMCAs is also limiting to gain-of-function effects when Nptn or Basigin are overexpressed. This would explain the mild effects on dendritic Ca^{2+} clearance observed after transfection of Np55 or Basigin into hippocampal neurons (Fig. 19 C and 20 C). Of note, blockade of glutamate receptors abolished this effect (Fig. 19 F and 20 F), suggesting that overexpressed Np55 or Basigin primarily act on Ca^{2+} of synaptic origin. In fact, a linkage between PMCA2b and NMDA receptors *via* the postsynaptic scaffold protein PSD-95 has been proposed

(Garside *et al.,* 2009), suggesting that PMCA2b controls NMDA receptor-dependent Ca^{2+} signals (Garside *et al.,* 2009, Lisek *et al.,* 2017, Scheuss *et al.,* 2006).

In this work all isoforms were found in synaptic junctional membrane fractions. These fractions, however, are likely to include plasma membrane from the periphery of synaptic contacts. In contrast to other isoforms, specific splice variants of PMCA2 have been detected by immuno-electronmicroscopy inside presynaptic AZs and PSDs, respectively (Burette *et al.,* 2009, Burette *et al.,* 2010). Moreover, PMCA2 (especially the a-form) has been described as a fast-acting isoform (Caride *et al.,* 2001). This isoform therefore appears to be well suited to limit synaptic plasticity (Jensen *et al.,* 2009). The finding that PMCA2 is the least affected isoform in synaptic junctional membrane fractions of Nptn-deficient cortex and hippocampus is therefore of particular interest and refined analysis should address, whether the a- and b-forms are affected equally.

Although Basigin compensates the loss of Nptn with regard to the stabilzation of PMCAs to quite some extent, it is important to note that the various western blot analyses in this study revealed increased levels of just one band that most likely represents the short, e.g. 2-Ig domain variant of Basigin. It is therefore highly unlikely that it can compensate for the loss of Np65-specific functions in $Nptn^{-/-}$ mice. This concerns, for example, the proposed homophilic adhesion function. Moreover, a most recent study has shown that the Np65-specific Ig1 domain interacts with the extracellular domain of the GluA1 subunit of AMPA receptors and that this interaction is highly relevant for the previously reported role of Np65 for the maintenance of LTP (Jiang *et al.,* 2021, Smalla *et al.,* 2000). Similarly, Basigin might be more or less restricted in its ability to replace Nptn as a binding partner for other proteins. For instance, Basigin might compensate for loss of Nptn concerning the interaction with the E3 ubiquitin ligase Traf6, which promotes spinogenesis (Vemula *et al.,* 2020). The binding motif for Traf6 is also present in the cytoplasmic tail of Basigin and binding of Basigin to the Traf6 paralog Traf2 has been decribed (Sakaguchi *et al.,* 2016). A few candidate synaptic interaction partners of Nptn have been checked in this work by

western blotting (Fig. 10), but no differences in the level of their expression were revealed in wild type versus Nptn$^{-/-}$ samples. Regardless of possible compensation by Basigin, one may of course not expect every interaction to be crucial at the level of protein stability.

PMCAs have been implicated in synaptic plasticity (Empson *et al.,* 2007, Jensen *et al.,* 2009, Scheuss *et al.,* 2006, Simons *et al.,* 2009) and are therefore likely to play specific roles in learning and memory. To date, however, neither PMCA-mutant mouse models nor studies in humans with inherited PMCA mutations have implicated (or excluded) these important regulators of Ca^{2+} homeostasis in amnesia-related memory deficits. This is not very surprising, as on one hand, PMCA isoforms may share functions (redundancy) and on the other hand constitutive mutations in individual isoforms typically affect various brain regions and may thus affect functions essential for behavorial testing in animal models. With regard to the striking memory deficits in pan-neuronal inducible Nptn$^{-/-}$ mice and their possible link to disturbed Ca^{2+} homeostasis, it was therefore obvious to address the effects on PMCAs in this condition. Although synaptic junctional membrane fractions were not addressed separately, the overall profile of PMCA reduction in crude membrane fractions 8 weeks after induction was found to resemble that of constitutive Nptn$^{-/-}$ mice. Therefore, the minimal conclusion is that none of the PMCA isoforms can be ruled out to play a crucial role in Nptn-related retrograde amnesia.

Additional genetic arrangements could help to further clarify, whether, where and when the reduction of PMCA in the brain can causes retrograde amnesia. This could, for instance, involve rescue and knockdown experiments, in which Nptn-expressing or Nptn-depleting (e.g. CRISPR/Cas9) viruses would be injected into specific brain areas. Such approaches could also be specific for splice variants or include mutated Nptn variants that specifically impair certain interactions, e.g. with PMCAs. For this it is important to characterize such interactions in detail and part of this work was dedicated to this. The TMD of Nptn and Basigin were identified as the essential interface for interaction with and stabilization of PMCAs. Several amino acid residues conserved

between the TMDs between Nptn, Basigin and *Drosophila* Basigin/Nptn were mutated, but none of these exchanges affected the ability to stabilize PMCA2b in HEK cells. In particular, replacing a glutamate residue in the center of the TMD by valine was expected to show an effect, because this residue is highly conserved between orthologs and paralogs. Moreover, it was shown to be crucial in rescue experiments with *d*Basigin/Nptn to restore the polarity of photoreceptor cells and neuron-glia interactions in *bsg*-mutant eyes (Munro *et al.,* 2010). On the other hand, changing the respective glutamate to alanine or glycine had no obvious effect on the interaction of Basigin with monocarboxylate transporters (MCT) (Deora *et al.,* 2005, Finch *et al.,* 2009). Interestingly, rescue experiments in *Drosophila* show that, in contrast to rNp55-TagRFPT, the rNp55^{E323V}-TagRFPT variant, though efficiently expressed, fails to restore PMCA levels at the glutamatergic neuromuscular junction when endogeneous *d*Basigin/Nptn is depleted by RNAi (X. Lin, U. Thomas, unpublished). The reason for this discrepancy is unclear. While the testing of the mutated Nptn variants was in progress, Gong et al. (2018) published the structure of hPMCA1 in complex with hNp55 based on cryo-electron microscopy. This revealed that the interface between the two proteins is made up by large hydrophobic residues present in the TMD of Nptn and in TMD10 and the linker between TMDs 8 and 9 of the PMCA. E232 was not part of the interface. While Nptn has been shown to be crucial for PMCA1 function none of the interface residues in the TMD of Nptn has been tested for functional relevance (Gong *et al.,* 2018). Two of the residues shown to be part of the interface, P226 and F227 (P225 and F226 in rNp55), were mutated in this work (to G and V, respectively). Although without effect on stabilizing PMCA2, it remains to be tested, if they are still able to support PMCA function.

In this work I also used Nptn-mutant mouse models to investigate the role of Nptn in the auditory system, primarily in the inner ear and with a particular focus on PMCA. In a first assessment, we could demonstrate that the severe hearing deficits associated with complete loss of Nptn originate upstream from the AC, which displayed normal basal synaptic transmission. However, in response to sound stimulation, no

thalamocortical input to the AC was detectable in 5-month old mice. Hearing is largely normal in the $Nptn^{lox/loxEmx1Cre}$ mice, implying that disturbed glutamatergic input to the AC is not a major cause for deafening, although more subtle deficits of hearing or processing of auditory information in these mutants cannot be excluded. Moreover, since the ABR was virtually absent, one may conclude that deafening in the $Nptn^{-/-}$ situation predominantly if not exclusively results from defects in the cochlea. In fact, I could detect Nptn in IHCs, OHCs and SGNs, i.e. in the cells that cooperate to convert sound into neural perception. Np65 was not detected, which was in agreement with the study by Zeng et al. (2016) but in disagreement with the study by Carrott et al. (2016). Of note, in the latter study mice heterozygous for the $Nptn^{pitch}$ allele rather than wild type controls were used for immohistological detection of Np65. Thus, at present, it cannot be ruled out that the pitch allele is associated with ectopic expression of the Np65-specific Ig1 domain, e.g. as part of a truncated gene product. Amuti et al. (2016) showed reduced freezing of Np65-deficient mice to a conditional cue of 87dB, which may indicate an increased hearing threshold but which might also point to impaired processing downstream in the auditory pathway. Therefore, it would be interesting to investigate these Np65-specific mutants for their hearing function in further detail.

The immunostainings presented in this work reveal strong colocalization of Nptn with the prevailing PMCA isoform in the plasma membrane of either type of hair cell, i.e. with PMCA1 mainly in the cell body of IHCs and with PMCA2 in the stereocilia of OHCs. Loss of Nptn in hair cells is always accompanied with loss or severe reduction of the associated PMCA in adult mice. The comparison between young and older mice, however, pointed to a progressive loss of cells, most prominently OHCs. While PMCA1 in IHCs and the cells themselves still appeared normal in young (P18) Nptn-deficient mice, PMCA2 was almost undetectable at this stage in OHCs (Fig. 27). Importantly, the OHCs by then still appeared mostly alive, meaning that severe loss of PMCA2 precedes the degeneration of OHCs. Basigin levels were elevated and showed the same subcellular distribution as Nptn and the PMCAs in wild type IHCs and OHCs, respectively. Basigin may be sufficient to maintain a detectable level of PMCA1 in IHCs up to P18, but available Basigin in OHCs obviously stabilizes only a small percentage

of PMCA2. The IHCs and OHCs are particularly challenged by Ca^{2+} influx and Ca^{2+} homeostasis is critically dependent on PMCA function (Fettiplace and Nam 2019). Basigin expression appears too low to serve as an efficient back-up for Nptn in these cells. Elevated Ca^{2+} concentration has been hypothesized to trigger the degeneration of hair cells (Fridberger *et al.,* 1998) and my findings clearly support this assumption. In fact, loss of PMCA and/or Nptn and Basigin has been shown to cause apoptotic cell death in various other cell types (Schmidt *et al.,* 2017, VanHouten *et al.,* 2010). This may also involve Ca^{2+} overload-induced production of free radicals (Hajnoczky *et al.,* 2003, Krabbendam *et al.,* 2018). By using the inducible KO for Nptn, I could also show that the degeneration of hair cells and progressive deafening can be triggered by a late onset of Nptn depletion.

The closest paralog of Nptn, Basigin (also referred to as CD147, less so as EMMPRIN), has attracted much attention, mainly for its involvement as a potentially "drugable" player in cancer, and most recently in COVID-19 (Kumar *et al.,* 2019, Landras and Mourah 2020, Liu *et al.,* 2020). Likewise, Nptn bears the potential to serve as a target for therapeutic treatments of diseases associated with various cell types, including neurons. The development of peptides binding specifically to Nptn/Np65 may be considered as proof-of-principle for this notion (Owczarek *et al.,* 2010, Owczarek *et al.,* 2011). The close association with PMCAs links Nptn to Ca^{2+} homeostasis and thus to many functions and their pathophysiological impairments such as disease- or aging-related memory decline. This work contributes insights on how and to what extent loss of Nptn affects PMCAs in the mouse brain and the inner ear.

6 References

1. Airaksinen MS, Eilers J, Garaschuk O, Thoenen H, Konnerth A, Meyer M. (1997): Ataxia and altered dendritic calcium signaling in mice carrying a targeted null mutation of the calbindin D28k gene. Proc Natl Acad Sci U S A 94:1488-1493.
2. Amuti S, Tang Y, Wu S, Liu L, Huang L, Zhang H*, et al.* (2016): Neuroplastin 65 mediates cognitive functions via excitatory/inhibitory synapse imbalance and ERK signal pathway. Neurobiol Learn Mem 127:72-83.
3. Augustine GJ, Santamaria F, Tanaka K. (2003): Local calcium signaling in neurons. Neuron 40:331-346.
4. Beesley PW, Herrera-Molina R, Smalla KH, Seidenbecher C. (2014): The Neuroplastin adhesion molecules: key regulators of neuronal plasticity and synaptic function. J Neurochem 131:268-283.
5. Berridge MJ, Lipp P, Bootman MD. (2000): The versatility and universality of calcium signalling. Nat Rev Mol Cell Biol 1:11-21.
6. Besse F, Mertel S, Kittel RJ, Wichmann C, Rasse TM, Sigrist SJ*, et al.* (2007): The Ig cell adhesion molecule Basigin controls compartmentalization and vesicle release at Drosophila melanogaster synapses. J Cell Biol 177:843-855.
7. Bhattacharya S, Herrera-Molina R, Sabanov V, Ahmed T, Iscru E, Stober F*, et al.* (2017): Genetically Induced Retrograde Amnesia of Associative Memories After Neuroplastin Ablation. Biol Psychiatry 81:124-135.
8. Blaustein MP, Juhaszova M, Golovina VA, Church PJ, Stanley EF. (2002): Na/Ca exchanger and PMCA localization in neurons and astrocytes: functional implications. Ann N Y Acad Sci 976:356-366.
9. Bortolozzi M, Mammano F. (2018): PMCA2 pump mutations and hereditary deafness. Neurosci Lett 663:18-24.
10. Bozulic LD, Malik MT, Powell DW, Nanez A, Link AJ, Ramos KS*, et al.* (2007): Plasma membrane Ca(2+) -ATPase associates with CLP36, alpha-actinin and actin in human platelets. Thromb Haemost 97:587-597.
11. Brini M, Cali T, Ottolini D, Carafoli E. (2013): Intracellular calcium homeostasis and signaling. Met Ions Life Sci 12:119-168.
12. Brini M, Cali T, Ottolini D, Carafoli E. (2014): Neuronal calcium signaling: function and dysfunction. Cell Mol Life Sci 71:2787-2814.
13. Brini M, Carafoli E. (2011): The plasma membrane Ca(2)+ ATPase and the plasma membrane sodium calcium exchanger cooperate in the regulation of cell calcium. Cold Spring Harb Perspect Biol 3.
14. Brini M, Carafoli E, Cali T. (2017): The plasma membrane calcium pumps: focus on the role in (neuro)pathology. Biochem Biophys Res Commun 483:1116-1124.
15. Bublitz M, Morth JP, Nissen P. (2011): P-type ATPases at a glance. J Cell Sci 124:2515-2519.
16. Burette A, Rockwood JM, Strehler EE, Weinberg RJ. (2003): Isoform-specific distribution of the plasma membrane Ca2+ ATPase in the rat brain. J Comp Neurol 467:464-476.

17. Burette AC, Strehler EE, Weinberg RJ. (2009): "Fast" plasma membrane calcium pump PMCA2a concentrates in GABAergic terminals in the adult rat brain. J Comp Neurol 512:500-513.
18. Burette AC, Strehler EE, Weinberg RJ. (2010): A plasma membrane Ca2+ ATPase isoform at the postsynaptic density. Neuroscience 169:987-993.
19. Carafoli E, Santella L, Branca D, Brini M. (2001): Generation, control, and processing of cellular calcium signals. Crit Rev Biochem Mol Biol 36:107-260.
20. Caride AJ, Filoteo AG, Penheiter AR, Paszty K, Enyedi A, Penniston JT. (2001): Delayed activation of the plasma membrane calcium pump by a sudden increase in Ca2+: fast pumps reside in fast cells. Cell Calcium 30:49-57.
21. Caride AJ, Filoteo AG, Penniston JT, Strehler EE. (2007): The plasma membrane Ca2+ pump isoform 4a differs from isoform 4b in the mechanism of calmodulin binding and activation kinetics: implications for Ca2+ signaling. J Biol Chem 282:25640-25648.
22. Caride AJ, Penheiter AR, Filoteo AG, Bajzer Z, Enyedi A, Penniston JT. (2001): The plasma membrane calcium pump displays memory of past calcium spikes. Differences between isoforms 2b and 4b. J Biol Chem 276:39797-39804.
23. Carrott L, Bowl MR, Aguilar C, Johnson SL, Chessum L, West M*, et al.* (2016): Absence of Neuroplastin-65 Affects Synaptogenesis in Mouse Inner Hair Cells and Causes Profound Hearing Loss. J Neurosci 36:222-234.
24. Casale J, Browne T, Murray I, Gupta G. Physiology, Vestibular System. StatPearls. Treasure Island (FL)2020.
25. Chicka MC, Strehler EE. (2003): Alternative splicing of the first intracellular loop of plasma membrane Ca2+-ATPase isoform 2 alters its membrane targeting. J Biol Chem 278:18464-18470.
26. Clapham DE. (2007): Calcium signaling. Cell 131:1047-1058.
27. Daniels RW, Rossano AJ, Macleod GT, Ganetzky B. (2014): Expression of multiple transgenes from a single construct using viral 2A peptides in Drosophila. PLoS One 9:e100637.
28. DeCoster MA. (1995): Calcium dynamics in the central nervous system. Adv Neuroimmunol 5:233-239.
29. DeMarco SJ, Strehler EE. (2001): Plasma membrane Ca2+-atpase isoforms 2b and 4b interact promiscuously and selectively with members of the membrane-associated guanylate kinase family of PDZ (PSD95/Dlg/ZO-1) domain-containing proteins. J Biol Chem 276:21594-21600.
30. Deora AA, Philp N, Hu J, Bok D, Rodriguez-Boulan E. (2005): Mechanisms regulating tissue-specific polarity of monocarboxylate transporters and their chaperone CD147 in kidney and retinal epithelia. Proc Natl Acad Sci U S A 102:16245-16250.
31. Desrivieres S, Lourdusamy A, Tao C, Toro R, Jia T, Loth E*, et al.* (2015): Single nucleotide polymorphism in the neuroplastin locus associates with cortical thickness and intellectual ability in adolescents. Mol Psychiatry 20:263-274.
32. Di Leva F, Domi T, Fedrizzi L, Lim D, Carafoli E. (2008): The plasma membrane Ca2+ ATPase of animal cells: structure, function and regulation. Arch Biochem

Biophys 476:65-74.
33. DiPolo R, Beauge L. (1983): The calcium pump and sodium-calcium exchange in squid axons. Annu Rev Physiol 45:313-324.
34. Dreses-Werringloer U, Lambert JC, Vingtdeux V, Zhao H, Vais H, Siebert A*, et al.* (2008): A polymorphism in CALHM1 influences Ca2+ homeostasis, Abeta levels, and Alzheimer's disease risk. Cell 133:1149-1161.
35. Driver EC, Kelley MW. (2020): Development of the cochlea. Development 147 (12): dev1622263
36. Empson RM, Garside ML, Knopfel T. (2007): Plasma membrane Ca2+ ATPase 2 contributes to short-term synapse plasticity at the parallel fiber to Purkinje neuron synapse. J Neurosci 27:3753-3758.
37. Evans RC, Blackwell KT. (2015): Calcium: amplitude, duration, or location? Biol Bull 228:75-83.
38. Fettiplace R, Nam JH. (2019): Tonotopy in calcium homeostasis and vulnerability of cochlear hair cells. Hear Res 376:11-21.
39. Finch NA, Linser PJ, Ochrietor JD. (2009): Hydrophobic interactions stabilize the basigin-MCT1 complex. Protein J 28:362-368.
40. Fridberger A, Flock A, Ulfendahl M, Flock B. (1998): Acoustic overstimulation increases outer hair cell Ca2+ concentrations and causes dynamic contractions of the hearing organ. Proc Natl Acad Sci U S A 95:7127-7132.
41. Gandhi S, Wood-Kaczmar A, Yao Z, Plun-Favreau H, Deas E, Klupsch K*, et al.* (2009): PINK1-associated Parkinson's disease is caused by neuronal vulnerability to calcium-induced cell death. Mol Cell 33:627-638.
42. Garside ML, Turner PR, Austen B, Strehler EE, Beesley PW, Empson RM. (2009): Molecular interactions of the plasma membrane calcium ATPase 2 at pre- and post-synaptic sites in rat cerebellum. Neuroscience 162:383-395.
43. Gomez-Varela D, Schmidt M, Schoellerman J, Peters EC, Berg DK. (2012): PMCA2 via PSD-95 controls calcium signaling by alpha7-containing nicotinic acetylcholine receptors on aspiny interneurons. J Neurosci 32:6894-6905.
44. Gong D, Chi X, Ren K, Huang G, Zhou G, Yan N*, et al.* (2018): Structure of the human plasma membrane Ca(2+)-ATPase 1 in complex with its obligatory subunit neuroplastin. Nat Commun 9:3623.
45. Gorski JA, Talley T, Qiu M, Puelles L, Rubenstein JL, Jones KR. (2002): Cortical excitatory neurons and glia, but not GABAergic neurons, are produced in the Emx1-expressing lineage. J Neurosci 22:6309-6314.
46. Gundelfinger ED, Fejtova A. (2012): Molecular organization and plasticity of the cytomatrix at the active zone. Curr Opin Neurobiol 22:423-430.
47. Hajnoczky G, Davies E, Madesh M. (2003): Calcium signaling and apoptosis. Biochem Biophys Res Commun 304:445-454.
48. Happel MF, Jeschke M, Ohl FW. (2010): Spectral integration in primary auditory cortex attributable to temporally precise convergence of thalamocortical and intracortical input. J Neurosci 30:11114-11127.
49. Herrera-Molina R, Mlinac-Jerkovic K, Ilic K, Stober F, Vemula SK, Sandoval M*, et al.* (2017): Neuroplastin deletion in glutamatergic neurons impairs selective

brain functions and calcium regulation: implication for cognitive deterioration. Sci Rep 7:7273.

50. Herrera-Molina R, Sarto-Jackson I, Montenegro-Venegas C, Heine M, Smalla KH, Seidenbecher CI*, et al.* (2014): Structure of excitatory synapses and GABAA receptor localization at inhibitory synapses are regulated by neuroplastin-65. J Biol Chem 289:8973-8988.
51. Hill IE, Selkirk CP, Hawkes RB, Beesley PW. (1988): Characterization of novel glycoprotein components of synaptic membranes and postsynaptic densities, gp65 and gp55, with a monoclonal antibody. Brain Res 461:27-43.
52. Hudspeth AJ. (2008): Making an effort to listen: mechanical amplification in the ear. Neuron 59:530-545.
53. Jensen TP, Buckby LE, Empson RM. (2009): Reduced expression of the "fast" calcium transporter PMCA2a during homeostatic plasticity. Mol Cell Neurosci 41:364-372.
54. Jensen TP, Filoteo AG, Knopfel T, Empson RM. (2007): Presynaptic plasma membrane Ca2+ ATPase isoform 2a regulates excitatory synaptic transmission in rat hippocampal CA3. J Physiol 579:85-99.
55. Jiang CH, Wei M, Zhang C, Shi YS. (2021): The amino-terminal domain of GluA1 mediates LTP maintenance via interaction with neuroplastin-65. Proc Natl Acad Sci U S A 118(9): e2019194118
56. Kim E, DeMarco SJ, Marfatia SM, Chishti AH, Sheng M, Strehler EE. (1998): Plasma membrane Ca2+ ATPase isoform 4b binds to membrane-associated guanylate kinase (MAGUK) proteins via their PDZ (PSD-95/Dlg/ZO-1) domains. J Biol Chem 273:1591-1595.
57. Korthals M, Langnaese K, Smalla KH, Kahne T, Herrera-Molina R, Handschuh J*, et al.* (2017): A complex of Neuroplastin and Plasma Membrane Ca(2+) ATPase controls T cell activation. Sci Rep 7:8358.
58. Krabbendam IE, Honrath B, Culmsee C, Dolga AM. (2018): Mitochondrial Ca(2+)-activated K(+) channels and their role in cell life and death pathways. Cell Calcium 69:101-111.
59. Kreutz MR, Langnaese K, Dieterich DC, Seidenbecher CI, Zuschratter W, Beesley PW*, et al.* (2001): Distribution of transcript and protein isoforms of the synaptic glycoprotein neuroplastin in rat retina. Invest Ophthalmol Vis Sci 42:1907-1914.
60. Kruger WA, Monteith GR, Poronnik P. (2010): The plasma membrane Ca(2+)-ATPase: regulation by PSD-95/Dlg/Zo-1 scaffolds. Int J Biochem Cell Biol 42:805-808.
61. Kuhn S, Ingham N, Pearson S, Gribble SM, Clayton S, Steel KP*, et al.* (2012): Auditory function in the Tc1 mouse model of down syndrome suggests a limited region of human chromosome 21 involved in otitis media. PLoS One 7:e31433.
62. Kumar D, Vetrivel U, Parameswaran S, Subramanian KK. (2019): Structural insights on druggable hotspots in CD147: A bull's eye view. Life Sci 224:76-87.
63. Landras A, Mourah S. (2020): [CD147: role and therapeutic targeting of a promising molecule in the treatment of cancers]. Med Sci (Paris) 36 Hors serie

n degrees 1:47-49.
64. Langnaese K, Beesley PW, Gundelfinger ED. (1997): Synaptic membrane glycoproteins gp65 and gp55 are new members of the immunoglobulin superfamily. J Biol Chem 272:821-827.
65. Langnaese K, Mummery R, Gundelfinger ED, Beesley PW. (1998): Immunoglobulin superfamily members gp65 and gp55: tissue distribution of glycoforms. FEBS Lett 429:284-288.
66. Lazarevic V, Schone C, Heine M, Gundelfinger ED, Fejtova A. (2011): Extensive remodeling of the presynaptic cytomatrix upon homeostatic adaptation to network activity silencing. J Neurosci 31:10189-10200.
67. Leistner C. Proteomische Charakterisierung von neuronalen Interaktomen des Zelladhasionsmolekuls Neuroplastin [Bachelor thesis] 2016, Hochschule Zittau/ Görlitz-Leibniz Institut für Neurobiologie Magdeburg
68. Li H, Liu Y, Gao X, Liu L, Amuti S, Wu D*, et al.* (2019): Neuroplastin 65 modulates anxiety- and depression-like behavior likely through adult hippocampal neurogenesis and central 5-HT activity. FEBS J 286:3401-3415.
69. Liao CS. Isoform diversity and PMCA-dependent expression of Basigin at glutamatergic neuromuscular junctions in Drosophila [Master thesis] 2018, Otto von Guericke Universtät/ Leibniz Institut für Neurobiologie Magdeburg.
70. Lin X, Brunk MGK, Yuanxiang P, Curran AW, Zhang E, Stober F*, et al.* (2021): Neuroplastin expression is essential for hearing and hair cell PMCA expression. Brain Struct Funct 226:1533-1551.
71. Lisek M, Boczek T, Zylinska L. (2018): Calcium as a Trojan horse in mental diseases-The role of PMCA and PMCA-interacting proteins in bipolar disorder and schizophrenia. Neurosci Lett 663:48-54.
72. Lisek M, Ferenc B, Studzian M, Pulaski L, Guo F, Zylinska L*, et al.* (2017): Glutamate Deregulation in Ketamine-Induced Psychosis-A Potential Role of PSD95, NMDA Receptor and PMCA Interaction. Front Cell Neurosci 11:181.
73. Liu C, von Brunn A, Zhu D. (2020): Cyclophilin A and CD147: novel therapeutic targets for the treatment of COVID-19. Med Drug Discov 7:100056.
74. Liu J, Tang TS, Tu H, Nelson O, Herndon E, Huynh DP*, et al.* (2009): Deranged calcium signaling and neurodegeneration in spinocerebellar ataxia type 2. J Neurosci 29:9148-9162.
75. Lopreiato R, Giacomello M, Carafoli E. (2014): The plasma membrane calcium pump: new ways to look at an old enzyme. J Biol Chem 289:10261-10268.
76. Mammano F. (2011): Ca2+ homeostasis defects and hereditary hearing loss. Biofactors 37:182-188.
77. Marzban H, Khanzada U, Shabir S, Hawkes R, Langnaese K, Smalla KH*, et al.* (2003): Expression of the immunoglobulin superfamily neuroplastin adhesion molecules in adult and developing mouse cerebellum and their localisation to parasagittal stripes. J Comp Neurol 462:286-301.
78. Mitzdorf U. (1985): Current source-density method and application in cat cerebral cortex: investigation of evoked potentials and EEG phenomena. Physiol Rev 65:37-100.

79. Moser T, Starr A. (2016): Auditory neuropathy--neural and synaptic mechanisms. Nat Rev Neurol 12:135-149.
80. Munro M, Akkam Y, Curtin KD. (2010): Mutational analysis of Drosophila basigin function in the visual system. Gene 449:50-58.
81. Neher E, Sakaba T. (2008): Multiple roles of calcium ions in the regulation of neurotransmitter release. Neuron 59:861-872.
82. Niggli V, Adunyah ES, Penniston JT, Carafoli E. (1981): Purified (Ca2+-Mg2+)-ATPase of the erythrocyte membrane. Reconstitution and effect of calmodulin and phospholipids. J Biol Chem 256:395-401.
83. Nishimune H, Numata T, Chen J, Aoki Y, Wang Y, Starr MP*, et al.* (2012): Active zone protein Bassoon co-localizes with presynaptic calcium channel, modifies channel function, and recovers from aging related loss by exercise. PLoS One 7:e38029.
84. Owczarek S, Kiryushko D, Larsen MH, Kastrup JS, Gajhede M, Sandi C*, et al.* (2010): Neuroplastin-55 binds to and signals through the fibroblast growth factor receptor. FASEB J 24:1139-1150.
85. Owczarek S, Soroka V, Kiryushko D, Larsen MH, Yuan Q, Sandi C*, et al.* (2011): Neuroplastin-65 and a mimetic peptide derived from its homophilic binding site modulate neuritogenesis and neuronal plasticity. J Neurochem 117:984-994.
86. Padanyi R, Xiong Y, Antalffy G, Lor K, Paszty K, Strehler EE*, et al.* (2010): Apical scaffolding protein NHERF2 modulates the localization of alternatively spliced plasma membrane Ca2+ pump 2B variants in polarized epithelial cells. J Biol Chem 285:31704-31712.
87. Perny M, Roccio M, Grandgirard D, Solyga M, Senn P, Leib SL. (2016): The Severity of Infection Determines the Localization of Damage and Extent of Sensorineural Hearing Loss in Experimental Pneumococcal Meningitis. J Neurosci 36:7740-7749.
88. Preiano BS, Guerini D, Carafoli E. (1996): Expression and functional characterization of isoforms 4 of the plasma membrane calcium pump. Biochemistry 35:7946-7953.
89. Regehr WG. (1997): Interplay between sodium and calcium dynamics in granule cell presynaptic terminals. Biophys J 73:2476-2488.
90. Ren T, Gillespie PG. (2007): A mechanism for active hearing. Curr Opin Neurobiol 17:498-503.
91. Rimessi A, Coletto L, Pinton P, Rizzuto R, Brini M, Carafoli E. (2005): Inhibitory interaction of the 14-3-3{epsilon} protein with isoform 4 of the plasma membrane Ca(2+)-ATPase pump. J Biol Chem 280:37195-37203.
92. Saito A, Fujikura-Ouchi Y, Kuramasu A, Shimoda K, Akiyama K, Matsuoka H*, et al.* (2007): Association study of putative promoter polymorphisms in the neuroplastin gene and schizophrenia. Neurosci Lett 411:168-173.
93. Sakaguchi M, Yamamoto M, Miyai M, Maeda T, Hiruma J, Murata H*, et al.* (2016): Identification of an S100A8 Receptor Neuroplastin-beta and its Heterodimer Formation with EMMPRIN. J Invest Dermatol 136:2240-2250.
94. Saldeitis K, Happel MF, Ohl FW, Scheich H, Budinger E. (2014): Anatomy of

the auditory thalamocortical system in the Mongolian gerbil: nuclear origins and cortical field-, layer-, and frequency-specificities. J Comp Neurol 522:2397-2430.

95. Sarto-Jackson I, Milenkovic I, Smalla KH, Gundelfinger ED, Kaehne T, Herrera-Molina R*, et al.* (2012): The cell adhesion molecule neuroplastin-65 is a novel interaction partner of gamma-aminobutyric acid type A receptors. J Biol Chem 287:14201-14214.
96. Schatzmann HJ. (1966): ATP-dependent Ca++-extrusion from human red cells. Experientia 22:364-365.
97. Scheuss V, Yasuda R, Sobczyk A, Svoboda K. (2006): Nonlinear [Ca2+] signaling in dendrites and spines caused by activity-dependent depression of Ca2+ extrusion. J Neurosci 26:8183-8194.
98. Schmidt N, Kollewe A, Constantin CE, Henrich S, Ritzau-Jost A, Bildl W*, et al.* (2017): Neuroplastin and Basigin Are Essential Auxiliary Subunits of Plasma Membrane Ca(2+)-ATPases and Key Regulators of Ca(2+) Clearance. Neuron 96:827-838 e829.
99. Schuh K, Uldrijan S, Gambaryan S, Roethlein N, Neyses L. (2003): Interaction of the plasma membrane Ca2+ pump 4b/CI with the Ca2+/calmodulin-dependent membrane-associated kinase CASK. J Biol Chem 278:9778-9783.
100. Schultz JM, Yang Y, Caride AJ, Filoteo AG, Penheiter AR, Lagziel A*, et al.* (2005): Modification of human hearing loss by plasma-membrane calcium pump PMCA2. N Engl J Med 352:1557-1564.
101. Simons SB, Escobedo Y, Yasuda R, Dudek SM. (2009): Regional differences in hippocampal calcium handling provide a cellular mechanism for limiting plasticity. Proc Natl Acad Sci U S A 106:14080-14084.
102. Smalla KH, Matthies H, Langnase K, Shabir S, Bockers TM, Wyneken U*, et al.* (2000): The synaptic glycoprotein neuroplastin is involved in long-term potentiation at hippocampal CA1 synapses. Proc Natl Acad Sci U S A 97:4327-4332.
103. Sneyd J, Han JM, Wang L, Chen J, Yang X, Tanimura A*, et al.* (2017): On the dynamical structure of calcium oscillations. Proc Natl Acad Sci U S A 114:1456-1461.
104. Spiden SL, Bortolozzi M, Di Leva F, de Angelis MH, Fuchs H, Lim D*, et al.* (2008): The novel mouse mutation Oblivion inactivates the PMCA2 pump and causes progressive hearing loss. PLoS Genet 4:e1000238.
105. Strehler EE, Caride AJ, Filoteo AG, Xiong Y, Penniston JT, Enyedi A. (2007a): Plasma membrane Ca2+ ATPases as dynamic regulators of cellular calcium handling. Ann N Y Acad Sci 1099:226-236.
106. Strehler EE, Filoteo AG, Penniston JT, Caride AJ. (2007b): Plasma-membrane Ca(2+) pumps: structural diversity as the basis for functional versatility. Biochem Soc Trans 35:919-922.
107. Stutzmann GE, Smith I, Caccamo A, Oddo S, Laferla FM, Parker I. (2006): Enhanced ryanodine receptor recruitment contributes to Ca2+ disruptions in young, adult, and aged Alzheimer's disease mice. J Neurosci 26:5180-5189.

108. Supper V, Schiller HB, Paster W, Forster F, Boulegue C, Mitulovic G, *et al.* (2016): Association of CD147 and Calcium Exporter PMCA4 Uncouples IL-2 Expression from Early TCR Signaling. J Immunol 196:1387-1399.
109. Surmeier DJ, Schumacker PT. (2013): Calcium, bioenergetics, and neuronal vulnerability in Parkinson's disease. J Biol Chem 288:10736-10741.
110. Szymczak AL, Workman CJ, Wang Y, Vignali KM, Dilioglou S, Vanin EF, *et al.* (2004): Correction of multi-gene deficiency in vivo using a single 'self-cleaving' 2A peptide-based retroviral vector. Nat Biotechnol 22:589-594.
111. Tidow H, Poulsen LR, Andreeva A, Knudsen M, Hein KL, Wiuf C, *et al.* (2012): A bimodular mechanism of calcium control in eukaryotes. Nature 491:468-472.
112. VanHouten J, Sullivan C, Bazinet C, Ryoo T, Camp R, Rimm DL, *et al.* (2010): PMCA2 regulates apoptosis during mammary gland involution and predicts outcome in breast cancer. Proc Natl Acad Sci U S A 107:11405-11410.
113. Vemula SK, Malci A, Junge L, Lehmann AC, Rama R, Hradsky J, *et al.* (2020): The Interaction of TRAF6 With Neuroplastin Promotes Spinogenesis During Early Neuronal Development. Front Cell Dev Biol 8:579513.
114. von Lewinski F, Keller BU. (2005): Ca2+, mitochondria and selective motoneuron vulnerability: implications for ALS. Trends Neurosci 28:494-500.
115. Weber P, Metzger D, Chambon P. (2001): Temporally controlled targeted somatic mutagenesis in the mouse brain. Eur J Neurosci 14:1777-1783.
116. Willmott T, Skitsa I, Hill I, Mummery R, Beesley PW. (1992): Molecular characterisation and structural relationship of the synapse-enriched glycoproteins gp65 and gp55. J Neurochem 58:2037-2043.
117. Willott JF. (2006): Measurement of the auditory brainstem response (ABR) to study auditory sensitivity in mice. Curr Protoc Neurosci Chapter 8:Unit8 21B.
118. Wilson MC, Kraus M, Marzban H, Sarna JR, Wang Y, Hawkes R, *et al.* (2013): The neuroplastin adhesion molecules are accessory proteins that chaperone the monocarboxylate transporter MCT2 to the neuronal cell surface. PLoS One 8:e78654.
119. Yang YM, Lee J, Jo H, Park S, Chang I, Muallem S, *et al.* (2014): Homer2 protein regulates plasma membrane Ca(2)(+)-ATPase-mediated Ca(2)(+) signaling in mouse parotid gland acinar cells. J Biol Chem 289:24971-24979.
120. Yoshida S, Shibata M, Yamamoto S, Hagihara M, Asai N, Takahashi M, *et al.* (2000): Homo-oligomer formation by basigin, an immunoglobulin superfamily member, via its N-terminal immunoglobulin domain. Eur J Biochem 267:4372-4380.
121. Zeng WZ, Grillet N, Dewey JB, Trouillet A, Krey JF, Barr-Gillespie PG, *et al.* (2016): Neuroplastin Isoform Np55 Is Expressed in the Stereocilia of Outer Hair Cells and Required for Normal Outer Hair Cell Function. J Neurosci 36:9201-9216.
122. Zuccato C, Valenza M, Cattaneo E. (2010): Molecular mechanisms and potential therapeutical targets in Huntington's disease. Physiol Rev 90:905-981.

7 Publications

- Katrina E. Deane, Michael G.K. Brunk, Andrew W. Curran, Marina M. Zepeltzi, Jing Ma, **Xiao Lin**, Francesca Abela, Sümeyra Aksit, Matthias Deliano, Frank W. Ohl, Max F.K. Happel. Ketamine anaesthesia induces gain enhancement via recurrent excitation in granular input layers of the auditory cortex. J Physiol. 2020; 598 (13): 2741-2755.

- **Xiao Lin,** Michael G.K. Brunk, Pingan Yuanxiang, Andrew W. Curran, Enqi Zhang, Franziska Stöber, Jürgen Goldschmidt, Eckart D. Gundelfinger, Maike Vollmer, Max F. K. Happel, Rodrigo Herrera-Molina, Dirk Montag. Neuroplastin expression is essential for hearing and hair cell PMCA expression. Brain Struct Funct. 2021; 226 (5): 1533-1551.

- **Xiao Lin,** Yi Liang. Rodrigo Herrera-Molina, Dirk Montag. Neuroplastin in neuropsychiatric diseases. Genes. 2021; 12 (10): 1507.

8 Ehrenerklärung

Ich versichere hiermit, dass ich die vorliegende Arbeit ohne unzulässige Hilfe Dritter und ohne Benutzung anderer als der angegebenen Hilfsmittel angefertigt habe; verwendete fremde und eigene Quellen sind als solche kenntlich gemacht.

Ich habe insbesondere nicht wissentlich:

- Ergebnisse erfunden oder widersprüchliche Ergebnisse verschwiegen,
- statistische Verfahren absichtlich missbraucht, um Daten in ungerechtfertigter Weise zu interpretieren,
- fremde Ergebnisse oder Veröffentlichungen plagiiert,
- fremde Forschungsergebnisse verzerrt wiedergegeben.

Mir ist bekannt, dass Verstöße gegen das Urheberrecht Unterlassungs- und Schadensersatzansprüche des Urhebers sowie eine strafrechtliche Androhung durch die Strafverfolgungsbehörden begründen kann.

Ich erkläre mich damit einverstanden, dass die Arbeit ggf. mit Mitteln der elektronischen Datenverarbeitung auf Plagiate überprüft werden kann.

Die Arbeit wurde bisher weder im Inland noch im Ausland in gleicher oder ähnlicher Form als Dissertation eingereicht und ist als Ganzes auch noch nicht veröffentlicht.

Magdeburg, 26.03.2021 Unterschrift

Ort, Datum Xiao Lin